Structural Studies of Bacterial RND-Transporters

Dissertation

zur
Erlangung der naturwissenschaftlichen Doktorwürde
(Dr. sc. nat.)

vorgelegt der
Mathematisch-naturwissenschaftlichen Fakultät
der
Universität Zürich

von
GABY SENNHAUSER

aus
Kirchberg SG

Promotionskomitee
Prof. Dr. Markus G. Grütter (Vorsitz)
Prof. Dr. Raimund Dutzler
Prof. Dr. Andreas Plückthun
Zürich 2008

Die vorliegende Arbeit wurde von der Mathematisch-naturwissenschaftlichen Fakultät der Universität Zürich auf Antrag von Prof. Dr. Markus G. Grütter, Prof. Dr. Raimund Dutzler und Prof. Dr. Andreas Plückthun als Dissertation angenommen.

Vol 10 No 2 March 2007

Current Opinion in Drug Discovery & Development

James A Bristol, Paul J Reider & David Brown EDITORS

In this issue

The Chemistry of Biological Products

Edited by James McAlpine, David Ecker & Alfredo Romano

Authoritative reviews covering aspects of alternatives to antibodies, RNA interference, protein engineering, vaccines and natural products

THOMSON

TABLE OF CONTENTS

RESEARCH SUMMARY

Even though transporters that extrude toxic compounds are found in all types of cells, they vary in the chemical diversity of their transported substrates, in their molecular architecture and in their energization source. In Gram-negative bacteria, drug transporters belonging to the resistance-nodulation-cell division (RND) family of proteins are especially abundant. A common feature of these RND-transporters is their utilization of the proton electrochemical gradient to energize the transport of substrates and that they transport a variety of chemically diverse substances. Among them are also several antibiotic agents, which often leads to clinically relevant multidrug resistance in bacteria. These multidrug-resistant bacteria represent a rising problem in the treatment of bacterial infections nowadays.

This doctoral thesis focused on the structural biology of members of the RND-transporter family. At the beginning of this thesis the X-ray crystal structure of one family member, *Escherichia coli* AcrB, was known at 3.5 Å resolution and revealed the general architecture of this family of proteins. Little was known, however, at the structural level, about how these transporters accomodate and translocate such a diversity of substrates. Our goal was therefore to gain further insight into the molecular mechanism of multidrug transport. As integral membrane proteins are notoriously difficult to crystallize, we made use of the designed ankyrin repeat protein (DARPin) technology to improve their crystallization behaviour. DARPins are built based on the natural ankyrin repeat protein fold onto which novel specificities were designed. A library consisting of a myriad of individual DARPin molecules was used in combination with the in vitro selection technique ribosome display, to select specific binders to several target transporters.

The X-ray structure of *Escherichia coli* AcrB in complex with a selected inhibitory DARPin at 2.54 Å resolution revealed a novel asymmetric conformation of the RND-transporter, where each subunit of the trimeric protein adapted a slightly different conformation. This study revealed novel mechanistic details of drug transport. The DARPin approach hereby greatly facilitated the crystallization of AcrB by stabilizing the asymmetric conformation and improved the resolution significantly.

To add structural information and to learn more about multidrug transport of RND-transporters, the X-ray structure of *Pseudomonas aeruginosa* MexB was determined at 3.0 Å resolution. Despite the importance of this transporter considering the pathogenicity and resistance properties of *P. aeruginosa*, this structure was not known. This represents only the second structure of a protein of this family of drug transporters. Not surprisingly, given the high sequence homology between them, MexB adopted an asymmetric fold very similar to AcrB but showed prominent conformational changes in one subunit. Moreover a detergent molecule, deriving from the purification, was bound in one of the binding cavities. Together with a high-resolution X-ray structure of AcrB in complex with its substrate minocycline we gained useful information on the detailed three-dimensional organization of the drug-binding site and on the capability of multidrug transporter to exhibit such broad substrate specificity. Since RND-transporters are usually part of a multicomponent efflux system, the structures of single-components and hopefully also of whole three-component systems in the future, will help to develop agents able to act as efflux inhibitors, thereby reviving the effectiveness of many efflux-affected antibiotics.

ZUSAMMENFASSUNG

Transporterproteine, welche giftige Stoffe aus der Zelle transportieren, kommen zwar in allen Zelltypen vor, unterscheiden sich aber in der Verschiedenartigkeit der von ihnen transportierten Substanzen, in ihrer molekularen Architektur und ihrer Energiequelle. In Gram-negativen Bakterien findet man besonders häufig Transporter die zur sogenannten „resistance-nodulation-cell division“ (Widerstand-Knöllchenbildung-Zellteilungs, RND) Proteinfamilie gehören. Eine Gemeinsamkeit dieser RND-Transporter ist es, dass sie alle den elektrochemischen Protonengradienten als Energiequelle für den Transport von Stoffen nützen, und dass sie eine grosse Anzahl von chemisch sehr unterschiedlichen Substanzen transportieren. Unter diesen befinden sich auch einige antibiotisch wirkende Substanzen, was oft zur klinisch bedeutenden Resistenz gegenüber verschiedensten Medikamenten führt. Diese mehrfach resistenten Bakterien stellen gegenwärtig ein grosses Problem in der Behandlung von bakteriellen Infektionen dar.

Diese Doktorarbeit konzentrierte sich auf die Strukturbiologie von Vertretern dieser RND-Transporter Familie. Zu Beginn dieser Arbeit war die Röntgenkristallstruktur von einem Familienmitglied, AcrB, bei einer Auflösung von 3.5 Å bekannt und hat die generelle Architektur dieser Proteinfamilie aufgezeigt. Nur wenig war jedoch bekannt, wie genau diese Transporter eine solche Vielfalt an Substanzen aufnehmen und durchschleusen können. Unser Ziel war es deshalb weitere Einsichten in den molekularen Mechanismus dieses vielfältigen Transports zu gewinnen. Da in einer Membran sitzende Proteine bekanntermassen schwer zu kristallisieren sind, haben wir sogenannte massgeschneiderte Ankyrin Repeat Proteine (DARPins) benutzt, um ihre Kristallisationseigenschaften zu verbessern. DARPins gründen auf der Faltung von natürlichen Ankyrin Repeat Proteinen, auf welche neue Spezifitäten gebaut wurden. Eine Protein Bibliothek, bestehend aus unzähligen individuellen DARPin Molekülen, wurde zusammen mit der Technik „ribosome display“ verwendet, um spezifische Binder für mehrere Zieltransporter zu finden.

Bei einer Auflösung von 2.54 Å zeigte die Röntgenstruktur des *Escherichia coli* Proteins AcrB in einem Komplex mit einem gefundenen hemmenden DARPin eine neue asymmetrische Gestalt dieses RND-Transporters, in welcher jede Untereinheit des trimeren Proteins eine leicht andere Konformation einnahm. Diese Studie offenbarte neue mechanistische Details des Substanztransports. Durch die Stabilisierung der asymmetrischen Form mit dem Ansatz der DARPins wurde in diesem Falle die Kristallisation von AcrB beträchtlich vereinfacht und die Auflösung erheblich verbessert.

Um weitere strukturelle Informationen und Erkenntnisse über den Substanztransport dieser RND-Transporter Familie zu gewinnen, wurde die Röntgenstruktur von *Pseudomonas aeruginosa* MexB, bei einer Auflösung von 3.0 Å gelöst. Diese Struktur war trotz der Wichtigkeit dieses Transporters in Bezug auf *P. aeruginosa* als Krankheitserreger und seine Resistenzeigenschaften, nicht bekannt. Sie ist daher erst die zweite Struktur dieser Proteinfamilie. MexB nimmt eine sehr ähnliche asymmetrische Form ein wie AcrB, was nicht erstaunt, wenn man die grosse Sequenzähnlichkeit der beiden bedenkt, aber MexB zeigt markante Änderungen in einer Untereinheit auf. Ausserdem ist ein Detergensmolekül aus der Reinigung in einer der Bindungstaschen gebunden. Zusammen mit einer hochaufgelösten Röntgenstruktur von AcrB mit gebundenem Substrat Minocyclin haben wir nützliche Erkenntnisse über das detaillierte dreidimensionale Aussehen der Substratbindungsstelle und über die Fähigkeit so viele verschiedene Stoffe zu transportieren, gewonnen. Weil RND-Transporter gewöhnlich Teil von Mehrkomponentsystemen sind, werden die Strukturen von Einzelkomponenten and hoffentlich in Zukunft auch die von ganzen Dreikomponentsystemen, in der Entwicklung von Stoffen helfen, welche den Transport hemmen können und so die Wirksamkeit von vielen vom Transport betroffenen Antibiotika wiederbeleben.

CHAPTER 1

BACTERIAL MULTIDRUG RESISTANCE

With the discovery of antibacterial drugs in the first half of the 20th century and the availability of a number of different antibiotic compounds in the 1980ties bacterial infections were considered no longer life-threatening and a lot of infectious diseases seemed to be eradicated. Nevertheless, almost as soon as these `magic bullets` were in use, bacterial strains evolved ways to overcome them. The excessive use of antibiotics has further increased the emergence of antibiotic-resistant pathogens. Particularly in hospitals, where various microbes can come in close contact with one another, resistance has been reported in many bacteria and often results in severe treatment failure. Furthermore, efflux-caused drug resistance is a medical problem not only restricted to bacterial infections, it is also arising in many tumours exhibiting resistance to anticancer therapy.

1.1 Efflux as resistance mechanism to antibacterial drugs

Resistance may occur as an intrinsic feature of an organism, or when it is not, the transfer of normally susceptible into resistant may be acquired either through mutation, or by obtaining the genetic information that encodes resistance from other bacteria. Generally, bacteria can resist the action of antibiotics through three strategies: inactivation of the antibiotic drug, alteration of the target protein, and reduced drug accumulation due to a decrease in membrane permeability and active efflux of the agent [1]. Clinically relevant levels of resistance can be explained, in many cases, by a synergy between these mechanisms. Multidrug resistance, however, defined as resistance of an organism to more then one class of antibiotics, is almost exclusively associated with the expression of drug exporters. Except a few examples where these genes are found on mobile elements, almost all multidrug transporters are chromosomally encoded [2].

The phenomenon of antibiotic efflux was first described in 1978 for transport proteins that expel tetracyclines from *Escherichia coli* [3]. Tetracycline transporters are specific, transporting only one given drug or class of drugs. In contrast, multidrug transporters are broad-specific, accomodating compounds with very diverse structures and cellular targets. In either case, specific or broad-specific, the effect of all these drug exporters is the extrusion of toxic substances from the cell before they can reach their site of action. Thereby the effective intracellular drug concentration is

reduced and the susceptibility of a bacterial cell to an antibiotic agent can be decreased by several orders of magnitude. In combination with other resistance mechanisms this can lead to clinically relevant levels of antibiotic resistance.

The natural physiological function of these bacterial drug exporters has been much debated in the literature and still is a widely discussed subject [4]. In antibiotic-producing organisms, like the tetracycline-producing *Streptomyces spp.*, the expression of such a protecting drug transporter is self-explanatory. From these organisms such genes could have been acquired then by other bacteria. The extrusion of exogenous toxic compounds produced by the host is another discussed intended function of multidrug transporters. The transport capability of substances such as bile salts and fatty acids by the AcrAB-TolC system from *Enterobacteria* and its homologs in other Gram-negative bacteria is a well known example to explain the survival of these organisms in high concentrations of these substances encountered in the gut of mammals. The expulsion of endogenous metabolites whose presence could be toxic above certain concentrations has also been discussed [5] and recently it was proposed that efflux pumps could play also a role in the pathogenicity of the bacterium, exporting virulence factors that are important for the colonization and infection of cells [4]. In these contexts, it seems that antibiotics are simply subject to efflux because they share the necessary basic structural features for efflux such as the presence of a relatively large hydrophobic part or the amphiphile character.

1.2 Bacterial multidrug transporters

Despite their individual differences, multidrug transporters share the ability to expel a wide variety of structurally diverse compounds. Bacterial multidrug transporters can be assigned to five larger classes of transporters, independent of their substrates [6]: the ATP-binding cassette (ABC) superfamily, the major facilitator superfamily (MFS), the multidrug and toxic-compound extrusion (MATE) family, the small multidrug resistance (SMR) family and the resistance-nodulation-cell division (RND) family (Fig. 1). Transporters within a superfamily are related with regard to primary/secondary structure and energization requirements. Multidrug transporters are found in virtually all bacteria and often a single organism expresses transporters from more than one family and several types belonging to the same family.

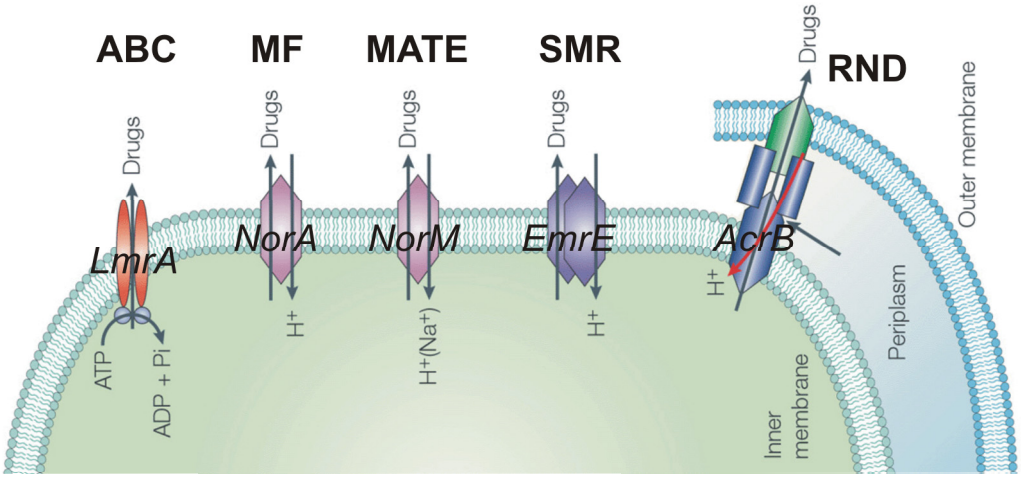

Fig. 1.

Schematic illustration of the five classes of bacterial drug transporters. Shown are representative members of the corresponding families: *Lactococcus lactis* LmrA, *Staphylococcus aureus* NorA, *Vibrio parahaemolyticus* NorM, *Escherichia coli* EmrE, and *Escherichia coli* AcrB. The RND-transporter family is shown as multicomponent system, together with an outer membrane protein and a membrane fusion protein, representing their functional architecture in Gram-negative bacteria. Adapted from [7].

Most of the transporters function as secondary transporters using the transmembrane electrochemical gradient of ions to mediate drug export. The transporters belonging to the MF-, RND- and SMR-families are H^+-driven, whereas those of the MATE-family are mostly Na^+-driven. The exception is the ABC superfamily whose members derive their energy for transport through ATP-hydrolysis and are therefore primary transporters. Drug transporters of the ABC family are especially abundant in eukaryotic cells, where they confer resistance to chemotherapeutic drugs, but are not very common in bacteria. Classical drug transporters, such as the ones found in Gram-positive bacteria, consist of a single component with several transmembrane spanning domains. Especially abundant and clinically significant in Gram-positive bacteria are efflux pumps of the MF superfamily. More elaborate systems exist in Gram-negative bacteria, which have a much higher level of intrinsic resistance compared to the Gram-positive. The majority of multidrug transporters there is organized as multi-component systems, to ensure a complete removal of an agent across both membranes (Fig. 1). Although RND-transporters are not unique to Gram-negative bacteria [8], they are the most prominent in these organisms and most relevant in respect of intrinsic and acquired resistance to

clinically significant antibiotics [9]. Most RND-transporters studied to date are multidrug transporters [5].

1.3 RND-transporter family

RND-transporters are large proteins composed typically of around 1000 amino acid residues. They all display an unusual topology consisting of 12 transmembrane helices (TMs) with two large periplasmic loops between TM1 and 2 and TM7 and 8 (Fig. 2). The N-terminal halves resemble the C-terminal halves and, as such, these proteins are believed to have arisen from an intragenic duplication event during evolution [10]. Reconstitution studies have confirmed that the RND-transporters are H^+/substrate antiporters [11] and substitutions of three conserved charged residues in the transmembrane domain (Asp-407 and Asp-408 of TM4 and Lys-940 (AcrB) or Lys-939 (MexB) of TM10) led to a complete loss of transport activity, indicating a probable function in proton translocation [12].

The determination of the structure of the *E. coli* RND-transporter AcrB in 2002 was a major breakthrough [13]. It was not only the first structure of an RND-family member but also the first multidrug and the first proton coupled transporter. The overall structure was shown to be a trimer (Fig. 2A). Besides the 36-helix transmembrane domain, the periplasmic loops fold into two prominent domains parallel to the membrane, the adjacent pore domain and the docking domain, being 40 Å and 30 Å thick respectively. Interestingly, the docking domain forms a funnel-like opening, with an internal diameter of 30 Å which is connected by a pore to a large central cavity formed by the transmembrane domains of the subunits. Originally it was thought that this symmetric structure represents the closed structure of AcrB and substrates are transported upon opening of the pore in an “elevator-like” mechanism via this central pathway. The pore domain is further arranged into four subdomains, PN1, PN2, PC1, and PC2, each comprising two $\beta-\alpha-\beta$–motifs and the docking domain is composed of two subdomains, DN and DC (Fig. 2B). The whole trimer is held together by a hairpin structure formed by subdomain DN that protrudes from each subunit into the next subunit.

Most RND-transporters promote resistance to a wide range of substrates. Nevertheless, the type and number of agents varies from organism to organism, even for pumps with a high degree of sequence homology. It is not clear whether these differences reflect the actual substrate specificity of these transporters. Variations in the intrinsic outer membrane permeability of the host organism and the presence of other drug transporters could compromise the drug resistance pattern of an organism. The best studied transporters, AcrB of *E. coli* and MexB of *P. aeruginosa* expel mostly lipophilic and amphiphilic compounds, many of them carrying either positive or negative or even both charges. One common feature of the majority of the substrates, however, appears to be a large hydrophobic framework. How a single protein can recognize such a variety of chemically unrelated compounds is an intriguing question and was a point that was not answered by the first AcrB structures [13-15]. Several studies showed that the periplasmic loops of RND transporters are critical for substrate recognition [16-18]. Recent advances in the structural analysis of AcrB, including the work that was done in the course of this thesis, and the structures of a number of soluble multidrug-recognizing proteins such as the regulator proteins which can bind a similar broad range of drugs showed how these substrates are recognized. The proteins possess large hydrophobic binding sites and bind their substrates through a combination of stacking, van der Waals and electrostatic interactions, rather than a specific network of hydrogen bonds and other specific interactions like in most enzymes and receptors.

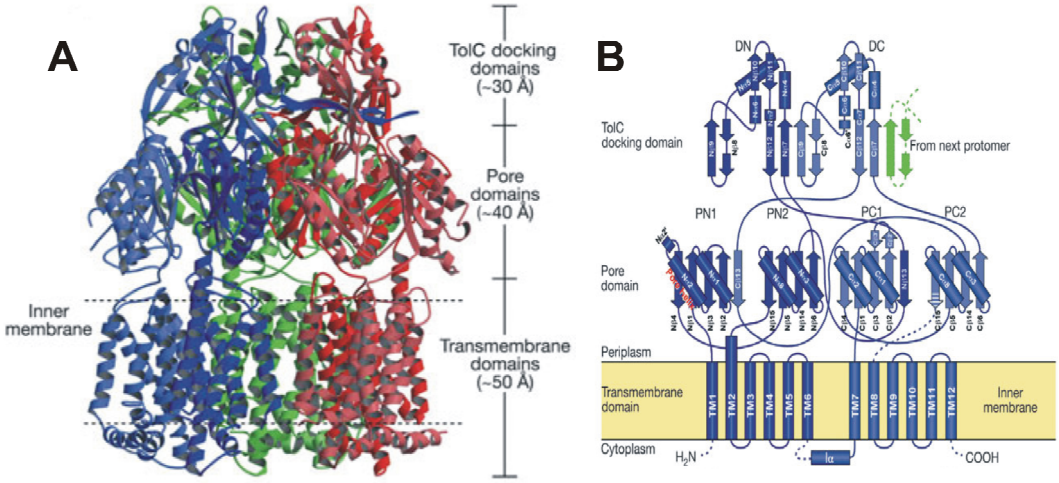

Fig. 2.

X-ray structure of the RND-transporter AcrB (1IWG). A Ribbon representation of the trimeric AcrB structure. The individual subunits are colored and the three main domains are labelled. **B** Topology diagram of AcrB with labelled subdomains. Adapted from [13].

1.4 Drug efflux in Gram-negative bacteria: The formation of tripartite efflux pumps

Gram-negative bacteria possess both a cytoplasmic and an outer membrane separated by the periplasmic space. As transport out of the cytoplasm only would be insufficient and as many antibiotic targets reside in the periplasm, like the cell wall components targeted by the β-lactams, effective removal of antibiotics requires transport also across the outer membrane. The outer membrane however, unable to maintain an electrochemical gradient or to access ATP, needs the inner membrane as source of energy. As a consequence, RND-transporters as well as some MFS- (e.g. the EmrAB-TolC system of *E. coli*) and ABC-transporters (e.g. the HlyBD-TolC system of *E. coli*) expressed by Gram-negativ bacteria typically operate as multiprotein efflux systems consisting of a an energy-providing transporter located in the cytoplasmic membrane, a pore-like outer membrane protein (OMP) and a periplasmic protein connecting them (a membrane-fusion protein (MFP) family member). It is thought that substrates are captured by the transporter protein and then are transported out of the cell through the OMP, which forms a channel through the outer membrane [19]. The most extensively characterized RND tripartite systems are the *E. coli* AcrAB-TolC and the *P. aeruginosa* MexAB-OprM system.

Many outer membrane components are multifunctional and can couple to different transporters located in the inner membrane, therefore their role in determining the specificity or directionality of transport seems not to be important. For example, TolC serves as general outer membrane channel in *E. coli.* It works together with different RND-transporters besides AcrB, and also with some MFS- and ABC-transporters. Similarly, OprM of *P. aeruginosa* can function with several RND-transporters [20]. The genes for such a tripartite system are often organized in one operon, in which a regulator gene is located adjacent to the gene encoding the MFP, which is located adjacent to the gene enconding the transporter, which in turn is located next to the OMP gene. All components are usually cotranscribed. Some OMPs, however, such as TolC, are located on the chromosome distant from the other tripartite components. As TolC is the universal OMP component of tripartite systems in *E. coli*, it has to interact with diverse transporters and its regulation independent of the individual transporters is not surprising.

The crystal structures of individual components of the two best characterized systems AcrAB-TolC and MexAB-OprM provided a structural basis to the current understanding of drug export through two membranes (see Chapters 3 and 4) (TolC [21], AcrB [13], MexA [22, 23], OprM [24], AcrA [25]). Nevertheless, the precise biochemical function, the specific association and the oligomeric state of the MFPs and therefore also the assembly of the whole tripartite system remains unknown and is discussed controversially. MFPs are fairly unifom in size (380-480 residues) [5] and are attached to the inner membrane by a single N-terminal transmembrane helix or by lipid modification of a conserved N-terminal cysteine residue after cleavage of the periplasmic signal sequence. However, the membrane attachment is not essential for drug efflux activity, since N-terminal mutants of the MFPs AcrA and MexA devoid of lipid modification, remained functional [26, 27].

The similarity in size and symmetry between the periplasmic end of the OMP and the tip of the periplasmic domain of RND-transporter has prompted the suggestion that these domains could directly interact. In vivo cross-linking experiments have indeed shown a close proximity between the RND and OMP components of both major efflux systems AcrB and TolC [28, 29] and MexB and OprM [30, 31]. AcrA was further shown to form stable interactions with both AcrB and

TolC [28, 32]. An often applied strategy to gain insight into the relevant parts for the assembly is the adaptation of the two best characterized efflux pumps AcrAB-TolC and MexAB-OprM to each other [33, 34]. These studies all showed that the α-helical hairpin of the MFPs interacts with the OMPs and the β-barrel and lipoyl-domain interacts with the RND-component.

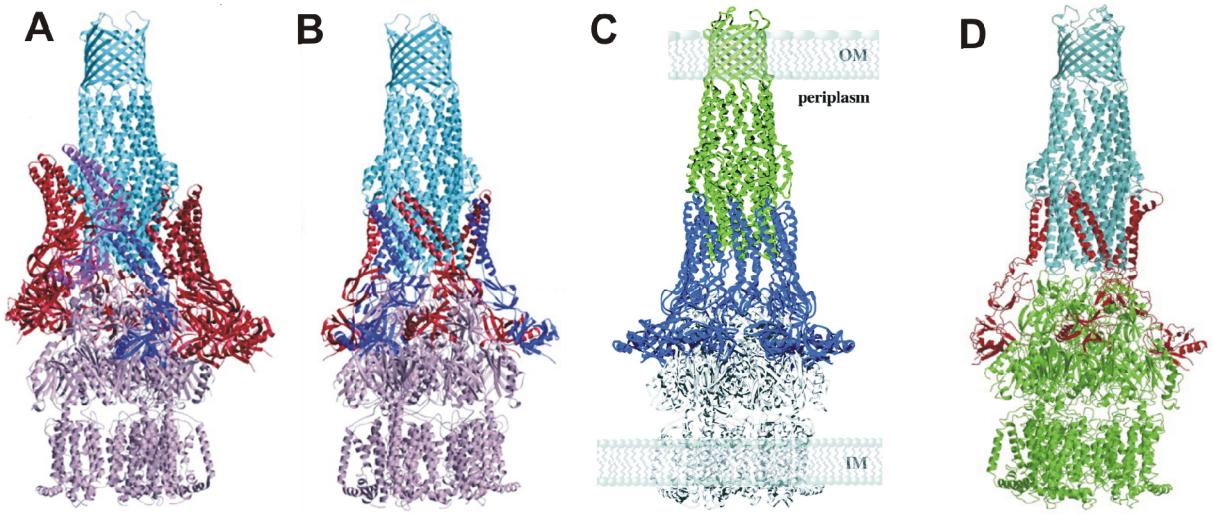

Fig. 3.

Models of the tripartite assembly. A MexA/MexB*-OprM [22] **B** MexA/MexB*-OprM [22] **C** MexA/AcrB-TolC [23] **D** AcrA*/AcrB-TolC [35]. *These structures derived from modeling on an available crystal structure of the homologous protein.

Based on the individual protein structures and molecular interaction studies, several models of the complete pump assembly have been proposed (Fig. 3) [19, 22, 23, 35]. They mainly differ in the oligomeric state and extend of the interaction of the MFP component. Akama et al. proposed two options: (i) a 12-mer sheath around both OprM and MexB similar to the oligomeric structure in the crystal and (ii) a threefold dimer model [22]. Higgins et al. proposed a model with nine monomers forming a sheath around OprM and MexB [23] and Fernandez-Recio et al. modelled an open conformation of TolC and predicted a subunit stoichiometry of 1:1:1 for the OMP:MFP:transporter components [35]. It is far from clear how these pumps assemble and if the MFPs simply stabilize the RND-OMP-complex or play a more active role in the transport event itself. But it seems that multidrug export systems are constitutively assembled independent of the presence of a substrate [28].

1.5 Regulation of multidrug transporter expression

A large number of studies have been undertaken to understand the complex regulation of efflux pump gene expression [36]. There are usually two ways how drug transporters are regulated, via local and global regulators (Fig. 4). Many pumps are controlled via repressors that are transcribed divergently to the efflux pump operon. The local repressor of the acrAB genes, AcrR belongs to the TetR repressor family [37], the one of the mexAB-oprM genes, MexR, to the MarR family [38]. These repress their own and the pump expression by binding to the promoter regions of the respective genes. In the case of AcrAB and MexAB-OprM the repression is generally loose, allowing constitutive expression of the proteins. Mutations in the repressor gene can fully inhibit the repression of the efflux pump gene and lead to overexpression of the latter.

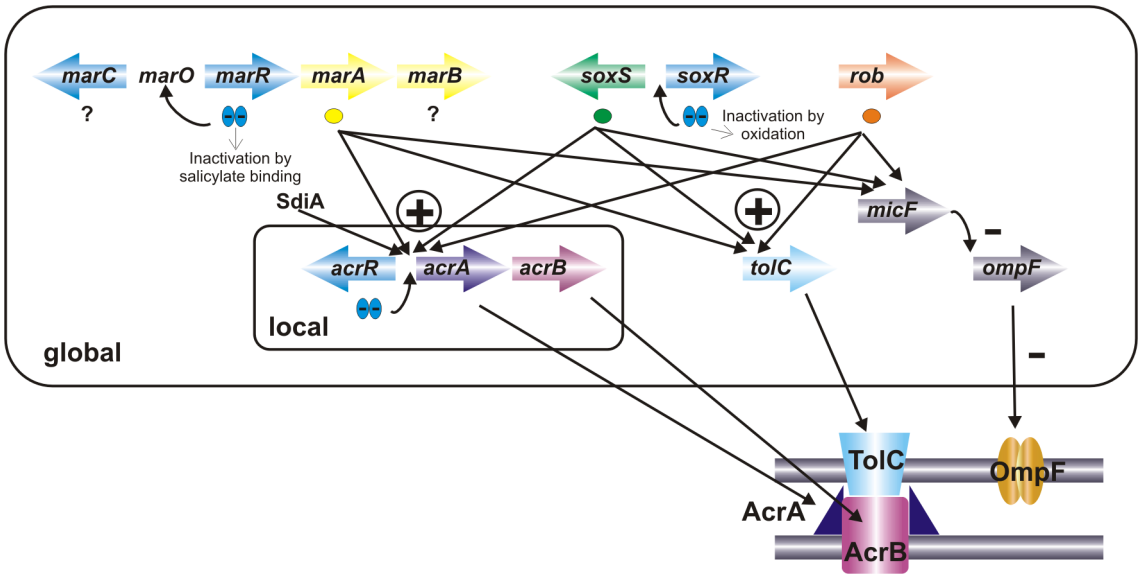

Fig. 4.

Local and global regulation of the AcrAB-TolC tripartite system expression in *E. coli*. Adapted from [39].

The global regulation of the AcrAB-TolC system is the best characterized so far. But it is believed that the expression of MexAB-OprM is also controlled by global regulators. AcrAB-TolC is tightly regulated through at least four global activators: MarA, SoxS, Rob and SdiA. Often these global regulators control also the expression of outer membrane porins (Fig. 4), thereby emphasizing again the important synergy

between different resistance mechanisms, here the active efflux and low outer membrane permeability.

1.6 References

1. McDermott, P.F., R.D. Walker, and D.G. White, *Antimicrobials: modes of action and mechanisms of resistance.* Int J Toxicol, 2003. 22(2): p. 135-43.

2. Butaye, P., A. Cloeckaert, and S. Schwarz, *Mobile genes coding for efflux-mediated antimicrobial resistance in Gram-positive and Gram-negative bacteria.* Int J Antimicrob Agents, 2003. 22(3): p. 205-10.

3. Levy, S.B. and L. McMurry, *Plasmid-determined tetracycline resistance involves new transport systems for tetracycline.* Nature, 1978. 276(5683): p. 90-2.

4. Piddock, L.J., *Multidrug-resistance efflux pumps - not just for resistance.* Nat Rev Microbiol, 2006. 4(8): p. 629-36.

5. Li, X.Z. and H. Nikaido, *Efflux-mediated drug resistance in bacteria.* Drugs, 2004. 64(2): p. 159-204.

6. Putman, M., H.W. van Veen, and W.N. Konings, *Molecular properties of bacterial multidrug transporters.* Microbiol Mol Biol Rev, 2000. 64(4): p. 672-93.

7. Krulwich, T.A., et al., *Do physiological roles foster persistence of drug/multidrug-efflux transporters? A case study.* Nat Rev Microbiol, 2005. 3(7): p. 566-72.

8. Tseng, T.T., et al., *The RND permease superfamily: an ancient, ubiquitous and diverse family that includes human disease and development proteins.* J Mol Microbiol Biotechnol, 1999. 1(1): p. 107-25.

9. Nikaido, H., *Multidrug efflux pumps of gram-negative bacteria.* J Bacteriol, 1996. 178(20): p. 5853-9.

10. Saier, M.H., Jr., et al., *Two novel families of bacterial membrane proteins concerned with nodulation, cell division and transport.* Mol Microbiol, 1994. 11(5): p. 841-7.

11. Zgurskaya, H.I. and H. Nikaido, *Bypassing the periplasm: reconstitution of the AcrAB multidrug efflux pump of Escherichia coli.* Proc Natl Acad Sci U S A, 1999. 96(13): p. 7190-5.

12. Guan, L. and T. Nakae, *Identification of essential charged residues in transmembrane segments of the multidrug transporter MexB of Pseudomonas aeruginosa.* J Bacteriol, 2001. 183(5): p. 1734-9.

13. Murakami, S., et al., *Crystal structure of bacterial multidrug efflux transporter AcrB.* Nature, 2002. 419(6907): p. 587-93.

14. Yu, E.W., et al., *Structural basis of multiple drug-binding capacity of the AcrB multidrug efflux pump.* Science, 2003. 300(5621): p. 976-80.

15. Yu, E.W., et al., *A periplasmic drug-binding site of the AcrB multidrug efflux pump: a crystallographic and site-directed mutagenesis study.* J Bacteriol, 2005. 187(19): p. 6804-15.

16. Mao, W., et al., *On the mechanism of substrate specificity by resistance nodulation division (RND)-type multidrug resistance pumps: the large periplasmic loops of MexD from Pseudomonas aeruginosa are involved in substrate recognition.* Mol Microbiol, 2002. 46(3): p. 889-901.

17. Elkins, C.A. and H. Nikaido, *Substrate specificity of the RND-type multidrug efflux pumps AcrB and AcrD of Escherichia coli is determined predominantly by two large periplasmic loops.* J Bacteriol, 2002. 184(23): p. 6490-8.

18. Tikhonova, E.B., Q. Wang, and H.I. Zgurskaya, *Chimeric analysis of the multicomponent multidrug efflux transporters from gram-negative bacteria.* J Bacteriol, 2002. 184(23): p. 6499-507.

19. Eswaran, J., et al., *Three's company: component structures bring a closer view of tripartite drug efflux pumps.* Curr Opin Struct Biol, 2004. 14(6): p. 741-7.

20. Aires, J.R., et al., *Involvement of an active efflux system in the natural resistance of Pseudomonas aeruginosa to aminoglycosides.* Antimicrob Agents Chemother, 1999. 43(11): p. 2624-8.

21. Koronakis, V., et al., *Crystal structure of the bacterial membrane protein TolC central to multidrug efflux and protein export.* Nature, 2000. 405(6789): p. 914-9.

22. Akama, H., et al., *Crystal structure of the membrane fusion protein, MexA, of the multidrug transporter in Pseudomonas aeruginosa.* J Biol Chem, 2004. 279(25): p. 25939-42.

23. Higgins, M.K., et al., *Structure of the periplasmic component of a bacterial drug efflux pump.* Proc Natl Acad Sci U S A, 2004. 101(27): p. 9994-9.

24. Akama, H., et al., *Crystal structure of the drug discharge outer membrane protein, OprM, of Pseudomonas aeruginosa: dual modes of membrane anchoring and occluded cavity end.* J Biol Chem, 2004. 279(51): p. 52816-9.

25. Mikolosko, J., et al., *Conformational flexibility in the multidrug efflux system protein AcrA.* Structure, 2006. 14(3): p. 577-87.

26. Zgurskaya, H.I. and H. Nikaido, *AcrA is a highly asymmetric protein capable of spanning the periplasm.* J Mol Biol, 1999. 285(1): p. 409-20.

27. Yoneyama, H., et al., *Function of the membrane fusion protein, MexA, of the MexA, B-OprM efflux pump in Pseudomonas aeruginosa without an anchoring membrane.* J Biol Chem, 2000. 275(7): p. 4628-34.

28. Touze, T., et al., *Interactions underlying assembly of the Escherichia coli AcrAB-TolC multidrug efflux system.* Mol Microbiol, 2004. 53(2): p. 697-706.

29. Tamura, N., et al., *Direct interaction of multidrug efflux transporter AcrB and outer membrane channel TolC detected via site-directed disulfide cross-linking.* Biochemistry, 2005. 44(33): p. 11115-21.

30. Nehme, D., et al., *Assembly of the MexAB-OprM multidrug efflux system of Pseudomonas aeruginosa: identification and characterization of mutations in mexA compromising MexA multimerization and interaction with MexB.* J Bacteriol, 2004. 186(10): p. 2973-83.

31. Mokhonov, V.V., et al., *Role of the membrane fusion protein in the assembly of resistance-nodulation-cell division multidrug efflux pump in Pseudomonas aeruginosa.* Biochem Biophys Res Commun, 2004. 322(2): p. 483-9.

32. Tikhonova, E.B. and H.I. Zgurskaya, *AcrA, AcrB, and TolC of Escherichia coli Form a Stable Intermembrane Multidrug Efflux Complex.* J Biol Chem, 2004. 279(31): p. 32116-24.

33. Krishnamoorthy, G., E.B. Tikhonova, and H.I. Zgurskaya, *Fitting periplasmic membrane fusion proteins to inner membrane transporters: mutations that enable Escherichia coli AcrA to function with Pseudomonas aeruginosa MexB.* J Bacteriol, 2008. 190(2): p. 691-8.

34. Bokma, E., et al., *Directed evolution of a bacterial efflux pump: adaptation of the E. coli TolC exit duct to the Pseudomonas MexAB translocase.* FEBS Lett, 2006. 580(22): p. 5339-43.

35. Fernandez-Recio, J., et al., *A model of a transmembrane drug-efflux pump from Gram-negative bacteria.* FEBS Lett, 2004. 578(1-2): p. 5-9.

36. Grkovic, S., M.H. Brown, and R.A. Skurray, *Regulation of bacterial drug export systems.* Microbiol Mol Biol Rev, 2002. 66(4): p. 671-701, table of contents.

37. Li, M., et al., *Crystal structure of the transcriptional regulator AcrR from Escherichia coli.* J Mol Biol, 2007. 374(3): p. 591-603.

38. Lim, D., K. Poole, and N.C. Strynadka, *Crystal structure of the MexR repressor of the mexRAB-oprM multidrug efflux operon of Pseudomonas aeruginosa.* J Biol Chem, 2002. 277(32): p. 29253-9.

39. Kumar, A. and H.P. Schweizer, *Bacterial resistance to antibiotics: active efflux and reduced uptake.* Adv Drug Deliv Rev, 2005. 57(10): p. 1486-513.

CHAPTER 2

MEMBRANE PROTEIN CRYSTALLIZATION

Membrane proteins, like the RND-transporters, are biological macromolecules that mediate diverse functions in all organisms by allowing molecules to pass a lipophilic membrane or to send a signal through it. Analysis of genomic data revealed that they account for between 25 and 30% of all encoded proteins [1]. Despite their significant abundance, high-resolution structures are available only for a limited number of this special class of proteins. Only 157 different membrane proteins have been characterized structurally whereas the number of all entries in the Protein Data Bank exceeded 50000. This low number reflects the difficulties encountered in structural biology with these challenging proteins.

2.1 Problems and Solutions

Atomic-resolution structures of membrane proteins are indispensable to understand their function. A prerequisite for the structural characterization of any biological macromolecule is the homogeneity of the sample in terms of purity, quality (secondary modifications or proteolytic cleavage) and conformational uniformity. Many recombinantly expressed and purified soluble proteins do not fulfill these requirements. The situation is even more complex for membrane proteins and even more difficulties arise. Apart from the ones mentioned above, membrane proteins are naturally embedded within the lipid bilayer of a cell or an organelle. Therefore they contain both a hydrophobic part buried within the lipids and a hydrophilic part exposed to the solvent. In order to purify such lipid embedded molecules it is beneficial to extract them from their environment since the lipid bilayer is very complex and not suitable for crystallization. The amphipathic nature of detergents is well suited to stand in for the lipids. They mimic the lipid bilayer by covering the hydrophobic part of the protein with their hydrophobic tail and simultaneously interact with the aequous environment via their polar head groups. These interactions prevent the aggregation of the hydrophobic region of a membrane protein. However, choosing the wrong detergent can have dramatic effects on a protein e.g. by partly denaturing it. A loss of stability or function is therefore an often encountered problem upon solubilization with a detergent. Choosing the right detergent, in contrast, can have a dramatic effect on the crystallization behaviour of a membrane protein and can be the key to successful crystallization.

The next step towards the structural characterization of a protein is the formation of well-ordered crystals. This requires specific intermolecular interactions of one molecule to another one. In contrast to soluble proteins which can use their entire surface for crystal contacts, membrane proteins have often only a limited surface to form such contacts, namely the small hydrophilic surface loops. Normally, the detergent molecules which form a micelle around the hydrophobic region, which is the major part of the surface for many membrane proteins, do not form crystal contacts. Furthermore, membrane proteins often adopt several conformations in order to fulfill their transport function.

One way to enhance the chance of crystallizing a membrane protein is to use either a natural ligand, a synthetic binding molecule or a bioengineered protein ligand. The complex formation of a target molecule with a binding protein can have several beneficial effects: (i) a thermodynamic stabilization of the target, (ii) a stabilization of a particular conformation, and (iii) an enlargement of the hydrophilic surface. Furthermore, the protein complex can form different crystal contacts in comparison to the single protein, due to the altered surface. However, most of natural interaction partners are not known, not easy to obtain or not suitable for crystallization in terms of affinity, homogeneity, flexibility etc. or in many cases there is no natural binding partner at all. The desire to use synthetic or engineered ligands therefore is easily explained. Antibodies or fragments thereof are the best-known binding molecules. They have been used to determine crystal structures of soluble proteins and membrane proteins complexes [2, 3].

However antibodies and antibody fragments are not ideal for use in structural biology because of several reasons. These limitations have prompted the search for alternative frameworks with the same binding capabilities, but with superior properties to antibodies. One of these alternative frameworks is the designed ankyrin repeat proteins (DARPins).

A general introduction into designed ankyrin repeat proteins and their successful application for the structure determination of diverse proteins is reviewed in the following publication.

2.2 References

1. Byrne, B. and S. Iwata, *Membrane protein complexes.* Curr Opin Struct Biol, 2002. 12(2): p. 239-43.

2. Kovari, L.C., C. Momany, and M.G. Rossmann, *The use of antibody fragments for crystallization and structure determinations.* Structure, 1995. 3(12): p. 1291-3.

3. Ostermeier, C. and H. Michel, *Crystallization of membrane proteins.* Curr Opin Struct Biol, 1997. 7(5): p. 697-701.

2.3

CHAPERONE-ASSISTED CRYSTALLOGRAPHY WITH DARPINS

GABY SENNHAUSER & MARKUS G. GRÜTTER

SUBMITTED.

Chaperone-assisted Crystallography with DARPins

Gaby Sennhauser[1] and Markus G. Grütter[1]*

[1]Department of Biochemistry, University of Zurich, CH-8057 Zurich, Switzerland

*To whom correspondence should be addressed. E-mail: gruetter@bioc.uzh.ch

The structure of proteins that are difficult to crystallize can often be solved by forming a noncovalent complex with a helper protein – a crystallization "chaperone". Although several such applications have been described to date, their handling usually is still very laborious. A valuable addition to the present repertoire of binding proteins is the recently developed designed ankyrin repeat protein (DARPin) technology. DARPins are built based on the natural ankyrin repeat protein fold with randomized surface residue positions allowing specific binding to virtually any target protein. The broad potential of these binding proteins for X-ray crystallography is illustrated by five cocrystal structures that have been determined recently comprising target proteins from distinct families, namely a sugar binding protein, two kinases, a caspase, and a membrane protein. This article reviews the opportunities of this technology for structural biology and the structural aspects of the DARPin-protein complexes.

Despite the continuous technical advances in protein crystallography due to the worldwide effort in structural genomics programs that promote the application of automated procedures in cloning, expression, purification, crystallization, data collection using synchrotron radiation and computational crystallography, the determination of some protein structures still remains a difficult task. Today, the main limitation is the growth of well-diffracting crystals - a pure

trial-and-error process – because the formation of protein crystals depends on several unpredictable variables. In particular, advances in microscaling methodology involving pipetting robots and automated imaging of individual experiments have allowed high throughput approaches boosting the field. However, even with these advances, many proteins resist forming suitable crystals on their own because of inherent structural flexibility and instability. Consequently, conformation stabilizing methods that help to crystallize proteins seem attractive.

Approaches in this direction are removal or mutation of surface residues known to be flexible (Lawson et al., 1991), the trimming of the protein's often flexible N- and C-terminal ends, or the analysis of stable domains of larger multi-domain proteins (Derewenda, 2004). Another successful approach to promote the crystallization of a particular protein has been the addition of a conformation-stabilizing ligand. Current crystallization tools include the building of complexes with diverse known natural or synthetic ligands, such as substrates, inhibitors, nucleic acid, cofactors, or protein ligands. The benefits of such noncovalent complexes can be manifold. A specific conformation of the target protein may be stabilized in such a complex. This increases the chances to obtain crystals of proteins that otherwise adopt several conformations and therefore resist forming crystals. In addition, novel surfaces can potentially provide better crystal contacts. Especially for membrane proteins, protein ligands also increase the hydrophilic surface area of an otherwise small non-transmembrane region. This strategy for the crystallization of membrane proteins has repeatedly led to successful structure determinations, as seen for many antibody fragment-membrane protein complexes (Dutzler et al., 2003; Hunte et al., 2000; Iwata et al., 1995; Zhou et al., 2001). Cocrystallization of a target protein in complex with a proteinaceous ligand of known structure potentially provides another advantage, namely the structure solution by molecular replacement allowing to avoid the often time-consuming determination of phases via heavy atoms as in single/multiple anomalous dispersion or multiple isomorphous replacement (MIR) techniques.

DNA and RNA binding proteins are often cocrystallized with their natural binding partner, fragments of DNA or RNA stabilizing the conformation of the protein (Anderson et al., 1984). In many cases however, the protein of interest lacks a natural binding partner, the natural binding partner might not be known or it might not be available for other reasons. Therefore, proteinaceous ligands, either natural or synthetic, have received a great deal of attention in the field of structural biology. Antibody and fragments thereof are the most successful molecules to be used as high-affinity and specific binding proteins in biomedical research and have not only been used as a binding protein but also assist in crystallization (Amit et al., 1986). In 1995, Ostermeier et al. selected monoclonal antibodies for the first time against a membrane protein, namely cytochrome c oxidase of *Paracoccus denitrificans*, finally allowing the successful structure determination of the oxidase in complex with a Fv fragment (Iwata et al., 1995; Ostermeier et al., 1995). In addition to the well-known Fab and Fv fragments, single-chain antibody domains such as camelid VHH fragments or scFvs led to successful structure determinations (Desmyter et al., 1996; Kortt et al., 1994). Recently, several studies using nonantibody scaffolds such as affibodies (Hogbom et al., 2003; Wahlberg et al., 2003), monobodies (Koide et al., 2007), and repeat proteins (Binz et al., 2004) have shown that these molecules are potential alternatives to antibody fragments in structural biology. These binding molecules were developed as tools for basic research, but their potential use in commercial applications (as specific reagents in biomedical research and as potential therapeutic molecules) was immediately apparent and quickly recognized (Gill and Damle, 2006). Many novel binding proteins have improved on the limitations of antibodies, in particular their rather low production yield and intrinsic stability. Simultaneously, they retain the beneficial properties of antibodies, namely specific and tight binding. Structural biologists likewise have a great interest in using these molecules as chaperones in crystallization.

In this review, we focus on one scaffold, the DARPins. The potential of DARPins as promising compounds in drug discovery and drug development has been reviewed recently (Stumpp and Amstutz, 2007). We examine the five recently determined X-ray structures of DARPin complexes and address several questions concerning DARPin-target interactions. The diversity of the successfully chosen antigens is paralleled by the diversity of the interaction partners of natural ankyrin repeat proteins, which indicates that the technology can be generally applied to a very broad range of target molecules.

Drawbacks of antibodies

The main advantage of antibodies is their ability to recognize a wide range of target molecules with high affinity and specificity. Besides proteins, antibodies can bind compounds such as peptides, sugars and small molecules. However, natural antibodies are complex multidomain molecules not well suited for cocrystallization due to their flexible linker regions between domains and their bivalent character. Therefore, only antibody fragments have been applied for cocrystallization purposes. Fab or Fv fragments contain the complete antigen recognition sites and are therefore sufficient to retain the specific antibody-antigen interaction. Nevertheless, these fragments often derive from monoclonal antibodies, and their classical production by hybridoma technology is time-consuming, expensive, and based on the use of living organisms. The selection using recombinant and synthetic libraries have facilitated their generation (Rothe et al., 2008) and let to successful structure determinations (Fellouse et al., 2007; Fellouse et al., 2005; Fellouse et al., 2004; Ye et al., 2008) but the complicated multidomain molecular architecture with disulfide bonds still complicates their handling, limits their use in reducing environments and requires special production precautions in bacterial expression systems such as expression in the periplasm to guarantee the correct disulfide bond formation. This often affects the production yield since the volume of the periplasm is limited. Despite these difficulties there are numerous structures in complex with

soluble target proteins (Bentley, 1996) as well as more demanding membrane proteins (Hunte and Michel, 2002) but the problems associated with all antibody-derived crystallization chaperones inspire continuously to search for alternative binding proteins with similar binding capabilities but superior properties regarding structure, stability and throughput.

What are DARPins?

DARPins are derived from the ankyrin repeat motif present in numerous naturally occurring proteins. In nature, ankyrin repeat containing proteins are involved in a wide variety of biological activities and are present in all three superkingdoms (Bork, 1993). Best documented is their involvement in specific protein-protein interactions. The diversity of their roles in a cellular context is further reflected in their localization, which can be the nucleus, cytoplasm and the extracellular space, where these proteins interact with a large diversity of partners. The number of repeats presented in a single ankyrin repeat protein and thus involved in binding is highly variable so that ankyrin domains can bind to host target molecules that vary considerably in size and shape.

The 33-residue sequence motif of an ankyrin repeat forms a well-defined architecture, consisting of a β-turn, followed by a pair of antiparallel α-helices and a loop that builds the connection to the next repeat (**Figure 1A**). The characteristic secondary structure components fold into an L-shaped conformation where the helices form the stem and the loop projects outward at an angle of about 90°. Not uncommon are insertions between or within repeats, mainly in the β-turn/loop region (Sedgwick and Smerdon, 1999). These insertions can be either a short helical segment or more complex motifs. The fully assembled ankyrin domain is elongated and slightly curved, manifested particularly in high repeat number ankyrin repeat proteins (**Figure 1B**). In naturally occurring complexes involving ankyrin repeat proteins, the concave surface, formed by the β-turn and the first α-helix, is commonly involved in binding the target molecules as shown by the X-ray structures determined to date: $p16^{INK4a}$-CDK6

(Russo et al., 1998), $p19^{INK4d}$-CDK6 (Brotherton et al., 1998; Russo et al., 1998), GABPα-GABPβ-DNA (Batchelor et al., 1998), IκBα-NFκB (Huxford et al., 1998; Jacobs and Harrison, 1998; Malek et al., 2003), $p18^{INK4c}$-CDK6 (Jeffrey et al., 2000), CSL-Notch-Mastermind (Wilson and Kovall, 2006), Nas6-Rpt3 (Nakamura et al., 2007b), Gankyrin-S6 (Nakamura et al., 2007a).

Recently, Plückthun and coworkers have chosen the traits of ankyrin repeat proteins for consensus-based protein library design (Binz et al., 2003). Heeding the lessons of nature, they created DNA libraries that encode DARPins consisting of different numbers of repeat modules and special capping repeats attached to the N and C termini of the protein (**Figure 1B**). Therefore, the molecules are termed NxC, where x indicates the number of ankyrin repeat modules. The consensus-designed idealized repeat module consists of conserved residues essential for the formation and stabilization of the repeat module itself and the interrepeat stacking interactions. These positions are invariant and build the framework of the individual repeats. In addition, positions not contributing to the structural integrity of the basic fold were defined to be adaptive surface residues (**Figure 1A**). These residues are positioned at the typical interface region of the natural ankyrin repeat, namely the tip of the β-turn and along the exposed surface of the first α-helix (**Figure 1C**). At these positions, the introduced diversification allows any amino acid except proline and glycine (structurally unfavorable) and cysteine (could form unwanted disulfide bonds). This design resulted in a virtually unlimited repertoire of molecular surfaces.

Selection process

Rapid and easy production is a prerequisite for alternative scaffolds suitable for co-crystallization. Repeat protein libraries (Binz et al., 2004; Binz et al., 2003) can be selected using powerful library selection technologies such as ribosome display (RD) (Hanes and Plückthun, 1997) or phage display (Smith, 1985), finally yielding specific binders to the target

protein. RD is a complete in vitro technology based on in vitro translation in which noncovalent ternary complexes consisting of mRNA, ribosome, and nascent protein chain are formed. These ternary complexes can then be tested for binding to a particular target protein. This system thereby guarantees the coupling of the genotype (mRNA) to the phenotype (protein) and allows immediate access to the genetic information of the binders. To achieve this, the coding sequence of the protein is genetically fused to a C-terminal spacer, allowing the correct folding of the nascent protein polypeptide chain, and the construct lacks a Stop codon, thus preventing release of the mRNA and the polypeptide from the ribosome. Low temperature and high concentrations of magnesium further stabilize the ternary complexes. The disassembly of the complexes results from depletion of magnesium, and the DNA is recovered via reverse transcription. RD is particularly well suited for large libraries, because no transformation steps limit the applicable library size. Furthermore, as a cell-free system, it enables the selection of cytotoxic proteins or of proteins with limited in vivo stability.

All the DARPin binders presented here were isolated from an N3C library and were selected by RD. DARPin binders could also be successfully selected from an N2C library, but these did not yield crystals. Ankyrin repeat proteins consisting of four to five repeats in total are very abundant in nature (Bork, 1993) and also many of the solved natural ankyrin repeat structures in complex with their target display such repeat numbers. The target proteins chosen here were all recombinantly expressed, purified, and either in vivo biotinylated at a specific lysine in the AviTag sequence (MBP, APH, and Caspase-2), in vitro biotinylated at diverse lysines on the surface (AcrB) or GST-tagged (Plk-1) for immobilization. Within a few RD cycles (usually 3 to 4), it was possible to enrich the resulting residual library with proteins that specifically and with high affinity bind to the target.

A subset of the DARPins obtained by RD was then tested individually for binding using approaches suitable for the particular target protein or the intended use of the binder. For MBP (Binz et al., 2004) and Plk-1 (Bandeiras et al., 2008), a standard ELISA was applied to

identify a high-affinity binder. In the case of caspase-2, an in vitro enzymatic activity test combined with a standard ELISA yielded an inhibitor (Schweizer et al., 2007). For APH (Amstutz et al., 2005; Kohl et al., 2005) and AcrB (Sennhauser et al., 2007), an in vivo assay was applied in which the inhibition of the target protein through the DARPins resulted in hypersusceptibility of the bacteria. Normally, the DNA of around 20 DARPins obtained from these assays was sequenced per target. The pools often seemed already quite enriched, revealing groups with similar sequences, although identical sequences were rarely observed. Depending on the sequence variability, five to ten complexes were then purified (yields between 50 and 200 mg/l), characterized, and subjected to crystallization.

Structures of DARPins in complex with different antigens

Maltose-binding protein: proof of principle

As a model protein for the approach of selecting a specific DARPin protein by RD, the maltose-binding protein from *Escherichia coli* was chosen and represents the first successful example for the selection and crystallization of a particular target protein in complex with a DARPin. The structure of the complex was determined at 2.3 Å resolution and the phases for this structure could be determined using a known structure of an unselected DARPin previously solved (Kohl et al., 2003). This was possible because the size of the DARPin (~18 kDa) relative to the size of maltose-binding protein (~43 kDa) was appropriate and there was only one complex in the asymmetric unit. Off7 binds the open form of MBP not involving the sugar-binding cleft but binding three helices at one side of the elongated MBP (**Figure 2A**). Four lysines forming a positive surface patch which account for 60 % of the buried surface area of MBP upon complexation interact closely with off7 (**Figure 3A**).

This first structure showed that the interface between the selected DARPin off7 and MBP indeed involves primarily residues from all three randomized repeat modules with the randomized repeat module 2 contributing most to the binding (**Figure 4A**). The two capping

repeats are not involved in the interaction. The binding interface is comparable to the lower limit of natural protein-protein interactions (Jones and Thornton, 1996) (**Table 1**) and is formed by the concave surface of off7 and a convex surface of MBP. It involves mainly amino acids at the randomized positions. Off7 contains three framework mutations, of which one (H125Y) is involved in MBP binding. The interface on the DARPin is further characterized by seven aromatic residues, four of these tyrosines, which account for 72% of the buried surface area of off7 upon complexation.

Aminoglycoside phosphotransferase (3')-IIIa: the first inhibiting DARPin

The bacterial kinase aminoglycoside phosphotransferase (3')-IIIa (APH) mediates antibiotic resistance to many pathogenic bacteria and is structurally homologous to eukaryotic protein kinases. A highly affine and potent intracellular kinase inhibitory DARPin, named 3a, was selected (Amstutz et al., 2005) and the structure of APH/3a with bound ADP was determined at a resolution of 2.15 Å with two heterodimeric complexes in the asymmetric unit. The DARPin binds to two helical segments in the C-terminal lobe of APH (**Figure 2B** and **3B**).

On the DARPin surface, the interaction residues are located mainly on the N-terminal capping repeat, on repeat modules 1 and 2, and, to a lesser extend, on module 3 (**Figure 4A**). As for MBP/off7 there are no interactions involving the C-terminal capping repeat, and as a consequence there was only weak density visible for this part of the molecule, indicating flexibility.

Whereas the structure of the DARPin is not affected by the binding (**Figure 4B**), 3a binds to the two helices A and B in the α-helical C-terminal lobe of APH, thereby stabilizing helix D in a conformation unable to bind substrate (**Figure 5A**). In addition, the aminoglycoside positioning loop connecting helices A and B is disordered. The structure of the C-terminal lobe of the complex differs significantly from the structure of APH alone. This affects in particular the C-terminal amino acid Phe264 of helix D which is critically involved in

substrate binding as revealed by the kanamycin A bound APH structure (Hon et al., 1997). In the DARPin complex, this interaction is distorted, and thus the enzyme is unable to bind the antibiotic.

Polo-like kinase-1: an arduously crystallizable target

The Ser/Thr protein kinase polo-like kinase-1 (Plk-1) is a key regulator of mitosis and is a well-validated drug target in cancer therapy. Crystallization attempts for various constructs of the wild-type kinase domain of Plk-1 using a multi-parallel cloning and expression approach have failed in the past. Therefore, binders from a DARPin library selective for Plk-1 have been generated and have been used in cocrystallization trials. In this way, the first structure of wild-type apo Plk-1 could be determined in complex with the DARPin 3H10 at 2.3 Å resolution with two complexes in the asymmetric unit. The DARPin binds to the C-terminal lobe of the kinase directly below the ATP binding site (**Figure 2C**). The binding epitope recognized by DARPin 3H10 is especially rich in Arg, Lys and Glu residues (66% of the buried surface area) enabling crystallization by masking a surface patch of Plk-1 that is unfavourable for forming crystal contacts similar to the surface residue mutation method (**Figure 3C**). Such residues have high conformational freedom and are considered counterproductive for crystal contact formation due to a loss of entropy (Derewenda and Vekilov, 2006). As revealed by isothermal calorimetry measurements, the overall interaction is endothermic and apparently driven by entropy alone.

The three repeat modules are solely responsible for the interaction, and again there are mainly residues at the randomized positions involved (**Figure 4A**). The N-terminal capping repeat is not involved in binding. Interestingly, the C-terminal capping repeat is fully disordered in the structure either due to the binding of the kinase or due to clashings with the noncrystallographic symmetry-related DARPin during crystal formation.

Caspase-2: the first specific Caspase-2 inhibitor

Caspases are key molecules in the signaling of apoptosis and inflammation. The DARPin F8 was found to inhibit caspase-2 with a subnanomolar inhibition constant. In addition, testing inhibition against other caspases showed that F8 was highly specific exclusively for caspase-2. The structure of the caspase-2/F8 complex at 3.24 Å resolution revealed the molecular basis for the specificity as well as the allosteric mechanism of inhibition which was also verified by kinetic analysis. The asymmetric unit contained three caspase-2 dimers with two bound DARPins each (**Figure 2D**). The main contact surface of caspase-2 is formed by the 381 loop, involving diverse residues (**Figure 3D**). Minor interactions involve the N-terminus of the other β-subunit of the caspase. Regarding F8, all three repeat modules and one framework residue in the N-terminal capping repeat are forming the interface on F8 (**Figure 4A**).

The 381 loop forms one side of the active site cleft (**Figure 5B**). The conformation of this loop is slightly shifted when compared to the caspase-2/peptide inhibitor structure (Schweizer et al., 2003), resulting in an opening of the active site cleft. Additional rearrangements in the surrounding of the active site cleft and the side chain of Tyr79 of F8 occupying partly the substrate subpocket S5 of caspase-2 are the main reasons for the inhibitory property of F8. The caspase-2/F8 complex shows that the allosteric inhibition of caspase-2 is extremely specific, which has significant advantages over orthosteric ligands which often lack specificity.

AcrB: the first integral membrane protein in complex with a DARPin

The multidrug exporter AcrB, the inner membrane component of the AcrAB-TolC drug efflux system in *Escherichia coli* is the major system contributing to efflux-caused drug resistance in this organism. This protein actively detoxifies the intracellular space by exporting drugs to the cell exterior while importing protons. To explain the molecular mechanism of this process, the

availability of high-resolution structural information is a prerequisite. For this, and to show the applicability of the DARPin combinatorial libraries and of the ribosome display selection method to membrane proteins, AcrB was chosen as model system. Although AcrB can be crystallized on its own due to its large periplasmic domain protruding from the lipid bilayer, the crystals of the AcrB/110819 complex diffracted to 2.54 Å resolution, substantially better than all the previously published crystals of AcrB alone (Murakami et al., 2002). In the structure, the DARPin binds to the periplasmic part of AcrB and due to the distinctly different conformations of the subunits only two DARPins bind to the trimeric protein (**Figure 2E**). The epitope on AcrB is mainly formed by a β-sheet connecting the pore domain with the TolC docking domain, which are subdomains of the periplasmic portion of the protein (**Figure 3E**). An additional interaction is formed involving a helical segment and a β-strand of the adjacent preceding subunit of AcrB via hydrophobic interactions and two hydrogen bonds. All five repeats (including both capping repeats) of the DARPin are involved in the interaction (**Figure 4A**). Comprising around 1100 $Å^2$ buried surface area on both the DARPin and AcrB, and 68 residues in total, this complex showed the largest buried surface area for a DARPin complex so far (**Table 1**).

Interestingly, the structure revealed a new conformation of the molecule where the three subunits of AcrB were locked in different conformations, revealing distinct channels in each subunit. Furthermore, the structure indicated how in the protein the coupling between the channel access, exit, and the putative proton translocation site is achieved. It suggests a transport pathway through the identified channels in the individual subunits by a rotary mechanism. At the same time, this new conformation was also observed without a bound DARPin by two individual groups (Murakami et al., 2006; Seeger et al., 2006). In further studies, DARPin 110819 also allowed the crystallization of otherwise uncrystallizable mutants (K.M. Pos, unpublished data).

General properties of DARPin-target interfaces

The structural properties forming the surface of the target proteins recognized by DARPins vary from complex to complex (**Figure 2**). A common trait between the different interfaces, however, is the overall curvature of the target protein interface area enclosed by DARPins. This curvature is complementary to the curvature of the randomized surface area of the DARPin. Furthermore, all three internal randomized repeat modules are involved in the interaction in all five complexes (**Figure 4A**). As set out in the design, the predominant interaction is mediated by residues in the randomized positions (**Figure 4C**); this is then also the reason for the high specificity of the selected molecules. Interestingly, the last residue of the individual repeat module, namely randomized position 33, is not involved in any interface. In contrast, position 3 is heavily buried in most of the repeat modules. In all complexes, framework residues also participate in the interaction with the target protein. In the case of the MBP and AcrB binders, there is a mutated framework position H125Y and D155N, respectively, contributing to the interaction. Such framework mutations can be explained as a result of the numerous PCR cycles the DARPin-encoding DNA passes during the selection process.

The involvement of the capping repeats in the interaction differs greatly between the different complexes. Whereas the N-terminal capping repeat is well ordered in all structures and involved in binding in the APH, caspase-2 and AcrB complexes, the C-terminal capping repeat is fully disordered in the Plk-1 complex and partially disordered in the APH and caspase-2 complex. It is solely involved in the AcrB/110819 complex, where 7 residues of the C-terminal capping repeat are participating in the interface. In having the first interacting residue at position 13 and the last at position 157, the full width of the 169 amino acid residue DARPin is used in this complex. This provides the most extensive interaction described to date.

The structures discussed here show that DARPins are not restricted to recognize any specific amino acid sequence or structure on the target. In all cases, the DARPins recognize native, nonlinear epitopes (**Figure 3**). There is no particular chemical character found neither for the epitopes (target interface) nor for the paratopes (DARPin interface). There are numerous aromatic residues on the paratopes, but they seem to be less preferred than in antibody paratopes (Padlan, 1990). An exception is the MBP-off7 complex where the aromatic residues account for 72% of the buried surface area of the DARPin. The proportion of aromatic residues in the epitopes is low, a fact that has been observed in antibody-antigen interactions as well (Davies and Cohen, 1996). Furthermore, charged residues seem to be important for the interaction, accounting for nearly half of the contact residues of the epitopes. Whereas all DARPins described here are composed of five repeat modules, the total interface sizes on the target molecules differ widely. The MBP/off7 complex presents by far the smallest interface, comprising 40 residues and a combined buried surface area of only 1264 $Å^2$ (**Table 1**). In contrast, the largest interface observed in the AcrB/110819 complex comprises 63 and 68 residues and buries 1986 and 2328 $Å^2$ of the AcrB surface in the two interfaces formed; all other complex interfaces are in between these values. However, the interfaces show great similarities to naturally occurring ankyrin repeat protein, heterodimeric protein-protein, and antibody-antigen complexes (**Table 1**).

Structural rearrangements in the target proteins and the DARPins

An often raised argument in the field of chaperone-assisted crystallization is that binders might induce a conformational change in the target molecules. Because the crystal structures of all target proteins chosen are available also without a binding partner, it is possible to investigate conformational changes of the targets on DARPin binding. The structures of MBP in the open conformation without a ligand (PDB ID code: 1LLS; (Rubin et al., 2002)) and complexed MBP are very similar, with an overall Cα rmsd below 1 Å. Also, in the case of

AcrB, the structures obtained in 2006 (Murakami et al., 2006; Seeger et al., 2006) are remarkably similar, considering the size of the protein (rmsd for 3110 Cα atoms ~ 1 Å). In addition, the observed asymmetry in the crystal structure could also be detected in solution (Sennhauser et al., 2007). The overall structure of Plk-1 is also very similar to two structures of a mutant solved at the same time, each harboring a different ligand (Kothe et al., 2007), again indicating that there is no binding protein induced conformational change.

The interaction of the DARPin inhibitors with APH and caspase-2 revealed conformations in which the target proteins were inactive. This information is useful for finding novel ways to inhibit the function of an enzyme. The structural rearrangements there are quite considerable. In APH, helices A, B, and D are significantly shifted with respect to kanamycin A bound APH (Hon et al., 1997), and the aminoglycoside positioning loop connecting helices A and B is disordered (**Figure 5A**). In caspase-2, the loops surrounding the active site cleft are altered when compared to the caspase-2/peptide inhibitor structure (Schweizer et al., 2003), resulting in an opening of the active site cleft (**Figure 5B**). Nevertheless, we do not believe that these structural rearrangements are caused by the DARPin, resulting in an induced fit. Recalling the DARPin selection strategy, it is more likely that the DARPins only bind to epitopes as presented by the target proteins in a “lock-and-key” like fashion. In this way, the selected DARPins can bind to proteins not only in their predominant conformation but also can trap the proteins in conformations which are probably present in solution but less populated thus inhibiting an enzyme in an allosteric way.

In all structures, the differences in the DARPin scaffold are minimal upon binding and showed no essential rearrangements of the global fold compared to an unselected DARPin alone (Kohl et al., 2003) (**Figure 4B**). In agreement with the participation of the individual repeats in the interaction, the strongest flexibility can be observed in the C-terminal capping repeat. In the DARPin binding Plk-1, the C-terminal capping repeat cannot even be localized

in the crystal structure. The β-turn regions of the individual repeat modules also show some minor adaptations when bound to a target protein.

DARPin mediated crystal contacts

The potential of DARPins to provide crystal contacts is best described for the MBP/off7 and the AcrB/110819 complex. As shown in **Figure 6A**, in the MBP/off7 complex the lattice interactions involve only DARPin-DARPin and MBP-MBP contacts, which occur within layers, and the direct binding interface between the two interaction partners is the sole contact form between the layers.

In the crystal formed by the AcrB/110819 complex, crystal contacts are mediated by the DARPin in such a way that, in addition to the interaction with the periplasmic domain of its target, the convex side of the DARPin simultaneously forms crystal contacts to the cytoplasmic polar surface of a symmetry-related molecule of AcrB (**Figure 6B**). Because the crystal has the space group $P2_12_12_1$, this contact critically contributes to the stability of the lattice (the mentioned contact occurs in all three dimensions) and thus to the higher diffraction limits of the complex crystal over the crystal formed by AcrB alone.

There are some proteins that could be crystallized only when complexed to a cognate Fab fragment (Laver et al., 1990). A similar case is Plk-1 that alone in its apo-form-a structure most useful for drug design-did not crystallize. In complex with the DARPin 3H10, however, Plk-1 did crystallize. Surprisingly, the DARPin makes direct crystal contacts to the other DARPin in the asymmetric unit via the third repeat module as the C-terminal capping repeat is fully disordered (**Figure 6C**).

It is worth mentioning that cocrystallization with a DARPin clearly was advantageous in the cases of AcrB and Plk-1, whereas the opposite was true for caspase-2. Here, the diffraction quality of the DARPin complex was clearly worse (3.24 Å) than caspase-2 in complex with a

peptide inhibitor (1.65 Å) (Schweizer et al., 2003). DARPins containing different numbers of internal repeats might be selected to obtain better diffracting crystals.

Conclusions

We have reviewed the recent results using DARPins as crystallization tools to crystallize difficult target proteins to understand the natural and alternative conformations of these proteins. DARPins are a class of designed binding molecules that represent a very promising alternative to antibodies. They retain the affinity and specificity of antibodies but are far more stable, and their simple architecture allows high-yield bacterial production. Their use in biomedical and biotechnological research is considerably more advantageous over antibodies. High-affinity DARPins to a given target can rapidly be selected from very large libraries within a few weeks. The use of in vitro selection systems such as phage or ribosome display represents an advantage over the traditional production of monoclonal antibodies in test animals, as the binders are selected to a native protein under defined buffer conditions. Therefore, the in vitro display techniques guarantee that surface epitopes of the presented target protein are selected. The use in structural biology is obvious from the structures described here, and not only enables crystallization of soluble and membrane proteins but also reveals conformations of the target proteins that otherwise are not detected when inhibitors are selected. In the cases of DARPin inhibitors of caspase-2 and APH, the crystals of the complex did not diffract better; rather, the diffraction was rather worse than of crystals of the target proteins with small molecule compounds bound to the active site. However, in both cases a conformation of the target protein was revealed in which the protein is inactive. This information is useful for finding new ways to modulate target protein function.

To expand the applicability of the technology in protein crystallography, heavy atom sites can be engineered into the capping repeats. Crystals of target proteins with a heavy atom-loaded DARPin is a great help in phasing using the single anomalous dispersion method. This has

already been successfully applied using a DARPin-MBP complex crystal (A. Plückthun and M.G. Grütter, unpublished data).

In conclusion, DARPins have the potential to (1) provide crystals of a target protein that is difficult to crystallize, (2) provide better diffracting crystals of the complex when the target protein alone only poorly diffracts, (3) provide initial phases for molecular replacement in cases where the DARPin and the target protein are not too different in size, (4) provide phases by single anomalous dispersion for complexes formed with heavy atom loaded DARPins, and (5) reveal new insight into the function of a target protein by stabilizing a conformation that in solution is less populated.

Acknowledgements

Support from the Swiss National Science Foundation in the framework of the National Center of Competence in Research Structural Biology is acknowledged. We would like to thank Patrick Amstutz for critical reading of the manuscript.

References

Amit, A.G., Mariuzza, R.A., Phillips, S.E., and Poljak, R.J. (1986). Three-dimensional structure of an antigen-antibody complex at 2.8 A resolution. Science (New York, N.Y 233, 747-753.

Amstutz, P., Binz, H.K., Parizek, P., Stumpp, M.T., Kohl, A., Grütter, M.G., Forrer, P., and Plückthun, A. (2005). Intracellular kinase inhibitors selected from combinatorial libraries of designed ankyrin repeat proteins. The Journal of biological chemistry 280, 24715-24722.

Anderson, J., Ptashne, M., and Harrison, S.C. (1984). Cocrystals of the DNA-binding domain of phage 434 repressor and a synthetic phage 434 operator. Proceedings of the National Academy of Sciences of the United States of America 81, 1307-1311.

Bandeiras, T.M., Hillig, R.C., Matias, P.M., Eberspaecher, U., Fanghanel, J., Thomaz, M., Miranda, S., Crusius, K., Putter, V., Amstutz, P., et al. (2008). Structure of wild-type Plk-1 kinase domain in complex with a selective DARPin. Acta crystallographica 64, 339-353.

Batchelor, A.H., Piper, D.E., de la Brousse, F.C., McKnight, S.L., and Wolberger, C. (1998). The structure of GABPalpha/beta: an ETS domain- ankyrin repeat heterodimer bound to DNA. Science (New York, N.Y 279, 1037-1041.

Bentley, G.A. (1996). The crystal structures of complexes formed between lysozyme and antibody fragments. Exs 75, 301-319.

Binz, H.K., Amstutz, P., Kohl, A., Stumpp, M.T., Briand, C., Forrer, P., Grütter, M.G., and Plückthun, A. (2004). High-affinity binders selected from designed ankyrin repeat protein libraries. Nature biotechnology 22, 575-582.

Binz, H.K., Stumpp, M.T., Forrer, P., Amstutz, P., and Plückthun, A. (2003). Designing repeat proteins: well-expressed, soluble and stable proteins from combinatorial libraries of consensus ankyrin repeat proteins. Journal of molecular biology 332, 489-503.

Bork, P. (1993). Hundreds of ankyrin-like repeats in functionally diverse proteins: mobile modules that cross phyla horizontally? Proteins 17, 363-374.

Brotherton, D.H., Dhanaraj, V., Wick, S., Brizuela, L., Domaille, P.J., Volyanik, E., Xu, X., Parisini, E., Smith, B.O., Archer, S.J., et al. (1998). Crystal structure of the complex of the cyclin D-dependent kinase Cdk6 bound to the cell-cycle inhibitor p19INK4d. Nature 395, 244-250.

Davies, D.R., and Cohen, G.H. (1996). Interactions of protein antigens with antibodies. Proceedings of the National Academy of Sciences of the United States of America 93, 7-12.

Derewenda, Z.S. (2004). The use of recombinant methods and molecular engineering in protein crystallization. Methods (San Diego, Calif 34, 354-363.

Derewenda, Z.S., and Vekilov, P.G. (2006). Entropy and surface engineering in protein crystallization. Acta crystallographica 62, 116-124.

Desmyter, A., Transue, T.R., Ghahroudi, M.A., Thi, M.H., Poortmans, F., Hamers, R., Muyldermans, S., and Wyns, L. (1996). Crystal structure of a camel single-domain VH antibody fragment in complex with lysozyme. Nature structural biology 3, 803-811.

Dutzler, R., Campbell, E.B., and MacKinnon, R. (2003). Gating the selectivity filter in ClC chloride channels. Science (New York, N.Y 300, 108-112.

Fellouse, F.A., Esaki, K., Birtalan, S., Raptis, D., Cancasci, V.J., Koide, A., Jhurani, P., Vasser, M., Wiesmann, C., Kossiakoff, A.A., et al. (2007). High-throughput generation of synthetic antibodies from highly functional minimalist phage-displayed libraries. Journal of molecular biology 373, 924-940.

Fellouse, F.A., Li, B., Compaan, D.M., Peden, A.A., Hymowitz, S.G., and Sidhu, S.S. (2005). Molecular recognition by a binary code. Journal of molecular biology 348, 1153-1162.

Fellouse, F.A., Wiesmann, C., and Sidhu, S.S. (2004). Synthetic antibodies from a four-amino-acid code: a dominant role for tyrosine in antigen recognition. Proceedings of the National Academy of Sciences of the United States of America 101, 12467-12472.

Gill, D.S., and Damle, N.K. (2006). Biopharmaceutical drug discovery using novel protein scaffolds. Current opinion in biotechnology 17, 653-658.

Hanes, J., and Plückthun, A. (1997). In vitro selection and evolution of functional proteins by using ribosome display. Proceedings of the National Academy of Sciences of the United States of America 94, 4937-4942.

Hogbom, M., Eklund, M., Nygren, P.A., and Nordlund, P. (2003). Structural basis for recognition by an in vitro evolved affibody. Proceedings of the National Academy of Sciences of the United States of America 100, 3191-3196.

Hon, W.C., McKay, G.A., Thompson, P.R., Sweet, R.M., Yang, D.S., Wright, G.D., and Berghuis, A.M. (1997). Structure of an enzyme required for aminoglycoside antibiotic resistance reveals homology to eukaryotic protein kinases. Cell 89, 887-895.

Hunte, C., Koepke, J., Lange, C., Rossmanith, T., and Michel, H. (2000). Structure at 2.3 A resolution of the cytochrome bc(1) complex from the yeast Saccharomyces cerevisiae co-crystallized with an antibody Fv fragment. Structure 8, 669-684.

Hunte, C., and Michel, H. (2002). Crystallisation of membrane proteins mediated by antibody fragments. Current opinion in structural biology 12, 503-508.

Huxford, T., Huang, D.B., Malek, S., and Ghosh, G. (1998). The crystal structure of the IkappaBalpha/NF-kappaB complex reveals mechanisms of NF-kappaB inactivation. Cell 95, 759-770.

Iwata, S., Ostermeier, C., Ludwig, B., and Michel, H. (1995). Structure at 2.8 A resolution of cytochrome c oxidase from Paracoccus denitrificans. Nature 376, 660-669.

Jacobs, M.D., and Harrison, S.C. (1998). Structure of an IkappaBalpha/NF-kappaB complex. Cell 95, 749-758.

Jeffrey, P.D., Tong, L., and Pavletich, N.P. (2000). Structural basis of inhibition of CDK-cyclin complexes by INK4 inhibitors. Genes & development 14, 3115-3125.

Jones, S., and Thornton, J.M. (1996). Principles of protein-protein interactions. Proceedings of the National Academy of Sciences of the United States of America 93, 13-20.

Kohl, A., Amstutz, P., Parizek, P., Binz, H.K., Briand, C., Capitani, G., Forrer, P., Plückthun, A., and Grütter, M.G. (2005). Allosteric inhibition of aminoglycoside phosphotransferase by a designed ankyrin repeat protein. Structure 13, 1131-1141.

Kohl, A., Binz, H.K., Forrer, P., Stumpp, M.T., Plückthun, A., and Grütter, M.G. (2003). Designed to be stable: crystal structure of a consensus ankyrin repeat protein. Proceedings of the National Academy of Sciences of the United States of America 100, 1700-1705.

Koide, A., Gilbreth, R.N., Esaki, K., Tereshko, V., and Koide, S. (2007). High-affinity single-domain binding proteins with a binary-code interface. Proceedings of the National Academy of Sciences of the United States of America 104, 6632-6637.

Kortt, A.A., Malby, R.L., Caldwell, J.B., Gruen, L.C., Ivancic, N., Lawrence, M.C., Howlett, G.J., Webster, R.G., Hudson, P.J., and Colman, P.M. (1994). Recombinant anti-sialidase single-chain variable fragment antibody. Characterization, formation of dimer and higher-molecular-mass multimers and the solution of the crystal structure of the single-chain variable fragment/sialidase complex. European journal of biochemistry / FEBS 221, 151-157.

Kothe, M., Kohls, D., Low, S., Coli, R., Cheng, A.C., Jacques, S.L., Johnson, T.L., Lewis, C., Loh, C., Nonomiya, J., et al. (2007). Structure of the catalytic domain of human polo-like kinase 1. Biochemistry 46, 5960-5971.

Laver, W.G., Air, G.M., Webster, R.G., and Smith-Gill, S.J. (1990). Epitopes on protein antigens: misconceptions and realities. Cell 61, 553-556.

Lawson, D.M., Artymiuk, P.J., Yewdall, S.J., Smith, J.M., Livingstone, J.C., Treffry, A., Luzzago, A., Levi, S., Arosio, P., Cesareni, G., and et al. (1991). Solving the structure of human H ferritin by genetically engineering intermolecular crystal contacts. Nature 349, 541-544.

Malek, S., Huang, D.B., Huxford, T., Ghosh, S., and Ghosh, G. (2003). X-ray crystal structure of an IkappaBbeta x NF-kappaB p65 homodimer complex. The Journal of biological chemistry 278, 23094-23100.

Murakami, S., Nakashima, R., Yamashita, E., Matsumoto, T., and Yamaguchi, A. (2006). Crystal structures of a multidrug transporter reveal a functionally rotating mechanism. Nature 443, 173-179.

Murakami, S., Nakashima, R., Yamashita, E., and Yamaguchi, A. (2002). Crystal structure of bacterial multidrug efflux transporter AcrB. Nature 419, 587-593.

Nakamura, Y., Nakano, K., Umehara, T., Kimura, M., Hayashizaki, Y., Tanaka, A., Horikoshi, M., Padmanabhan, B., and Yokoyama, S. (2007a). Structure of the oncoprotein gankyrin in complex with S6 ATPase of the 26S proteasome. Structure 15, 179-189.

Nakamura, Y., Umehara, T., Tanaka, A., Horikoshi, M., Padmanabhan, B., and Yokoyama, S. (2007b). Structural basis for the recognition between the regulatory particles Nas6 and Rpt3 of the yeast 26S proteasome. Biochemical and biophysical research communications 359, 503-509.

Ostermeier, C., Iwata, S., Ludwig, B., and Michel, H. (1995). Fv fragment-mediated crystallization of the membrane protein bacterial cytochrome c oxidase. Nature structural biology 2, 842-846.

Padlan, E.A. (1990). On the nature of antibody combining sites: unusual structural features that may confer on these sites an enhanced capacity for binding ligands. Proteins 7, 112-124.

Rothe, C., Urlinger, S., Lohning, C., Prassler, J., Stark, Y., Jager, U., Hubner, B., Bardroff, M., Pradel, I., Boss, M., et al. (2008). The human combinatorial antibody library HuCAL GOLD combines diversification of all six CDRs according to the natural immune system with a novel display method for efficient selection of high-affinity antibodies. Journal of molecular biology 376, 1182-1200.

Rubin, S.M., Lee, S.Y., Ruiz, E.J., Pines, A., and Wemmer, D.E. (2002). Detection and characterization of xenon-binding sites in proteins by 129Xe NMR spectroscopy. Journal of molecular biology 322, 425-440.

Russo, A.A., Tong, L., Lee, J.O., Jeffrey, P.D., and Pavletich, N.P. (1998). Structural basis for inhibition of the cyclin-dependent kinase Cdk6 by the tumour suppressor p16INK4a. Nature 395, 237-243.

Schweizer, A., Briand, C., and Grütter, M.G. (2003). Crystal structure of caspase-2, apical initiator of the intrinsic apoptotic pathway. The Journal of biological chemistry 278, 42441-42447.

Schweizer, A., Roschitzki-Voser, H., Amstutz, P., Briand, C., Gulotti-Georgieva, M., Prenosil, E., Binz, H.K., Capitani, G., Baici, A., Plückthun, A., and Grütter, M.G. (2007). Inhibition of Caspase-2 by a Designed Ankyrin Repeat Protein: Specificity, Structure, and Inhibition Mechanism. Structure 15, 625-636.

Sedgwick, S.G., and Smerdon, S.J. (1999). The ankyrin repeat: a diversity of interactions on a common structural framework. Trends in biochemical sciences 24, 311-316.

Seeger, M.A., Schiefner, A., Eicher, T., Verrey, F., Diederichs, K., and Pos, K.M. (2006). Structural asymmetry of AcrB trimer suggests a peristaltic pump mechanism. Science (New York, N.Y 313, 1295-1298.

Sennhauser, G., Amstutz, P., Briand, C., Storchenegger, O., and Grütter, M.G. (2007). Drug Export Pathway of Multidrug Exporter AcrB Revealed by DARPin Inhibitors. PLoS Biology 5, e7.

Smith, G.P. (1985). Filamentous fusion phage: novel expression vectors that display cloned antigens on the virion surface. Science (New York, N.Y 228, 1315-1317.

Stumpp, M.T., and Amstutz, P. (2007). DARPins: a true alternative to antibodies. Current opinion in drug discovery & development 10, 153-159.

Wahlberg, E., Lendel, C., Helgstrand, M., Allard, P., Dincbas-Renqvist, V., Hedqvist, A., Berglund, H., Nygren, P.A., and Hard, T. (2003). An affibody in complex with a target protein: structure and coupled folding. Proceedings of the National Academy of Sciences of the United States of America 100, 3185-3190.

Wilson, J.J., and Kovall, R.A. (2006). Crystal structure of the CSL-Notch-Mastermind ternary complex bound to DNA. Cell 124, 985-996.

Ye, J.D., Tereshko, V., Frederiksen, J.K., Koide, A., Fellouse, F.A., Sidhu, S.S., Koide, S., Kossiakoff, A.A., and Piccirilli, J.A. (2008). Synthetic antibodies for specific recognition and crystallization of structured RNA. Proceedings of the National Academy of Sciences of the United States of America 105, 82-87.

Zhou, Y., Morais-Cabral, J.H., Kaufman, A., and MacKinnon, R. (2001). Chemistry of ion coordination and hydration revealed by a K+ channel-Fab complex at 2.0 A resolution. Nature 414, 43-48.

Table 1. Structural features of the interfaces of DARPin-protein complexes

Complex	K_D (nM)[b]	Resolution (Å)	N_{res}			Buried surface area (Å^2)			Percentage of total surface area (%)		N_{HB}	N_{SB}
			Target	DARPin	Total	Target	DARPin	Total	Target	DARPin		
1svx												
MBP-off7 (B-A)[a]	4.4	2.3	19	21	40	649	615	1264	4.2	8.1	8	2
2bkk												
APH-3a (A-B)	1.7	2.15	21	27	48	925	850	1775	6.7	10.8	15	8
2v5q												
Plk1-3H10 (A-D)	75	2.3	21	25	46	857	885	1742	6.0	14.3	14	9
2p2c												
C2-F8 (BDA-P)	4.1	3.24	25	26	51	937	885	1822	12.1	10.2	8	9
C2-F8 (DBC-Q)			23	25	48	830	809	1639	10.5	9.7	6	9
2j8s												
AcrB-110819 (BA-D)	28	2.54	35	33	68	1142	1186	2328	2.5	15.3	12	3
AcrB-110819 (AC-E)			32	31	63	969	1017	1986	2.2	13.4	11	2
Antibody-antigen[c]						777 ± 135					8.2 ± 0.7	
Heterodimeric protein-protein complexes[c]						983 ± 582					11.1 ± 2.7	

Analyzed with the Protein Interfaces, Surfaces and Assemblies service PISA. The numbers may be at variance with those found by the original authors owing to different programs used. Only the interface features of one complex are shown when there were several complexes in the asymmetric unit.

[a] Characters in parentheses show the chains participating in the interface as designated in the PDB file (target - DARPin).

[b] Affinities were determined by BIAcore technology. For Plk-1-3H10 a K_D measured by competition ELISA was described.

[c] According to (Jones and Thornton, 1996). The values for N_{HB} were calculated from the tabulated hydrogen bonds/100 Å^2 ΔASA.

N_{res} – number of residues from the specified molecule that take part in the interface; **N_{HB}** – number of potential hydrogen bonds across the interface; **N_{SB}** – number of potential salt bridges across the interface.

Figure 1

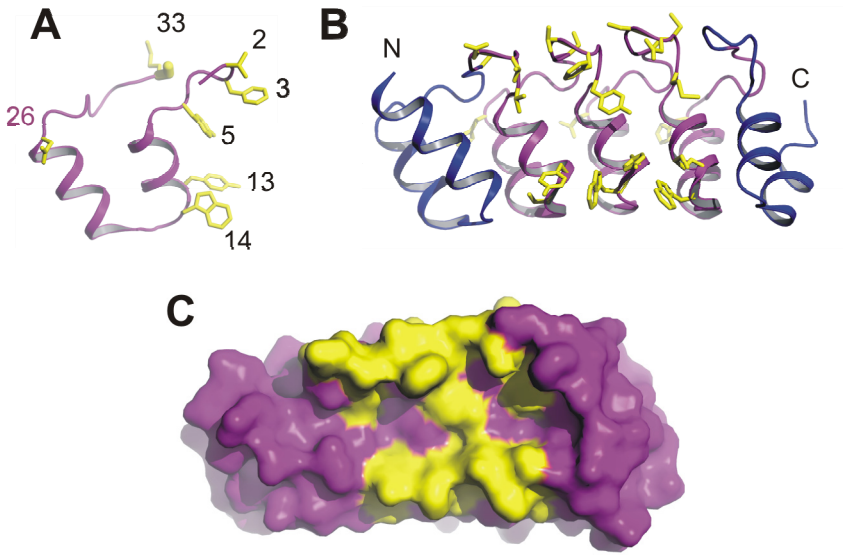

Figure 1. Structure and potential interaction surface of a DARPin

(A) Ribbon representation of a designed ankyrin repeat module. The side chains of the six randomized positions and the randomized framework residue (position 26) are shown as yellow sticks, and their positions within the 33-amino acid conserved framework are labeled. Side chains of the conserved residues are not shown for clarity.
(B) An N3C DARPin library member. The three repeat modules are colored purple; the capping repeats are colored blue. The randomized positions, located mainly in the β-turns and the first α-helices of the individual repeat modules, are shown as yellow sticks.
(C) Randomized potential interaction surface of an N3C DARPin that normally provides the interaction site (in yellow). The orientation is the same as in (B).
All figures were prepared with PyMol (DeLano, 2002).

Figure 2

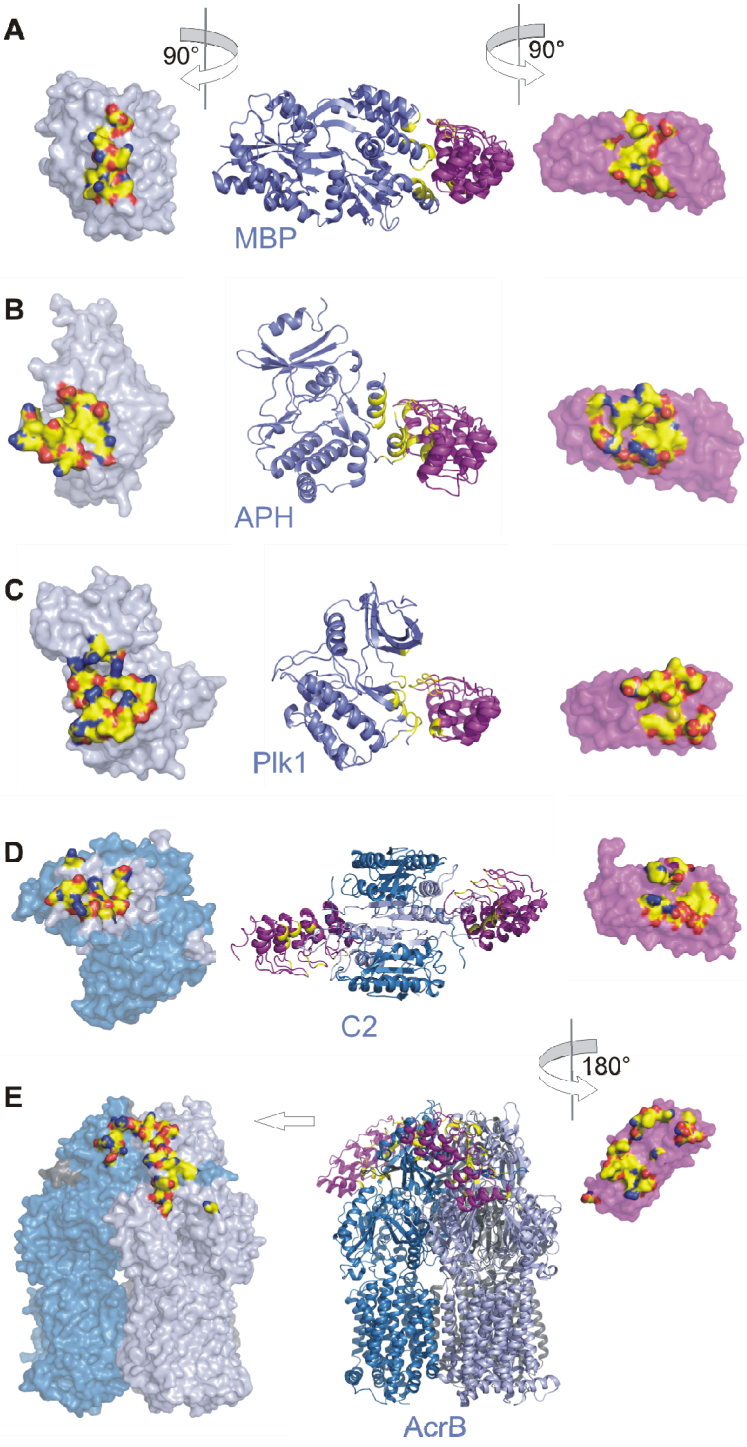

Figure 2. Open book illustrations of the interaction surfaces of DARPins and their respective target molecules

(A)-(D) Center: ribbon diagrams of the X-ray structures of the individual complexes. Target proteins and DARPins are colored blue and purple, respectively. Interfaces are highlighted in yellow. Left: The targets have been rotated clockwise. Right: The DARPins have been rotated counterclockwise. Residues that approach within 4 Å of the interaction partner are colored by element (C, N, and O atoms are colored yellow, blue, and red, respectively).
(A) DARPin off7 in complex with MBP (PDB entry code 1svx).
(B) DARPin 3a in complex with APH (PDB entry code 2bkk).
(C) DARPin 3H10 in complex with Plk-1 (PDB entry code 2v5q).
(D) DARPin F8 in complex with caspase-2 (PDB entry code 2p2c). Caspase-2 is colored dark blue for the α-subunits and light blue for the β-subunits.
(E) DARPin 110819 in complex with AcrB (PDB entry code 2j8s). The AcrB subunits A, B, and C are colored dark blue, light blue, and gray. Left: AcrB has been translated. Right: the DARPin has been rotated counterclockwise. Residues that approach within 4 Å of the DARPin are colored by element.

Figure 3

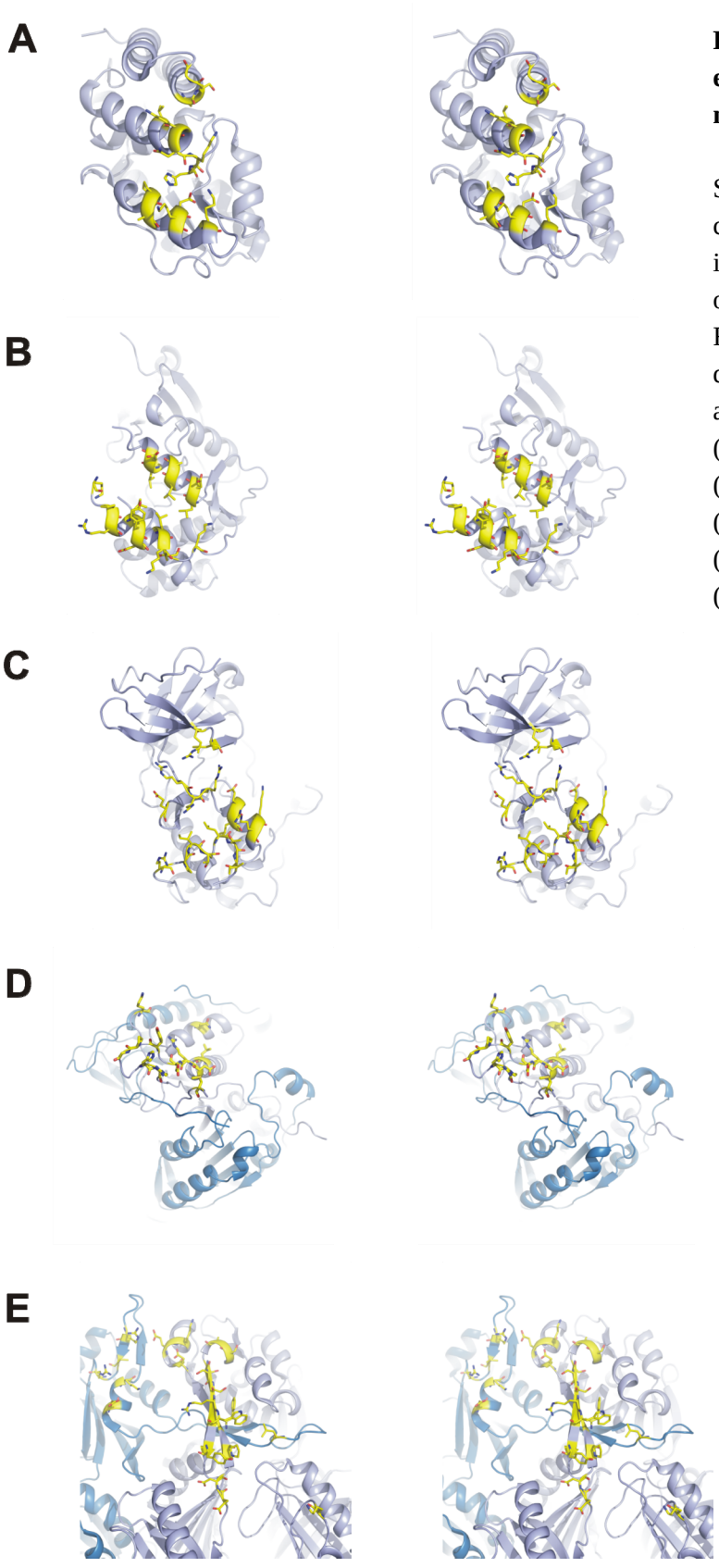

Figure 3. Comparison of the epitopes on the different target molecules

Stereo view of the targets of the complexes. The molecules are shown in ribbon representation in the same orientation as in the left panel of Figure 2. Interfacing residues (4 Å distance cutoff) are shown as sticks and are colored by element.
(A) MBP
(B) APH
(C) Plk-1
(D) Caspase-2
(E) Close-up view of AcrB

Figure 4

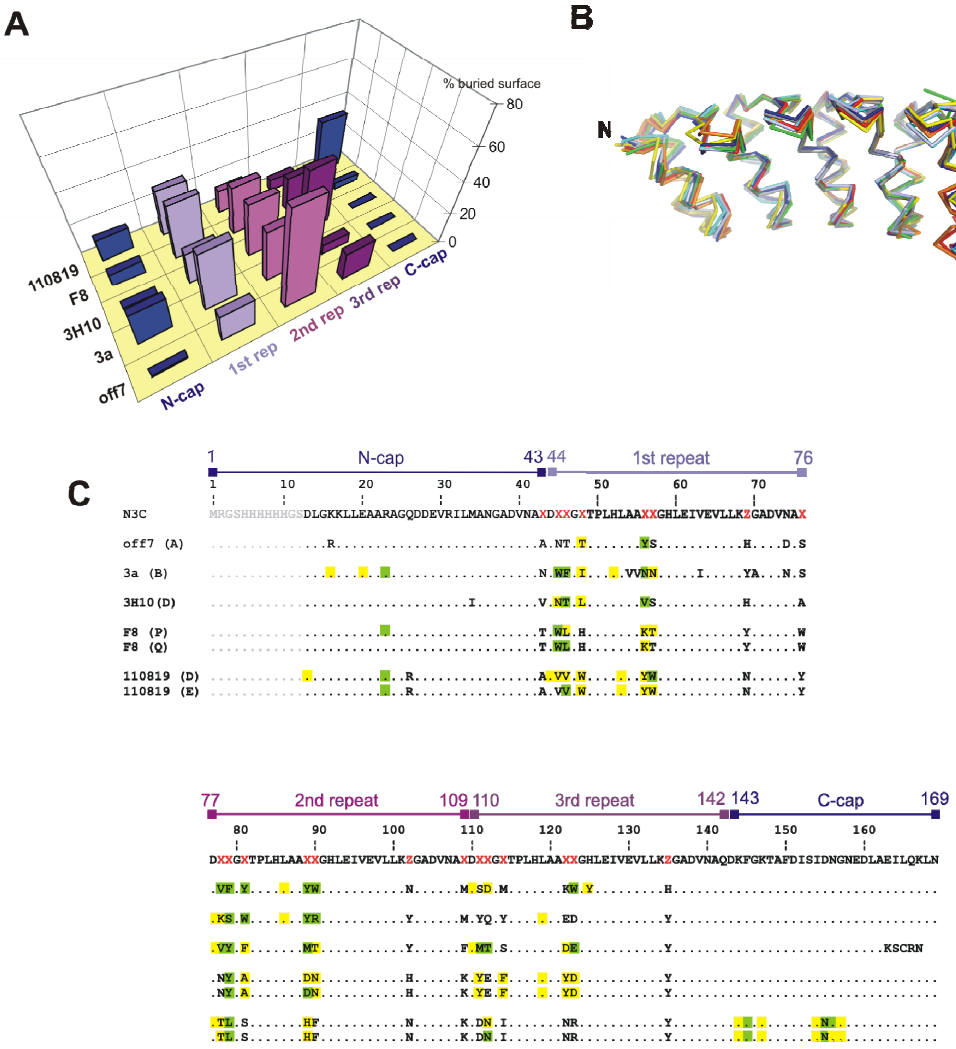

Figure 4. Structural differences between the binding DARPins

(A) Contribution of each repeat to the buried surface area of the paratope.
(B) Structures of the DARPins bound to the diverse target molecules. The Cα atoms of the DARPins were least-squares superimposed using the program coot and are shown in worm representation. The termini are labeled. The DARPins are colored as follows: red, unselected DARPin; orange, off7; yellow, 3a; green, 3H10; cyan and light blue, F8 molecules P and Q; dark blue and gray, 110819 molecules D and E.
(C) Amino acid sequence alignment of the DARPins. Positions marked with X and Z in the consensus represent the randomized positions where in the case of X any amino acid (except Cys, Gly, and Pro) or in the case of Z Asn, His, and Tyr is allowed. Residues marked in yellow and green indicate those involved in binding of the target in the crystal structure (distance < 4 Å; in green: accounts for more than 5% of the total buried surface area upon complex formation).

Figure 5

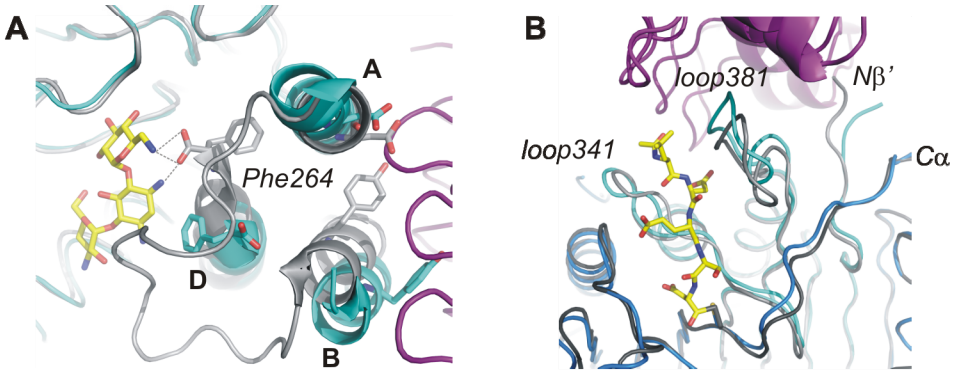

Figure 5. Conformations of the target molecules

(A) Close-up view of the superposition of the DARPin binding region of APH in complex with DARPin inhibitor 3a (blue and purple) and wtAPH (gray). The APH/3a complex displays a distorted drug binding site. The α-helices A and B in the C-terminal lobe of APH interacting with the DARPin are shifted, and the aminoglycoside positioning loop between these two helices is disordered. This rearrangement leads further to a 5- to 7-Å shift of helix D with respect to wtAPH which includes the C-terminal residue Phe264. Kanamycin A bound to wtAPH is shown in yellow, and hydrogen bonds to the mainchain carboxyl group of Phe264 are indicated as dashed lines.
(B) Close-up view of the active-site cleft region of caspase-2. Superimposed caspase-2 bound to Ac-LDESD-CHO (colored in gray and yellow), and to the DARPin F8 (colored in blue and red) is shown. In the DARPin-bound form, the loop 381 and the C-terminal part of the α subunit (Cα), which includes the active site cysteine, are shifted with respect to the peptide bound form.

Figure 6

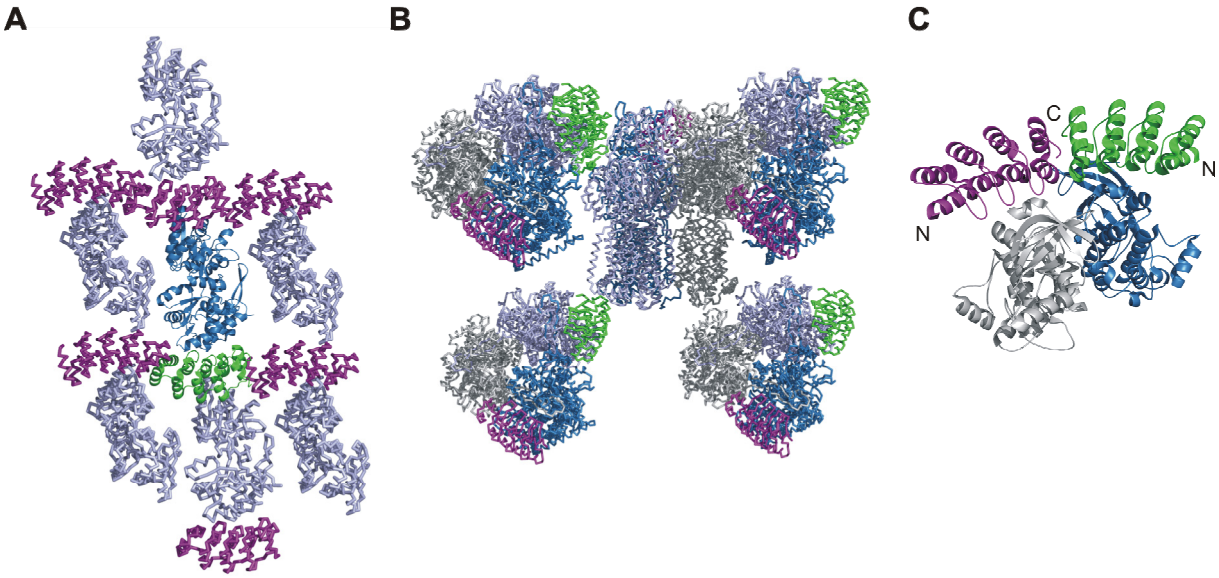

Figure 6. Diverse crystal contacts mediated by DARPins

(A) Crystal packing in the MBP-DARPin complex. The crystals belong to space group $P2_1$. One complex is shown in ribbon representation and colored dark blue (MBP) and green (DARPin). The neighbouring molecules are shown in worm representation in light blue and purple. Crystal contacts are mediated mainly between adjacent DARPin and MBP molecules.
(B) Crystal contacts of AcrB molecules and the DARPin. The crystals belong to space group $P2_12_12_1$. The AcrB subunits A, B, and C are colored dark blue, light blue, and gray, respectively. One of the two DARPins (in green) bound to the periplasmic part of AcrB mediates essential crystal contacts to the cytoplasmic part of a symmetry-related trimer, resulting in a different packing to AcrB crystallized without a DARPin.
(C) Asymmetric unit content of the Plk-1/DARPin crystal. The two complexes are shown in ribbon representation and are colored gray and blue (Plk-1) and purple and green (DARPin). The N- and C-terminal ends are labeled.

CHAPTER 3

MULTIDRUG EFFLUX IN *ESCHERICHIA COLI*: THE ACRAB-TOLC SYSTEM

Multidrug efflux systems are widespread in Gram-negative bacteria, although the contribution of many, if not most, of these to intrinsic or acquired resistance has not been demonstrated. Analysis of the *E. coli* genome has revealed the presence of seven RND-transporters (Table 1) [1]. Six of them have been functionally characterized to participate in multidrug efflux and one RND-transporter, CusA, was shown to confer resistance to copper. AcrF, MdtF and MdtB are not expressed at significant levels and seem therefore not important for the intrinsic resistance of *E. coli* as the knock-out of these did not alter the drug susceptibilities [2]. Interestingly, the overexpression of AcrF could suppress the hypersusceptible phenotype of acrAB mutants [3]. AcrD, although not associated with any gene for an MFP or an OMP, seems to work in complex with AcrA and TolC [4] and plays a role in efflux of aminoglycosides [5]. Nevertheless, as predominant pump in terms of efflux of clinically relevant antibiotics, AcrB is by far the best characterized of all RND transporters to date. An acr mutation on the chromosome that led to a hypersusceptible phenotype was already described in 1965 [6], but it was attributed for a long time to an alteration of the outer membrane permeability of the bacteria. The cloning of the AcrAB locus finally revealed that AcrB actually codes for a transporter [7]. In *E. coli*, AcrB is the major constitutively expressed drug efflux pump and works in a large multicomponent system together with two essential components - the first being the OMP TolC and the second the MFP-family member AcrA.

Table 1: RND efflux pumps of *E. coli*. Adapted from [8].

Efflux system			Substrate(s)	References
Genetic context	RND	OMP		
acrAB	**AcrB**	TolC	AC, BL, BS, CM, CV, EB, FA, FQ, ML, NO, OS, RF, SDS, TX	[7]
acrD	**AcrD**	TolC	AG, DC, FU, NO	[5]
acrEF (envC**D**)	**AcrF**	TolC	AC, BS, FQ, SDS, TX	[9]
mdtABCD (yegM**NO**B)	**MdtBC**	TolC	DC, NO	[10, 11]
yhiU**V**	**MdtF**	TolC	CV, DC, NO, SDS	[12]
cusCFBA (ylcBCD-**ybdE**)	**CusA**	CusC	Copper (silver)	[13]

AC = acriflavine; **AG** = aminoglycosides; **BL** = β-lactams; **BS** = bile salts; **CM** = chloramphenicol; **CV** = crystal violet; **DC** = deoxylcholate; **EB** = ethidium bromide; **FA** = fatty acids; **FQ** = fluoroquinolones; **FU** = fusidic acid; **ML** = macrolides, **NO** = novobiocin; **OS** = organic solvents; **RF** = rifampicin; **SDS** = sodium dodecyl sulfate; **TX** = Triton X-100.

3.1 TolC

TolC is a multifunctional protein, being involved in the translocation of both small drugs and large proteins, including enzymes and toxins such as haemolysin. It achieves these different roles by interacting with diverse transporters such as the RND-transporter AcrB or the ABC-transporter HlyB. The crystal structure of TolC at 2.1 Å resolution revealed a fold never observed before. TolC adopts a trimeric arrangement comprising a pore-like 40 Å β-barrel domain that spans the outer membrane and a 100 Å periplasmic α-helical barrel domain, [14] (Fig. 1A-C). The right-twisted β-barrel domain is composed of 12 β-strands in total. The left-twisted α-helical domain is formed by six pairs of antiparallel α-helices that form six coiled-coils each containing a long (67 residues) and two shorter (23 and 34 residues) helices. A third equatorial mixed α/β domain connecting the shorter helices forms a belt around this helical barrel. The β-barrel is constitutively open to the cell exterior but the coiled helices at the periplasmic end of the α-helical barrel seem to close off the periplasmic entrance. An opening of the channel was proposed based on the small differences in the superhelical twist between the three inner (helices 7 and 8) and three outer (helices 3 and 4) coiled coils (Fig. 1D). It was suggested that an iris-like untwisting of the inner coils with respect to the outer coils could open the channel. In vivo and in vitro mutational experiments supported this hypothesis [15, 16]. Furthermore, the inner and outer coiled coil helices are similar in sequence, suggesting that both coiled-coils can adopt both conformations.

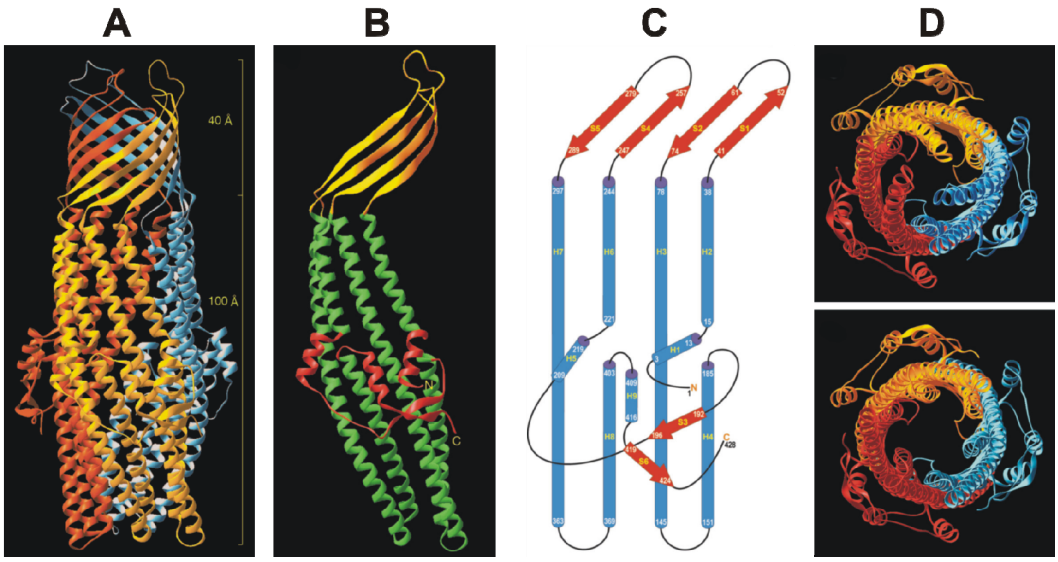

Fig. 1.

3D-Structure of TolC, the OMP of the AcrAB system of *E. coli* (PDB ID code: 1EK9). A The biologically active, trimeric molecule is depicted in a ribbon diagram with the three subunits colored individually. **B** Ribbon diagram of a single subunit. The β-barrel domain is colored in yellow, the α-helical barrel domain in green and the equatorial domain in red. **C** Topology diagram for the TolC monomer. **D** The closed and modelled open states of TolC. Adapted from [14].

3.2 AcrA

The crystal structure of AcrA (residues 45 to 312 of the 397 amino acid residues protein) was solved at 2.7 Å resolution. Similar to the homologous MexA structure (see chapter 4.2) [17], the AcrA structure revealed only the core of the protein, namely residues 53 to 299. The remaining residues were either not in the construct (residues 1 to 25), removed by proteolysis (residues 26 to 44 and 313 to 397) or not visible in the electron density. Furthermore, the AcrA construct contained four methionine substitutions which were constructed for MAD phase determination. This mutant diffracted significantly better than the wildtype protein. The introduction of these 4 methionine residues into the full length AcrA had functional consequences leading to hypersensitivity towards several substrates of the AcrAB-TolC pump while showing a drastic decrease in the expression level.

AcrA displayed a very similar structure as MexA, most likely a consequence of their 62% sequence identities. AcrA is an elongated molecule consisting of three domains: a β-barrel, a lipoyl domain and a coiled-coil α-helical hairpin (Fig. 2). The α-

helical hairpin in AcrA is seven residues longer than in MexA and displays five heptad repeats per helix.

In an attempt to define the biologically relevant oligomeric state of MFPs, the crystal packing was carefully analyzed. In contrast to MexA which crystallized as a tridecamer, AcrA crystallized as a dimer of dimers. The slightly different conformations of the four molecules were interpreted as conformational flexibility of the hinge region at the base of the α-helical hairpin domain, which could have an influence in opening of the OMP.

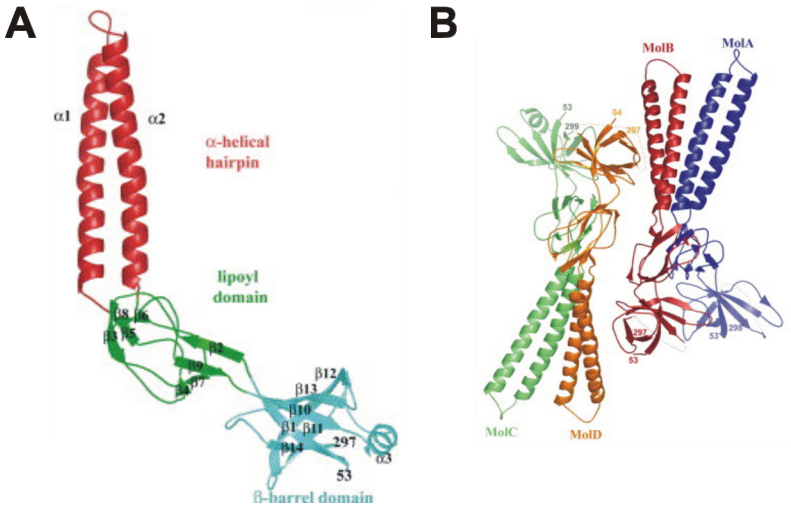

Fig. 2.

3D-Structure of AcrA, the MFP of the AcrAB system of *E. coli* (PDB ID code: 2F1M). A The AcrA monomer is depicted in a ribbon diagram, with the domains colored individually. The last residues visible in the electron density, the three domains and the secondary structures are indicated. **B** The dimer of dimers found in the asymmetric unit of the crystal. Adapted from [17].

3.3 AcrB

The crystal structure of AcrB was first determined in 2002 at 3.5 Å resolution and revealed the general architecture of an RND-transporter (see 1.4). AcrB consists of 1049 amino acids with a molecular mass of around 114 kDa. The structure confirmed many of the predictions regarding the functional unit of the transporter. It adopts a homotrimeric arrangement and comprises a transmembrane domain with 12 membrane-spanning α-helices per subunit and a large periplasmic domain. This

structure was followed by several structures harbouring substrates at diverse proposed binding sites [18, 19] suggesting a drug translocation pathway through the central region of the protein.

However, a convincing model for the transport mechanism and the multidrug binding capacity of this transporter was not provided by any of these studies. Therefore we attempted to determine the structure of AcrB in complex with a selected DARPin to higher resolution which should provide new insight into the transport mechanism of AcrB, and presumably other members of the RND-transporter family.

3.4 References

1. Nishino, K. and A. Yamaguchi, *Analysis of a complete library of putative drug transporter genes in Escherichia coli.* J Bacteriol, 2001. 183(20): p. 5803-12.

2. Sulavik, M.C., et al., *Antibiotic susceptibility profiles of Escherichia coli strains lacking multidrug efflux pump genes.* Antimicrob Agents Chemother, 2001. 45(4): p. 1126-36.

3. Nikaido, H., *Multidrug efflux pumps of gram-negative bacteria.* J Bacteriol, 1996. 178(20): p. 5853-9.

4. Elkins, C.A. and H. Nikaido, *Substrate specificity of the RND-type multidrug efflux pumps AcrB and AcrD of Escherichia coli is determined predominantly by two large periplasmic loops.* J Bacteriol, 2002. 184(23): p. 6490-8.

5. Rosenberg, E.Y., D. Ma, and H. Nikaido, *AcrD of Escherichia coli is an aminoglycoside efflux pump.* J Bacteriol, 2000. 182(6): p. 1754-6.

6. Nakamura, H., *Gene-Controlled Resistance to Acriflavine and Other Basic Dyes in Escherichia coli.* J Bacteriol, 1965. 90(1): p. 8-14.

7. Ma, D., et al., *Molecular cloning and characterization of acrA and acrE genes of Escherichia coli.* J Bacteriol, 1993. 175(19): p. 6299-313.

8. Kumar, A. and H.P. Schweizer, *Bacterial resistance to antibiotics: active efflux and reduced uptake.* Adv Drug Deliv Rev, 2005. 57(10): p. 1486-513.

9. Ma, D., et al., *Efflux pumps and drug resistance in gram-negative bacteria.* Trends Microbiol, 1994. 2(12): p. 489-93.

10. Baranova, N. and H. Nikaido, *The baeSR two-component regulatory system activates transcription of the yegMNOB (mdtABCD) transporter gene cluster in Escherichia coli and increases its resistance to novobiocin and deoxycholate.* J Bacteriol, 2002. 184(15): p. 4168-76.

11. Nagakubo, S., et al., *The putative response regulator BaeR stimulates multidrug resistance of Escherichia coli via a novel multidrug exporter system, MdtABC.* J Bacteriol, 2002. 184(15): p. 4161-7.

12. Nishino, K. and A. Yamaguchi, *EvgA of the two-component signal transduction system modulates production of the yhiUV multidrug transporter in Escherichia coli.* J Bacteriol, 2002. 184(8): p. 2319-23.

13. Munson, G.P., et al., *Identification of a copper-responsive two-component system on the chromosome of Escherichia coli K-12.* J Bacteriol, 2000. 182(20): p. 5864-71.

14. Koronakis, V., et al., *Crystal structure of the bacterial membrane protein TolC central to multidrug efflux and protein export.* Nature, 2000. 405(6789): p. 914-9.

15. Andersen, C., et al., *Transition to the open state of the TolC periplasmic tunnel entrance.* Proc Natl Acad Sci U S A, 2002. 99(17): p. 11103-8.

16. Eswaran, J., C. Hughes, and V. Koronakis, *Locking TolC entrance helices to prevent protein translocation by the bacterial type I export apparatus.* J Mol Biol, 2003. 327(2): p. 309-15.

17. Mikolosko, J., et al., *Conformational flexibility in the multidrug efflux system protein AcrA.* Structure, 2006. 14(3): p. 577-87.

18. Yu, E.W., et al., *Structural basis of multiple drug-binding capacity of the AcrB multidrug efflux pump.* Science, 2003. 300(5621): p. 976-80.

19. Yu, E.W., et al., *A periplasmic drug-binding site of the AcrB multidrug efflux pump: a crystallographic and site-directed mutagenesis study.* J Bacteriol, 2005. 187(19): p. 6804-15.

3.5

DRUG EXPORT PATHWAY OF MULTIDRUG EXPORTER ACRB REVEALED BY DARPIN INHIBITORS

GABY SENNHAUSER, PATRICK AMSTUTZ, CHRISTOPHE BRIAND, OTSO STORCHENEGGER, MARKUS G. GRÜTTER

PLOS BIOLOGY (2007) 5(1), E7.

OPEN ACCESS Freely available online PLOS BIOLOGY

Drug Export Pathway of Multidrug Exporter AcrB Revealed by DARPin Inhibitors

Gaby Sennhauser[1], Patrick Amstutz[1,2], Christophe Briand[1], Otso Storchenegger[1], Markus G. Grütter[1*]

1 Department of Biochemistry, University of Zurich, Zurich, Switzerland, **2** Molecular Partners AG, Zurich, Switzerland

The multidrug exporter AcrB is the inner membrane component of the AcrAB-TolC drug efflux system in *Escherichia coli* and is responsible for the resistance of this organism to a wide range of drugs. Here we describe the crystal structure of the trimeric AcrB in complex with a designed ankyrin-repeat protein (DARPin) inhibitor at 2.5-Å resolution. The three subunits of AcrB are locked in different conformations revealing distinct channels in each subunit. There seems to be remote conformational coupling between the channel access, exit, and the putative proton-translocation site, explaining how the proton motive force is used for drug export. Thus our structure suggests a transport pathway not through the central pore but through the identified channels in the individual subunits, which greatly advances our understanding of the multidrug export mechanism.

Citation: Sennhauser G, Amstutz P, Briand C, Storchenegger O, Grütter MG (2007) Drug export pathway of multidrug exporter AcrB revealed by DARPin inhibitors. PLoS Biol 5(1): e7. doi:10.1371/journal.pbio.0050007

Introduction

Drug resistance is a medical problem, ranging from cancer cells evading chemotherapy to bacteria surviving antibiotic treatment. Efflux pumps represent one class of integral membrane transport proteins in bacteria that confer antibiotic resistance [1]. These proteins actively detoxify the intracellular space by exporting drugs to the cell exterior. AcrB of *Escherichia coli* is such an efflux pump belonging to the subclass of resistance-nodulation-cell division transporters, which catalyze drug export driven by proton antiport [2]. AcrB associates with the outer membrane channel TolC [3] and the periplasmic protein AcrA [4] and allows direct and efficient transport of a wide range of toxic substances [5]. The structures of AcrB alone [6] and of AcrB in complex with substrates [7,8] revealed the general architecture of the transporter. However, despite all mutational and structural studies to date, the mechanism explaining how substrates are transported into the extracellular media was still unclear.

The use of antibody fragments as crystallization aids for membrane proteins has yielded a number of crystal structures [9,10]. The binding of such antibody fragments enlarges the hydrophilic extramembranal surface of integral membrane proteins, thereby providing additional surface for crystal contacts. They can also stabilize a specific conformation supporting the crystallization process. The drawback of the antibody fragment approach is that it is not always easy to get an antibody fragment that recognizes and binds to a particular conformation of a membrane protein. Further, the selected antibody fragment might be unstable or production might be difficult. To circumvent these problems, we applied an approach based on designed ankyrin-repeat proteins (DARPins) as an alternative to antibody fragments. DARPins can be selected to bind almost any given target protein with high affinity and specificity [11]. They are very stable and can be produced as soluble proteins in large amounts by bacterial expression. As DARPins interact with their target protein with an exposed interaction surface, they tend to bind to conformational epitopes rather than to peptidic ones. These characteristics make DARPins ideal tools to help the structural studies of membrane proteins.

Here we selected DARPins that not only bind to AcrB but also inhibit bacterial drug export. Crystals of a selected AcrB–DARPin complex were obtained, and the structure was determined at 2.5-Å resolution. It is the first structure of an integral membrane protein with a selected DARPin molecule binder. The structure reveals a previously unknown asymmetric conformation of the efflux pump, in which each of the three subunits has a unique well-defined conformation. The internal asymmetry of AcrB is underlined by the fact that only two of the three subunits of AcrB are recognized by DARPins in crystallo and in solution and is in contrast to the 3-fold symmetric structures reported to date [6–8]. The structural features described here together with the enhanced resolution allow us to deduce a pathway for drug export and a mechanism for the coupling of substrate export with proton import.

Results

DARPin Selection and Inhibitor Screening

DARPin binders were selected in vitro by ribosome display using a designed ankyrin-repeat protein library [11,12]. The selection was performed on purified and in vitro biotinylated AcrB under native conditions. Four rounds of ribosome display were sufficient to select a pool of specific DARPins binding to AcrB. These experiments are to our knowledge the first ribosome display selections performed in the presence of

Academic Editor: Gregory A. Petsko, Brandeis University, United States of America

Received August 18, 2006; **Accepted** November 3, 2006; **Published** December 26, 2006

Abbreviations: DARPin, designed ankyrin-repeat protein; IPTG, isopropyl-β-d-thiogalactopyranoside; R6G, rhodamine 6G; TM, transmembrane

* To whom correspondence should be addressed. E-mail: gruetter@bioc.unizh.ch

Author Summary

Bacterial resistance to antibiotics is a major challenge for the current treatment of infectious diseases. One way bacteria can escape destruction is by pumping out administered drugs through specific transporter proteins that span the cell membrane. We used designer proteins that bind to and stabilize proteins of interest in order to study the major drug efflux pump of *Escherichia coli,* AcrB. After selecting for designed ankyrin repeat proteins (DARPins) that inhibit this pump, we determined the crystal structure of a DARPin inhibitor in complex with AcrB. We confirmed that the AcrB is split into three subunits, each of which exhibits distinctly different conformations. Moreover, we show that each subunit has a differently shaped substrate transport channel; these variable channels provide unique snapshots of the different conformations adopted by AcrB during transport of a substrate. The structure also offers an explanation for how substrate export is structurally coupled to simultaneous proton import—thus significantly improving our understanding of the mechanism of AcrB. This is the first report of the selection and co-crystallization of a DARPin with a membrane protein, which demonstrates the potential of DARPins not only as inhibitors but also as tools for the structural investigation of integral membrane proteins.

detergent to select specific binders to an integral membrane protein.

The pool of specific binders was subjected to an in vivo screen, based on replica plating, to identify those AcrB-binding DARPins which lead to an inhibitory phenotype. As AcrB is crucial for the transport of certain substrates, its inhibition will consequently lead to accumulation of substrates in the bacterial cell and consequently to cell death. We chose Rhodamine 6G (R6G) as substrate for AcrB. The enriched pool after four rounds of ribosome display was cloned into an expression plasmid under the control of an isopropyl-β-D-thiogalactopyranoside (IPTG)-inducible promoter. *E. coli* strain XL1-blue was transformed and plated under nonselective conditions, in absence of R6G. About 1,500 colonies were subsequently replica-plated under selective conditions, in the presence of 32 μg/ml R6G. By this procedure, 18 single clones were identified which showed a rhodamine-sensitive phenotype. These selected clones were sequenced and assayed for expression. Analysis of the sequences showed that all 18 clones were different and unique.

The affinities of the AcrB inhibiting DARPins were analyzed by surface plasmon resonance using a BIAcore (http://www.biacore.com) instrument. The analysis was performed on AcrB-coated sensor surfaces with multiple concentrations of the DARPins and was evaluated with a global kinetic fit. The five inhibitors with highest affinity, having dissociation constants in the low nanomolar range (3.6 to 98.9 nM; Figure S1), were chosen for further characterization. Clone 1108__19, which was used for cocrystallization, had a dissociation constant K_D of 28 nM.

Inhibition Efficiency of the DARPins

We rated the inhibition efficiencies of the identified DARPins by spotting the clones onto selective plates with different R6G concentrations, ranging from 2 to 64 μg/ml (Figure 1). All inhibitors showed a significant increase of the sensitivity compared to cells expressing an unselected non-binding DARPin, termed E3__5 [13]. This control also showed that the expression of a nonbinding DARPin per se has no influence on R6G sensitivity or bacterial growth. The *acrB* gene-deletion strain KAM3 [14] causes hypersensitivity to R6G and was used as a sensitivity control. In absence of R6G, DARPins conferring R6G sensitivity did not influence *E. coli* growth by themselves. It should be noted, however, that the affinity of the inhibitors does not always correlate with the inhibition efficacy (Figure S1). Possible factors leading to this observation include different expression levels or different binding sites of the DARPins on AcrB. Moreover, the exact inhibition mechanism is not known, even for the inhibitor 1108__19 for which the structure was solved. Different inhibition mechanisms seem plausible ranging from allosteric inhibition of the rotary export mechanism of AcrB by the DARPin to simply preventing the interaction with TolC or AcrA to form the export complex.

Overall Structure of the AcrB–DARPin Complex: Loss of the 3-Fold Symmetry

AcrB exists as a homotrimer, with each subunit containing 12 transmembrane (TM) helices and a large periplasmic part formed by two loops between TM helices 1 and 2 and TM helices 7 and 8. The trimer consists of three prominent domains, the TM domain, and parallel to the membrane, the adjacent pore domain and the TolC docking domain (Figure 2A). The TM domain encompasses a large central cavity, 35 Å in diameter, through the membrane which is closed toward the central funnel formed by the TolC docking domain by three helices provided by the PN1 subdomains of the pore domain (Figure 2B and 2C). The export of substrates was proposed directly through this central pore. Several structures of ligand-free AcrB and with bound substrates have been solved at moderate resolution (between 3.5 and 3.8 Å). Yu et al. [7,8] reported structures of AcrB–ligand complexes showing ligand binding to the upper wall in the central cavity and additional substrate binding in the periplasmic domain, compatible with mutational studies, which indicated that discrimination between different toxic substrates occurs in the periplasmic domain, rather than in the TM domain [15,16]. All structures determined to date imply 3-fold symmetry and thus the three AcrB subunits displayed the same conformation.

To analyze the interaction and to characterize the inhibition property of a selected DARPin, we determined the crystal structure of one inhibitor (1108__19) in complex with AcrB. The crystals diffracted to 2.5-Å resolution and belonged to space group $P2_12_12_1$. The structure was solved by molecular replacement using the structure published by Murakami et al. [6] as a search model without using the phases of the DARPin. The results of the data collection and refinement are presented in Table 1.

The crystal structure of the AcrB–DARPin complex shows two DARPin molecules bound basically to two subunits, named A and B, in the homotrimeric transporter, while the third subunit, named C, is not bound (Figure 2A and 2B). Unlike previously determined crystal structures, there is no 3-fold symmetry of AcrB with the DARPin molecules stabilizing three distinct conformations of the subunits. The conformations of the DARPin-bound subunits A and B are similar to the known symmetric structure. A superposition on Protein Data Bank entry 1IWG [17] shows a few differences for these

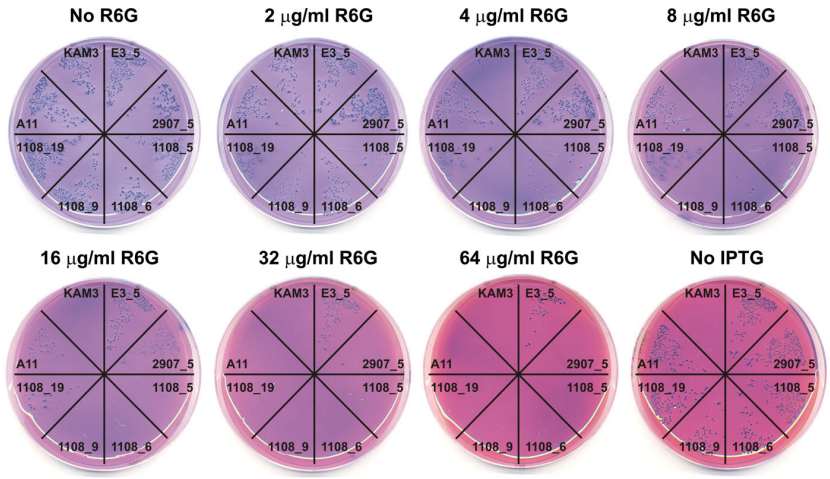

Figure 1. Phenotype of *E. coli* XL1-Blue Strain Expressing the Selected Inhibitory DARPins

Six AcrB inhibitors (2907_5, 1108_5, 1108_6, 1108_9, 1108_19, and A11), one unselected nonbinding DARPin (E3_5), and an *acrB* knockout strain (KAM3 [14], transformed also with E3_5) were ranked for their R6G sensitivity. Induction of the DARPins results in the inhibition of AcrB, yielding an R6G-sensitive phenotype. *E. coli* cells were transformed with the respective plasmid and plated under different conditions: nonselective, no R6G or no IPTG; selective where different R6G concentrations create an environment in which inhibitory DARPins repress growth. All plates contained IPTG (except plate no IPTG). The plates were colored with Coomassie brilliant blue for better visibility of the colonies.

doi:10.1371/journal.pbio.0050007.g001

two subunits with root-mean-square deviations of 1.72 Å and 1.98 Å, respectively, for 1,033 Cα atoms, compared to 2.95 Å for the third subunit C. To validate in solution the 3:2 (AcrB monomer to DARPin) stoichiometry observed in the crystal structure, we performed sedimentation velocity experiments. Single molecular weight species taking the detergent micelle into consideration were observed, with molecular masses of 374 ± 1.6 kDa for AcrB alone and 408 ± 1.7 kDa for the complex (Figure S2). The mass difference indicates that AcrB in solution is bound by two DARPins, with a calculated mass of 17.8 kDa each.

As can be seen in the crystal structure (Figure 2A and 2B), the DARPins bind mainly to the β-sheet connecting the pore domain with the TolC docking domain interacting, as expected, primarily through their randomized concave surface area. The interface buries a surface of around 1,000 $Å^2$ (see Table S1 for detailed interactions). Furthermore, each DARPin interacts with the adjacent preceding subunit of AcrB via one additional hydrophobic interaction involving Leu230 of the intersubunit connecting loop as well as two interactions involving the residues Arg263 and Lys248, again of the preceding subunit (Table S1). Subunit C is in a different orientation, and consequently no DARPin is bound. Notably, the DARPins not only stabilize the asymmetric conformation of AcrB but are also involved in direct interactions in the crystal lattice (Figure S3), resulting in a different crystal form $P2_12_12_1$.

Structure Reveals Channels Leading through the Individual Subunits

The three AcrB subunits are bound in three different conformations, revealing three distinct channels (Figure 3). The width of these channels is sufficient for the passage of typical AcrB substrates. In subunit A, a channel is observed, extending from the external depression through the large periplasmic domain reaching almost the central funnel at the top of the protein (Figure 4A). Here the side chains of residues Gln124, Gln125, and Tyr758 form a gate, closing the channel and therefore preventing direct access to the central funnel. The periplasmic channel entrance corresponds perfectly with the periplasmic binding site indicated in the AcrB–ligand structures of Yu et al. [8]. A similar channel, although a little wider, is present in subunit B (Figure 4B). In addition, the channel is open not only to the periplasm but also to the membrane bilayer at the periphery of the TM domain. In subunit C, the channel entrances are closed due to movements of PC2 and PN1 (Figure 4C). In contrast to subunits A and B, the gate to the central funnel at the top of the periplasmic domain formed by residues Gln124, Gln125, and Tyr758 is now open, allowing the substrate to enter the central funnel from where it most probably reaches TolC and is exported to the cell exterior.

Structural Rearrangements in the Putative Proton-Translocation Site

The opening and closing of the channel entrances and the gate is coupled to structural rearrangements in the putative proton-translocation site in the TM domain (Figure 5A) involving residues in the middle of the TM helix 4 (Asp407 and Asp408) and TM helix 10 (Lys940), respectively (Figure 5B). These charged residues are localized in the center of the hydrophobic TM domain and have been shown to be essential for the proper function of AcrB, since the mutation of these residues leads to complete loss of drug resistance [18]. In subunits A and B, Lys940 forms a salt bridge to the side chains of Asp407 and Asp408, which are also involved in H-bonds with Ser481 and Thr978 presenting the same conformation described to date [6]. In subunit C, this salt bridge is not formed; instead Lys940 is tilted away, forming new polar contacts to Asn941 and Thr978.

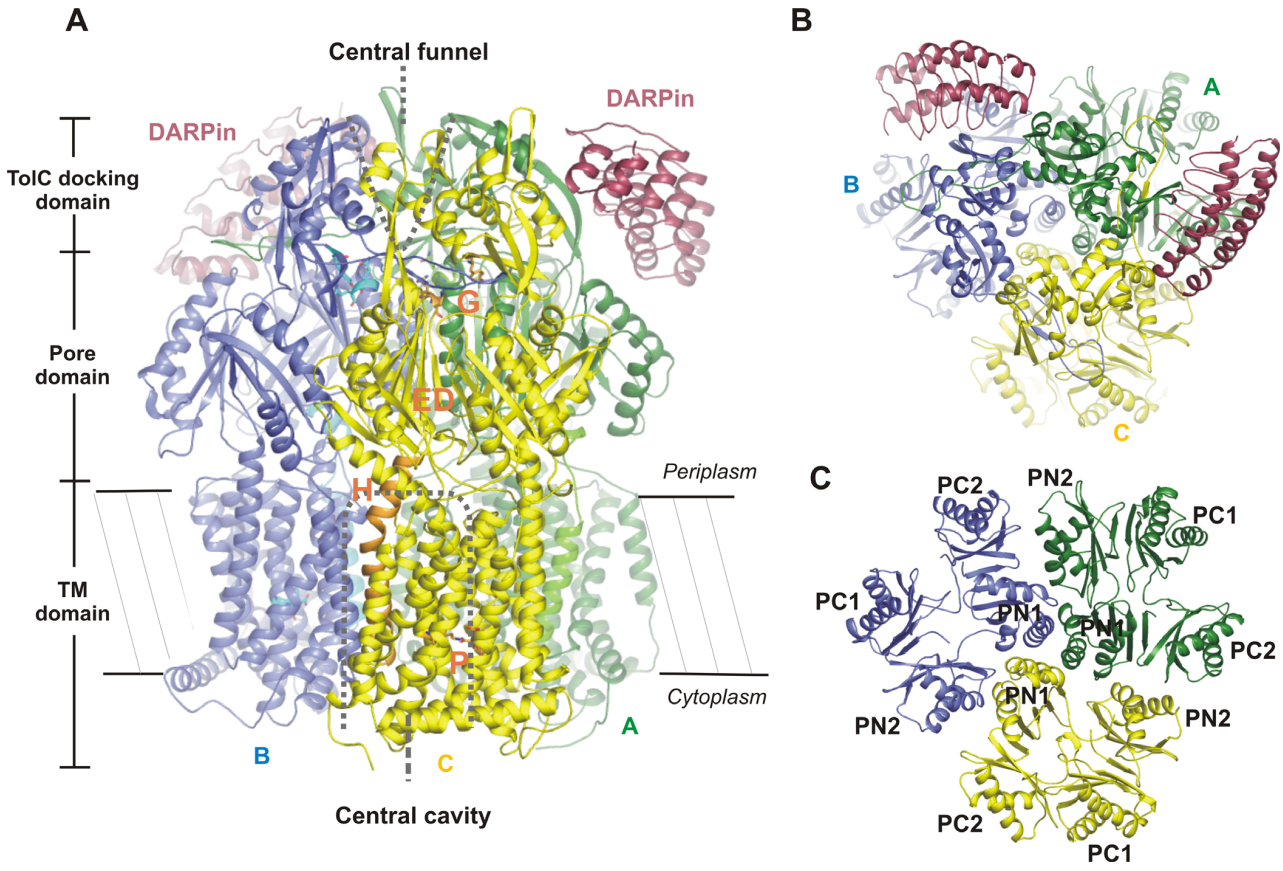

Figure 2. Crystal Structure of the AcrB–DARPin Complex

(A) Ribbon diagram of the overall AcrB–DARPin complex structure viewed from the side, depicted in three different colors for each subunit: green, blue, and yellow for A, B, and C, respectively. The DARPins are colored in red. This color code is used throughout all the figures. The locations of the three prominent domains are indicated and the important regions are highlighted and labeled in subunit C (G, gate; ED, external depression; P, putative proton translocation site; H, helix 8).

(B) Ribbon diagram of the overall AcrB–DARPin complex viewed from the periplasm.

(C) Ribbon diagram of the pore domain viewed as in (B). The subdomains are labeled.

All figures of the molecular models were generated with PyMOL [31].

doi:10.1371/journal.pbio.0050007.g002

The conformational changes described for the putative proton-translocation site are linked to the opening and closing of the channel entrances and the gate described above via rigid movements of TM helix 5 and TM helix 8 (Figure 5A). Distinct conformational differences of the polypeptide stretch that connects the N-terminal end of TM helix 8 to PC2 can be observed in each subunit (Figure 4). The functional importance of this connection is underlined by the fact that each subunit displays a different conformational state of this polypeptide stretch. In subunit A, the stretch shows a long random coil conformation, whereas in subunit B, it adopts partially a helical conformation but with still some random coil conformation. In subunit C, the polypeptide segment is in a completely α-helical conformation continuing the TM helix 8 up to the headpiece subdomain PC2.

The loss of the interaction of Asp407, Asp408 with Lys940 in the putative site for proton-translocation, the simultaneous closing of the channel entrances, and the opening of the gate are evident. This hints at a coordinated control or a coupling of drug export and proton-translocation. The coupling seems to occur via the polypeptide segment that connects TM helix 8 and PC2.

Comparison of Asymmetric AcrB Structures

During the review process of this manuscript, the asymmetric structure of AcrB was published by two other groups [19,20]. Our experimental approach, however, differs from theirs as we apply a new technology using DARPins as crystallization aid. This lead to a new crystal form, $P2_12_12_1$, and, finally, crystals diffracting to higher resolution. Notably, the structural comparison reveals that all three independent structure determinations of AcrB resulted all in almost identical structures. The root-mean-square deviations for 1,032 Cα atoms (Table S2 and Video S1) is around 1, which is a very good correlation at the given resolutions of the different structures (2J8S, 2.5 Å; 2DHH, 2.8 Å [19]; 2GIF, 2.9 Å [20]). Importantly, the region where the DARPins bind shows no significant differences in all the structures. This clearly demonstrates that the selected DARPins bind and stabilize an existing conformational state and do not induce a nonnative conformation upon binding. Murakami et al. [19] also crystallized the protein in the presence of two substrates, which greatly substantiates our findings. In conclusion, all three crystal structures lead to virtually identical conclusions

Table 1. Data Collection and Refinement Statistics

Method	Parameter	AcrB/1108_19
Data collection	Space group	$P2_12_12_1$
	Unit cell parameters (Å)	a = 146.18, b = 157.41, c = 246.04
	Resolution (Å)	35.00–2.54 (2.70–2.54)[a]
	Completeness (%)	95.0 (79.9)
	R_{merge}[b]	0.081 (0.321)
	I/σ(I)	20.75 (6.1)
Refinement	Resolution	25.00–2.54 (2.70–2.54)
	Number of reflections	177,557
	R/R_{free} (%)[c]	22.9/27.0
	RMS deviations	
	Bond lengths (Å)	0.008
	Bond angles (°)	1.3
	Ramachandran plot (%)	
	Most favored	88.4
	Allowed	10.8

[a]Values in parentheses are for the highest resolution shell.
[b]$R_{merge} = \sum_h\sum_j |<I>_h - I_{h,j}|/\sum_h\sum_j I_{h,j}$, where $<I>_h$ is the mean intensity of symmetry-equivalent reflections.
[c]$R = \sum|F_{obs} - F_{cal}|/\sum F_{obs}$. The formula for R_{free} is the same as that for R, except it is calculated with a portion of the structure factors that had not been used for refinement.
doi:10.1371/journal.pbio.0050007.t001

about the drug export pathway and we all proposed similar export mechanisms.

Discussion

Cocrystallization of the membrane protein AcrB and a DARPin inhibitor selected from a large combinatorial library resulted in crystals that diffract to high resolution. The significant higher resolution of our structure compared to the structures published to date allowed unambiguous modeling of the side chain conformations and the interpretation of structural rearrangements extending from the putative proton-translocation sites in the center of the membrane to the gate in the periplasmic domain. The quality of the structure is underlined by 11 resolved detergent molecules (Figure S4). Our work shows for the first time the structure of an integral membrane protein with a selected DARPin molecule, an experimental approach that has great potential for the structural biology of these exceedingly difficult proteins. DARPins may aid by stabilizing certain conformations and by extending the hydrophilic surface similar to antibody-derived protein fragments.

In contrast to the previously known R32 crystal form of AcrB with one monomer in the asymmetric unit, in our structure there are one AcrB trimer and two DARPins in the asymmetric unit, and therefore there are no constraints regarding the conformation of the individual subunits of AcrB. Indeed, the crystal structure shows different conformations for the three individual subunits and reveals channels extending either from the periplasm and the membrane bilayer to a gate near the central funnel at the top of the protein or as in one subunit extending from the gate directly into the central funnel. Moreover, we were able to confirm the 3:2 stoichiometry in solution, confirming the internal asymmetry of AcrB. We believe that the three conformations likely present intermediates in the transport cycle and suggest a rotary mechanism for drug transport where the three subunits strictly alternate their conformation in a concerted way (Figure 6). The R6G-sensitive phenotype of cells expressing the DARPin supports this hypothesis. AcrB may be locked by the DARPins and therefore the rotation of the molecule is stopped. It seems unlikely that the subunits export drugs independent of each other. If this was the case, subunit C would still be functional, and this would be in contrast to the observed inhibitory phenotype induced by the DARPin. Another possibility for the inhibitory effect of the DARPin is that either TolC or AcrA is unable to bind AcrB

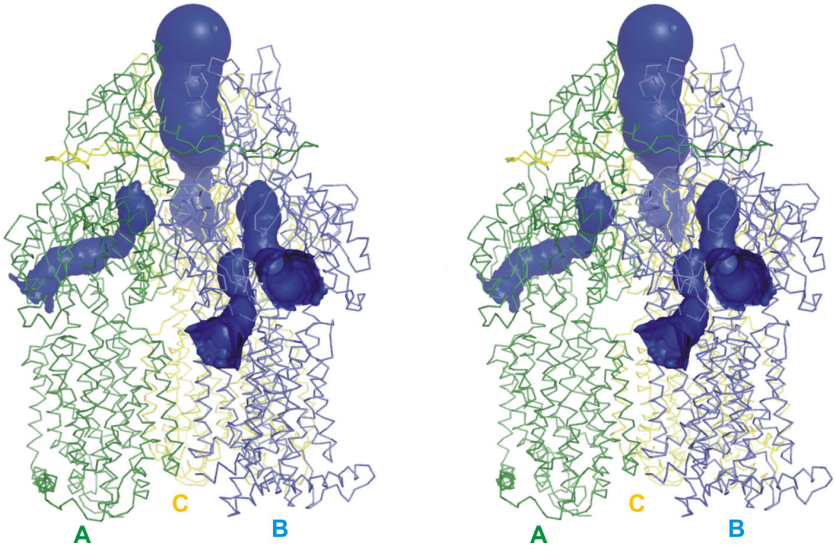

Figure 3. Channels in the AcrB Trimer

Stereo view of the channels leading through the periplasmic domain of AcrB. The structure of AcrB is shown as wire model and the DARPins omitted for clarity. The channels are shown as blue surfaces and were calculated using the program CAVER (http://loschmidt.chemi.muni.cz/caver).
doi:10.1371/journal.pbio.0050007.g003

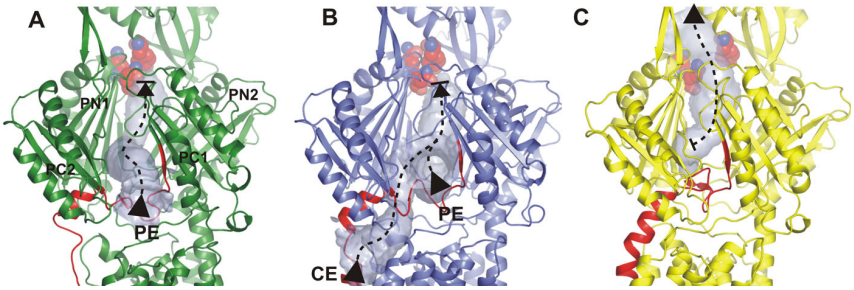

Figure 4. The Extension of the Channels in the Individual Subunits of AcrB

The view is the same as in Figure 2A. For simplicity, the DARPins are not shown. The channels are colored in transparent blue. The potential export pathway is represented by dashed lines. The loop forming the bottom of the periplasmic channel entrance (PE) and TM helix 8 are highlighted in red. The gate to the central funnel formed by the residues Gln124, Gln125, and Tyr758 is shown in space filling representation for clarity.
(A) In subunit A, the channel is opened to the periplasm, while the gate is in the closed conformation. The pore domain subdomains are labeled.
(B) In subunit B, the channel displays an open conformation to the periplasm and to the membrane bilayer (CE). The gate is in a closed conformation.
(C) Subunit C displays a closed conformation of the channel entrances, while the gate is open, extending the channel to the central funnel.
doi:10.1371/journal.pbio.0050007.g004

anymore, resulting in the loss of function of this resistance-nodulation-cell division–type transport protein.

We believe that AcrB operates through a mechanism resembling the alternating-access mechanism which is the substrate-translocation mechanism most commonly described to secondary membrane transporters [21]. We propose that substrates could enter the channel in subunit B via the transmembranal groove at the periphery of the TM domain or via the external depression in the periplasmic part of the structure close to the outer leaflet of the membrane. Substrate would then be specifically bound with the gate of the channel still closed to the central funnel at the top of the periplasmic headpiece. Upon protonation of the proton gating residues Asp407 and/or Asp408, conformational changes in the TM helix 8 take place, which in turn trigger the conformational changes in the periplasmic headpiece. The channel entrances then close through movements of subdomains PN1 and PC2 opening the gate toward the central funnel at the top of the headpiece, releasing the bound substrate into the funnel, from where it could reach TolC and finally the cell exterior.

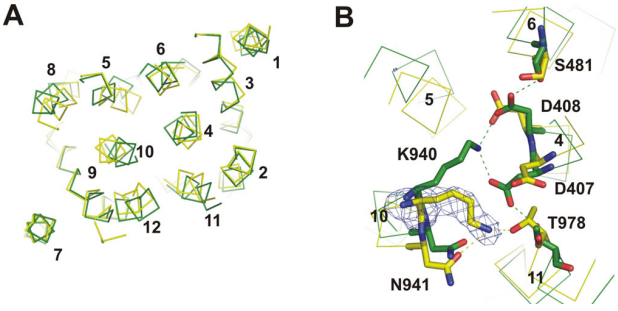

Figure 5. Conformational Changes in the TM Region of AcrB

(A) Wire model of the superpositioned TM domains of subunit A and subunit C viewed from the periplasmic side. Subunit B is omitted since it displays a similar conformation as subunit A. The individual helices are labeled.
(B) Detailed interactions of the amino acid residues in the putative proton-translocation site viewed in the same orientation as in (A). Residues involved in the hydrogen-bonded network (dashed lines) are labeled. The |Fo-Fc| omit electron density map (blue mesh) of Lys940 in subunit C is contoured at 3.5 σ.
doi:10.1371/journal.pbio.0050007.g005

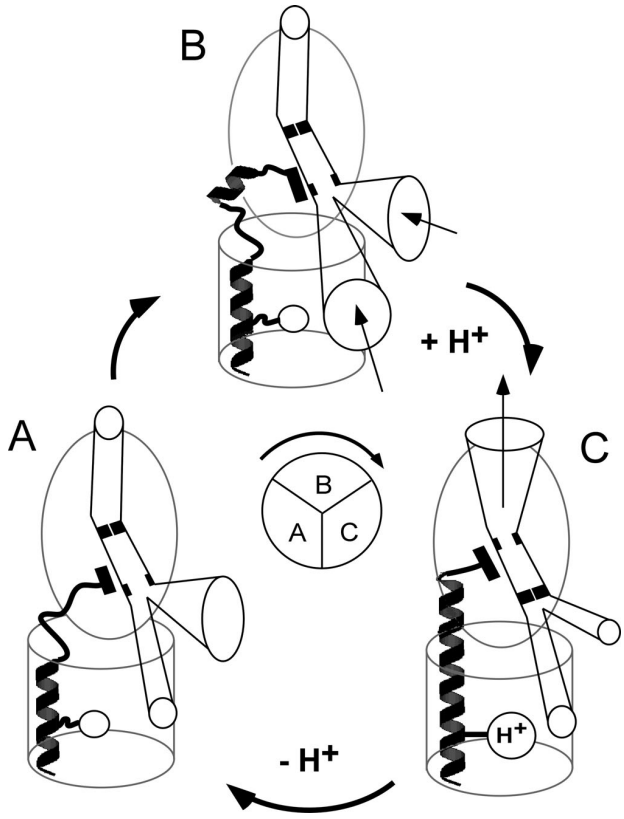

Figure 6. Schematic Drawing of the Transport Pathway of the AcrB Efflux Pump Suggesting a Rotary Mechanism

Proposed mechanism: Substrate may bind into the channel through the open entrances of subunit B. Helix 8 is only weakly pronounced and mostly random coil. Changes of the protonation state of residues of the putative translocation site induce the formation of helix 8 and thus the closing of the channel entrances and the simultaneous opening of the gate, extending the channel to the central funnel at the top of the headpiece showing the conformation of subunit C. The bound substrate can be released into the central funnel from where it reaches TolC and finally the cell exterior. Deprotonation takes place, leading to the collapse of helix 8, and the channel goes back to the original conformation (subunit A).
doi:10.1371/journal.pbio.0050007.g006

While this model is based on the interpretation of the structural information seen in the asymmetric structure, it contains all features necessary for the export of substrates and simultaneous import of protons. It is also consistent with mutational studies available to date [8,17]. Further experiments using the crystals of the complex with drug substrates may substantiate this mechanism. In fact, similar to the experiments performed by Murakami et al. [19], we also could show binding of minocycline in the identified channel at 2.5-Å resolution (unpublished data). The structural findings most likely rule out the previously proposed export of substrates directly through the central pore of the structure.

Materials and Methods

AcrB production and purification. AcrB was overexpressed in *E. coli* strain BL21 (DE3; Novagen, EMD Biosciences, http://www.emdbiosciences.com) overnight at 30 °C using a pET28 vector (Novagen) containing *acrB* with a hexahistidine-tag at the C terminus. Cells of 1-L bacterial culture were disrupted with a French pressure cell, and the membranes were collected and solubilized in buffer A (20 mM Tris-HCl [pH 7.5], 150 mM NaCl, 10 mM imidazole, 10% glycerol), containing 1% (w/v) *n*-dodecyl-β-D-maltoside (DDM) (Anatrace, http://www.anatrace.com). Lipids and debris were removed by ultracentrifugation at 100,000*g* for 1 h. The solubilized protein was purified with affinity chromatography using Ni-NTA (Qiagen, http://www.qiagen.com), equilibrated with buffer A, containing 0.03% DDM. The column was washed using this buffer and 50 mM imidazole, respectively. Purified AcrB was eluted with 200 mM imidazole added to the above buffer.

For biotinylation purposes, AcrB was eluted in 200 mM imidazole (pH 7.5) as the only buffering agent. The protein was chemically biotinylated using a 15 molar excess EZ-Link Sulfo-NHS-LC-Biotin (Pierce Biotechnology, http://www.piercenet.com) for 30 min at 4 °C. Free biotin was removed using a HiTrap Desalting column (5 ml; Amersham Biosciences, http://www.amersham.com) equilibrated in buffer B (20 mM Tris-HCl [pH 7.5], 150 mM NaCl, 0.03% [w/v] DDM).

In vitro selection by ribosome display. Four rounds of ribosome-display selection were carried out using an N3C DARPin library [11,12]. In vitro biotinylated AcrB was immobilized on neutravidin-coated wells blocked with BSA. To eliminate BSA- and neutravidin-binding library members as well as further unspecific binders, two pre-panning steps were applied, where neutravidin, BSA, and biotinylated maltose binding protein (MBP) [11] were present. In the actual panning step, binders to AcrB were thus selected. The panning procedure was performed exactly as described previously [11], with the modification that all buffers contained 0.03% (w/v) DDM, to keep AcrB stable and solubilized.

In vivo selection by replica plating. The pool of specific binders was subjected to an in vivo screen, based on replica plating, to identify those AcrB-binding DARPins with an inhibitory phenotype. For this purpose, the selected pool of binders was cloned into the vector pQIA [22]. This vector carries an expression cassette for the selected DARPins under the control of an IPTG-inducible T5 promoter.

The pool of binders was transformed into *E. coli* XL1-blue cells (recA1 endA1 gyrA96 thi-1 hsdR17 supE44 relA1 lac [F′ proAB lacIqZΔM15 Tn10 (Tetr)]; Stratagene, http://www.stratagene.com) and plated under nonselective conditions (ampicillin, IPTG, no R6G). About 1,500 colonies were subsequently replica-plated under selective conditions (ampicillin, IPTG, R6G [32 μg/ml]). By this procedure, 18 N3C clones were identified which showed a rhodamine-sensitive phenotype. The characterization of these DARPins included sequencing, expression tests, surface plasmon resonance, MIC determination, size exclusion chromatography studies, and cocrystallization.

Drug susceptibility assay. The susceptibility to R6G of *E. coli* XL1-blue cells expressing the selected DARPins were determined by sequential 2-fold dilutions with LB agar/glucose plates containing 0.1 mM IPTG. R6G was used at concentrations of 2, 4, 8, 16, 32, and 64 μg/ml. Bacterial growth was examined after 24 h at 37 °C.

Surface plasmon resonance. Surface plasmon resonance was measured using a BIAcore 3000 instrument at 20 °C. The running buffer was buffer B. An SA chip (BIAcore) was used with 700 RU of biotinylated AcrB immobilized. The DARPin binding was measured at a flow of 50 μl/min with 5-min buffer flow, 2-min injection of AcrB-binding DARPin in varying concentrations (2.5 nM to 60 nM), and an off-rate measurement of 30 min with buffer flow. The signal of an uncoated reference cell was subtracted from the measurements. The kinetic data of the interaction were evaluated using the program BIAevaluation 3.0 (BIAcore), and global fits were used to determine K_D. The possible avidity effect of the AcrB trimer was not taken into account in the fit.

Analytical ultracentrifugation. Sedimentation velocity experiments were conducted using a Beckman ProteomeLab XL-I (http://www.beckmancoulter.com) with an An-50 Ti analytical rotor (Beckman). The samples were equilibrated in buffer B at a concentration of 0.42 mg/ml. All data acquired from this experiment were obtained using the UV/Vis absorbance detection system (Perkin Elmer, http://www.perkinelmer.com) on the ultracentrifuge at 280 nm and double sector 12-mm charcoal-filled Epon centerpieces. The experiment was conducted at 4 °C at a speed of 40,000 rpm. The data of 300 scans were analyzed using the LAMM equation in the program SEDFIT [23].

Crystal preparation. To obtain crystals of the AcrB–DARPin complex, AcrB and the selected AcrB-inhibiting DARPin 1108__19 were purified separately as described [12]. A small molar excess of the DARPin with regard to the AcrB monomer was used to prepare the complex, followed by purification on a Tricorn Superdex-200 (Amersham Biosciences) column equilibrated in buffer B. The peak fractions containing AcrB in complex with the DARPin were concentrated using a 30-kDa-cutoff concentrator (Amicon Ultra; Millipore, http://www.millipore.com), exchanged into 10 mM HEPES (pH 7.5), 50 mM NaCl containing 0.03% (w/v) DDM, and again concentrated to 13 to 15 mg/ml.

Initial crystallization screening was done in 96-well, sitting drop crystallization plates (Greiner Bio-One, http://www.greinerbioone.com). The initial crystals were refined using standard techniques. The crystals used for data collection appeared within 4 d in 8% PEG 4000, 50 mM ADA (pH 6.5), 200 mM $(NH_4)_2SO_4$ in a hanging drop vapor diffusion experiment at 20 °C. For data collection, the crystals were soaked in six steps for about 15 s in the mother liquid containing 5% to 30% glycerol and flash frozen into liquid propane.

Data collection, phase determination, and structure refinement. Data were collected at the Swiss Light Source beamline PX (http://sls.web.psi.ch/view.php/about/index.html) and processed using the program XDS [24]. The crystal belonged to space group $P2_12_12_1$, with a Matthews coefficient V_M of 3.8 $Å^3$/Da, corresponding to an estimated water content of 67.7%.

The crystal structure was solved by molecular replacement using the program PHASER [25,26], with the structure of the AcrB monomer (Protein Data Bank code 1IWG [6]) used as search model. A PHASER search with the DARPin E3__5 (Protein Data Bank code 1MJO [13]) as search model did not yield a meaningful solution. The information obtained from the conventional PHASER protocol for the three AcrB monomers was sufficient to model one DARPin molecule into the resulting electron density with the program O [27]. The second DARPin also was positioned in O. Refinement of the structure was carried out through multiple cycles of manual rebuilding using the program Coot [28] and refinement using CNS [29] resulting in a final model with an R factor of 22.9 and an R_{free} factor of 27.9. The refined structure of the AcrB–DARPin complex was validated by the program PROCHECK [30]. Three-dimensional structural figures were prepared by using PyMOL [31].

Supporting Information

Figure S1. Surface Plasmon Resonance Analysis of the AcrB–DARPin Complexes

The binding kinetics of selected DARPins were analyzed using a BIAcore instrument. Different concentrations of DARPin (2.5, 5, 8, 15, 25, 40, and 60 nM) were applied to a flow cell with immobilized AcrB for 2 min, followed by washing with buffer flow. The global fit is indicated in the figure by black lines.

Found at doi:10.1371/journal.pbio.0050007.sg001 (64 KB DOC).

Figure S2. Sedimentation Velocity Analysis of AcrB and the AcrB–DARPin Complex Using the LAMM Equation in the Program SEDFIT

(A) AcrB. (B) AcrB–DARPin complex.

Found at doi:10.1371/journal.pbio.0050007.sg002 (27 KB DOC).

Figure S3. Crystal Packing of AcrB–DARPin Complex Crystals

The DARPins (in red) are involved in crystal contacts and thus account for the different space group and most likely for the high resolution of the structure.

Found at doi:10.1371/journal.pbio.0050007.sg003 (902 KB DOC).

Figure S4. Detergent Molecules in the Structure

The structure contains 11 *n*-dodecyl-β-D-maltoside (DDM) detergent molecules underlining the quality of the structure.

Found at doi:10.1371/journal.pbio.0050007.sg004 (738 KB DOC).

Table S1. Detailed Interactions of the AcrB–DARPin Complex

Direct hydrogen bonds between AcrB and the bound DARPins identified by the program LIGPLOT and the interface accessible surface area calculated with the Protein-Protein Interaction Server.

Found at doi:10.1371/journal.pbio.0050007.st001 (49 KB DOC).

Table S2. Comparison of the Asymmetric AcrB Structures

Root-mean-square deviations of Cα coordinates calculated by the program lsqman.

Found at doi:10.1371/journal.pbio.0050007.st002 (41 KB DOC).

Video S1. Comparison of the AcrB–DARPin Complex with Other Asymmetric AcrB Structures

Superposition of the Cα atoms of the AcrB–DARPin complex (green) with 2DHH (blue) and 2GIF (pink).

Found at doi:10.1371/journal.pbio.0050007.sv001 (3.2 MB WMV).

Accession Numbers

The atomic coordinates and structure factors of the described complex have been deposited in the Protein Data Bank (http://www.rcsb.org) with accession number 2J8S.

Acknowledgments

We thank Raimund Dutzler for reading the manuscript and Heinz Gut for his help in solving the structure and helpful discussions. We also thank the staff of beamline PX of the Swiss Light Source, Villigen, Switzerland, for excellent technical assistance.

Author contributions. GS and PA conceived and designed the experiments. GS performed all the experiments with the help of OS and CB. GS, CB, and MGG analyzed the data. GS, PA, and MGG wrote the paper.

Funding. This work was supported by the Swiss National Center of Competence in Research (NCCR) in Structural Biology.

Competing interests. The authors have declared that no competing interests exist.

References

1. Ma D, Cook DN, Hearst JE, Nikaido H (1994) Efflux pumps and drug resistance in gram-negative bacteria. Trends Microbiol 2: 489–493.
2. McKeegan KS, Borges-Walmsley MI, Walmsley AR (2004) Structural understanding of efflux-mediated drug resistance: Potential routes to efflux inhibition. Curr Opin Pharmacol 4: 479–486.
3. Koronakis V, Sharff A, Koronakis E, Luisi B, Hughes C (2000) Crystal structure of the bacterial membrane protein TolC central to multidrug efflux and protein export. Nature 405: 914–919.
4. Mikolosko J, Bobyk K, Zgurskaya HI, Ghosh P (2006) Conformational flexibility in the multidrug efflux system protein AcrA. Structure 14: 577–587.
5. Nikaido H (1998) Antibiotic resistance caused by gram-negative multidrug efflux pumps. Clin Infect Dis 27: S32–S41.
6. Murakami S, Nakashima R, Yamashita E, Yamaguchi A (2002) Crystal structure of bacterial multidrug efflux transporter AcrB. Nature 419: 587–593.
7. Yu EW, McDermott G, Zgurskaya HI, Nikaido H, Koshland DE Jr. (2003) Structural basis of multiple drug-binding capacity of the AcrB multidrug efflux pump. Science 300: 976–980.
8. Yu EW, Aires JR, McDermott G, Nikaido H (2005) A periplasmic drug-binding site of the AcrB multidrug efflux pump: A crystallographic and site-directed mutagenesis study. J Bacteriol 187: 6804–6815.
9. Iwata S, Ostermeier C, Ludwig B, Michel H (1995) Structure at 2.8 Å resolution of cytochrome *c* oxidase from *Paracoccus denitrificans*. Nature 376: 660–669.
10. Dutzler R, Campbell EB, MacKinnon R (2003) Gating the selectivity filter in ClC chloride channels. Science 300: 108–112.
11. Binz HK, Amstutz P, Kohl A, Stumpp MT, Briand C, et al. (2004) High-affinity binders selected from designed ankyrin repeat protein libraries. Nat Biotechnol 22: 575–582.
12. Binz HK, Stumpp MT, Forrer P, Amstutz P, Pluckthun A (2003) Designing repeat proteins: Well-expressed, soluble and stable proteins from combinatorial libraries of consensus ankyrin repeat proteins. J Mol Biol 332: 489–503.
13. Kohl A, Binz HK, Forrer P, Stumpp MT, Pluckthun A, et al. (2003) Designed to be stable: Crystal structure of a consensus ankyrin repeat protein. Proc Natl Acad Sci U S A 100: 1700–1705.
14. Morita Y, Kodama K, Shiota S, Mine T, Kataoka A, et al. (1998) NorM, a putative multidrug efflux protein, of *Vibrio parahaemolyticus* and its homolog in *Escherichia coli*. Antimicrob Agents Chemother 42: 1778–1782.
15. Elkins CA, Nikaido H (2002) Substrate specificity of the RND-type multidrug efflux pumps AcrB and AcrD of *Escherichia coli* is determined predominantly by two large periplasmic loops. J Bacteriol 184: 6490–6498.
16. Tikhonova EB, Wang Q, Zgurskaya HI (2002) Chimeric analysis of the multicomponent multidrug efflux transporters from gram-negative bacteria. J Bacteriol 184: 6499–6507.
17. Murakami S, Tamura N, Saito A, Hirata T, Yamaguchi A (2004) Extramembrane central pore of multidrug exporter AcrB in *Escherichia coli* plays an important role in drug transport. J Biol Chem 279: 3743–3748.
18. Guan L, Nakae T (2001) Identification of essential charged residues in transmembrane segments of the multidrug transporter MexB of *Pseudomonas aeruginosa*. J Bacteriol 183: 1734–1739.
19. Murakami S, Nakashima R, Yamashita E, Matsumoto T, Yamaguchi A (2006) Crystal structures of a multidrug transporter reveal a functionally rotating mechanism. Nature 443: 173–179.
20. Seeger MA, Schiefner A, Eicher T, Verrey F, Diederichs K, et al. (2006) Structural asymmetry of AcrB trimer suggests a peristaltic pump mechanism. Science 313: 1295–1298.
21. Huang Y, Lemieux MJ, Song J, Auer M, Wang DN (2003) Structure and mechanism of the glycerol-3-phosphate transporter from *Escherichia coli*. Science 301: 616–620.
22. Amstutz P, Binz HK, Parizek P, Stumpp MT, Kohl A, et al. (2005) Intracellular kinase inhibitors selected from combinatorial libraries of designed ankyrin repeat proteins. J Biol Chem 280: 24715–24722.
23. Schuck P (2000) Size-distribution analysis of macromolecules by sedimentation velocity ultracentrifugation and LAMM equation modeling. Biophys J 78: 1606–1619.
24. Kabsch W (1993) Automatic processing of rotation diffraction data from crystals of initially unknown symmetry and cell constants. J Appl Cryst 26: 795–800.
25. Storoni LC, McCoy AJ, Read RJ (2004) Likelihood-enhanced fast rotation functions. Acta Crystallogr D Biol Crystallogr 60: 432–438.
26. Read RJ (2001) Pushing the boundaries of molecular replacement with maximum likelihood. Acta Crystallogr D Biol Crystallogr 57: 1373–1382.
27. Jones TA, Zou JY, Cowan SW, Kjeldgaard (1991) Improved methods for building protein models in electron density maps and the location of errors in these models. Acta Crystallogr A 47: 110–119.
28. Emsley P, Cowtan K (2004) Coot: model-building tools for molecular graphics. Acta Crystallogr D Biol Crystallogr 60: 2126–2132.
29. Brunger AT, Adams PD, Clore GM, DeLano WL, Gros P, et al. (1998) Crystallography and NMR system: A new software suite for macromolecular structure determination. Acta Crystallogr D Biol Crystallogr 54: 905–921.
30. Laskowski RA, MacArthur MW, Moss DS, Thornton JM (1993) PROCHECK:A program to check the stereochemical quality of protein structures. J Appl Crystallogr 26.
31. DeLano WL (2002) The PyMOL molecular graphics system. San Carlos (California): DeLano Scientific.

Figure S1. Surface Plasmon Resonance Analysis of the AcrB-DARPin complexes

SPR analysis of 1108_19

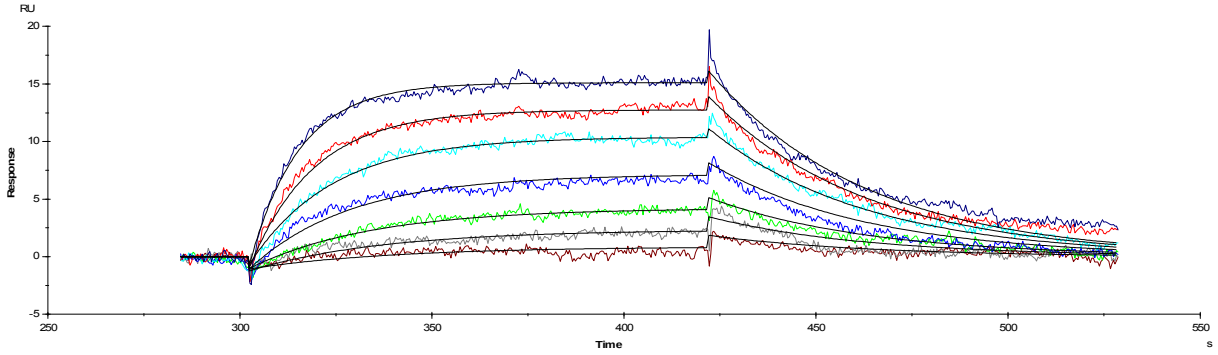

Clone	k_{on} [$M^{-1}s^{-1}$]	k_{off} [s^{-1}]	K_D [M]	R6G sensitivity [µg/ml R6G]
1108_19	$8.7 \cdot 10^{5}$	$2.4 \cdot 10^{-2}$	$28.0 \cdot 10^{-9}$	32
1108_05	$1.2 \cdot 10^{6}$	$6.5 \cdot 10^{-2}$	$52.3 \cdot 10^{-9}$	8
1108_06	$3.4 \cdot 10^{5}$	$3.4 \cdot 10^{-2}$	$98.9 \cdot 10^{-9}$	16
1108_09	$1.1 \cdot 10^{6}$	$4.1 \cdot 10^{-3}$	$3.6 \cdot 10^{-9}$	4
2907_05	$1.8 \cdot 10^{6}$	$4.2 \cdot 10^{-2}$	$23.4 \cdot 10^{-9}$	32

Figure S2. Sedimentation Velocity Analysis of (A) AcrB and (B) the AcrB-DARPin Complex

(A)

rmsd = 0.004265

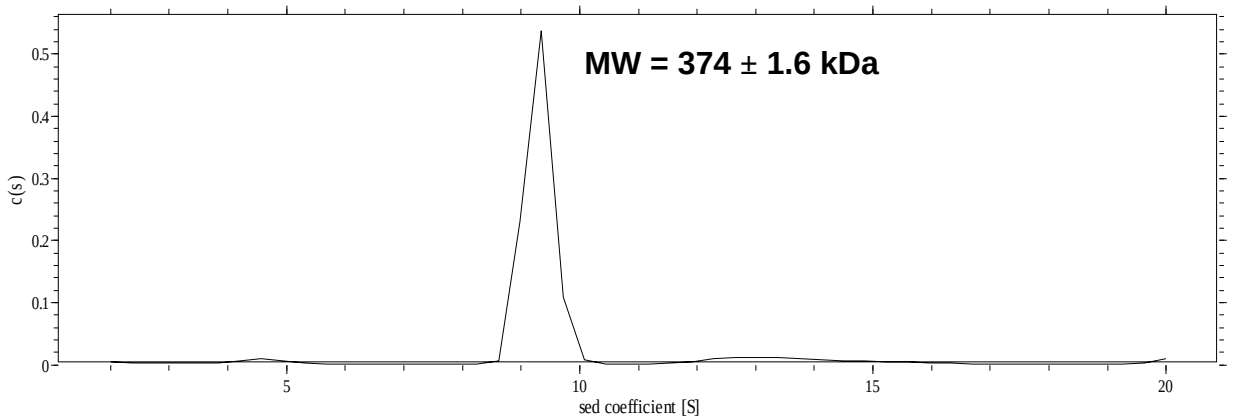

(B)

rmsd= 0.004182

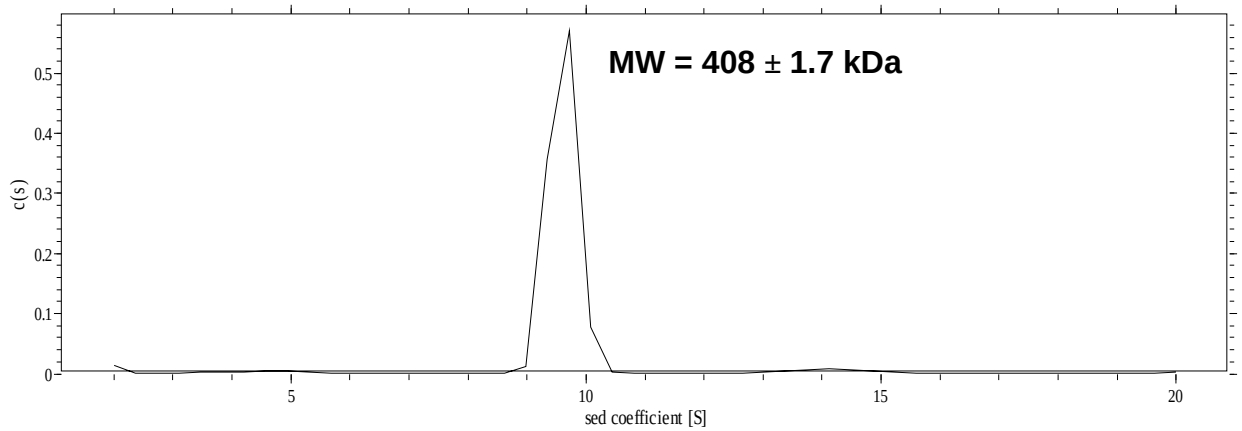

Figure S3. Crystal Packing of AcrB-DARPin Complex Crystals

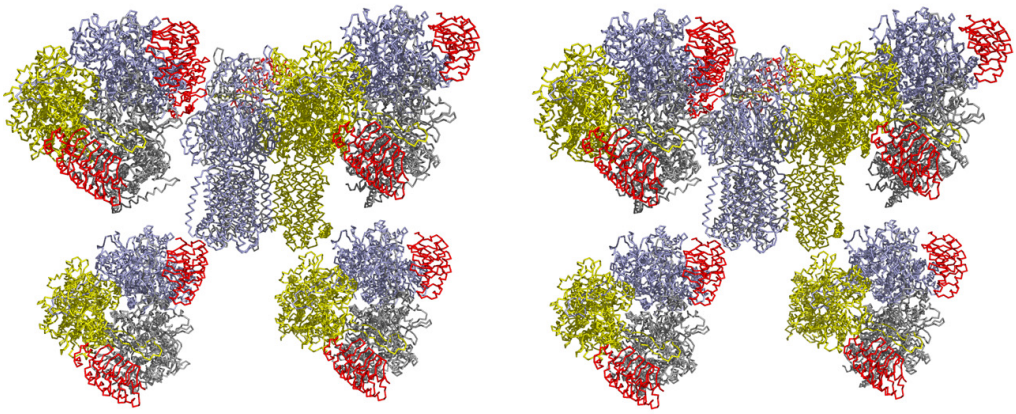

Figure S4. Detergent Molecules in the Structure

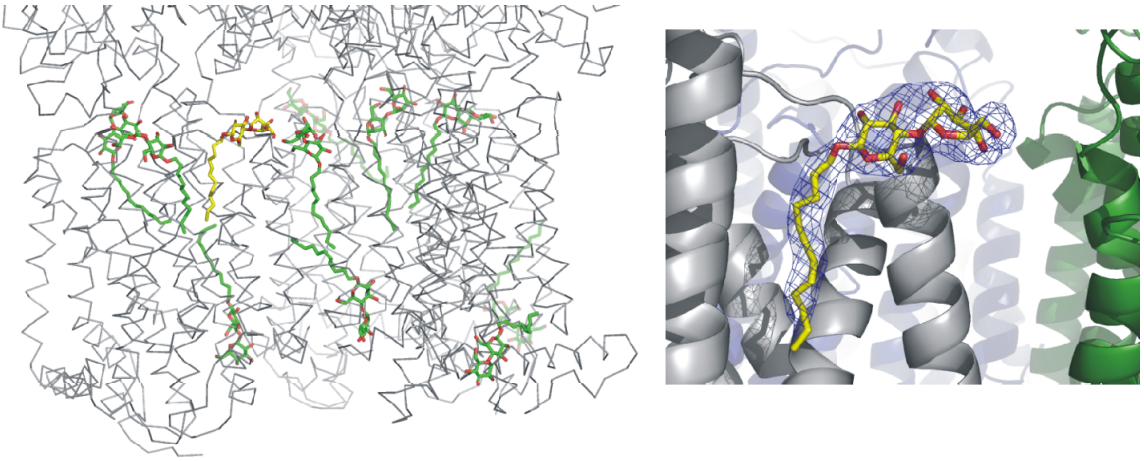

CHAPTER 4

MULTIDRUG EFFLUX IN *PSEUDOMONAS AERUGINOSA*: THE MEXAB-OPRM SYSTEM

The opportunistic Gram-negative pathogen *P. aeruginosa* causes life-threatening infections, affecting in particular immunocompromised patients and patients with cystic fibrosis. A well-known characteristic of *P. aeruginosa* is its high intrinsic resistance to a variety of antimicrobial agents. The low permeability of the outer membrane itself can not sufficiently explain this fact. Therefore, it is believed that the maintenance of such a high level of antibacterial resistance is largely attributable to the presence of multidrug efflux pumps [1]. The analysis of the genome sequence of *P. aeruginosa* has revealed the existence 13 putative RND-transporters (Table 1) [2, 3]. One exports heavy metals (CzcA), the others are drug transporters. Seven of these systems have been experimentally confirmed as multidrug efflux systems (Mex) systems so far. The role of the other RND-systems in drug transport, if any, has yet to be determined.

Table 1: RND efflux pumps of *P. aeruginosa*. Adapted from [4].

Efflux system			Substrate(s)	References
Genetic context	RND	OMP		
mexAB-oprM	**MexB**	OprM	AC, AG, BL, CM, CV, EB, FQ, ML, NO, SDS, TC, TM, TR	[1]
mexCD-oprJ	**MexD**	OprJ	CM, CP, FQ, TC, TR	[5]
mexEF-oprN	**MexF**	OprN	CM, FQ	[6]
mexXY	**MexY**	OprM	AG, ML, TC	[7]
mexGHI-opmD	**MexI**	OpmD	AC, EB, NO, RD, Vanadium	[8]
mexJK	**MexK**	OprM/OpmH	EM, TC, TR	[9]
mexVW	**MexW**	OprM	AC, CM, EB, EM, FQ, TC	[10]
PA3523-PA3522-opmE	**PA3522**	OpmE	?	
PA2528-PA2527-PA2526-opmB	**PA2527/PA2526**	OpmB	?	
PA1435-PA1436	**PA1436**	?	?	
PA156-PA157-PA158	**PA158**	?	?	
czcC-czcB-czcA	**CzcA**	?	Heavy metals	[11]

AC = acriflavine; **AG** = aminoglycoside; **BL** = β-lactams; **CM** = chloramphenicol; **CP** = cephalosporins; **CV** = crystal violet; **EB** = ethidium bromide; **EM** = erythromycin; **FQ** = fluoroquinolones; **ML** = macrolide; **NO** = novobiocin; **RD** = Rhodamine; **SDS** = sodium dodecyl sulfate; **TC** = tetracycline; **TM** = trimethoprim; **TR** = triclosan.

The MexAB-OprM system is the major responsible factor for the intrinsic resistance of *P. aeruginosa*. Acquired resistance is often associated with mutations in the adjacent repressor gene mexR, a phenotype also known as nalB mutants, and results in overexpression of this system. MexB exhibits the broadest substrate range of all characterized drug transporters in *P. aeruginosa* transporting β-lactams, β-lactamase inhibitors, quinolones, macrolides, tetracyclines, chloramphenicol,

novobiocin, sulfonamides, trimethoprim, thiolactomycin, dyes, detergents, triclosan and organic solvents [4]. Like other efflux pumps, the MexAB-OprM system consists of an MFP-, an RND-, and an OMP-component.

4.1 OprM

The structure of OprM was solved at 2.56 Å resolution [12]. Although the protein showed only 21% amino acid identity to its functional homologue TolC the two structures displayed a very similar fold (Fig. 1) (see chapter 3.1). OprM also forms a trimer consisting of a 12-stranded β-barrel domain, an α-helical barrel domain and an equatorial domain and similar to TolC the periplasmic end of OprM is closed by six coiled-coils. The major structural differences between the two structures are exhibited by the equatorial domain and in contrast to TolC, the β-barrel is much more constricted at the cell exterior by extracellular loops connecting the β-strands. This constriction is large enough to inhibit the passage of any antibiotic. These surface loops were disordered in the second trimer in the asymmetric unit, suggesting some flexibility for this part of the molecule. In contrast to TolC, OprM transports only small molecules and no proteins. Furthermore, OprM is fatty acid acylated at its N-terminus which could have a function in anchoring the protein to the outer membrane. But as with the acylated MFPs, the acylation seems not to be necessary for function [13].

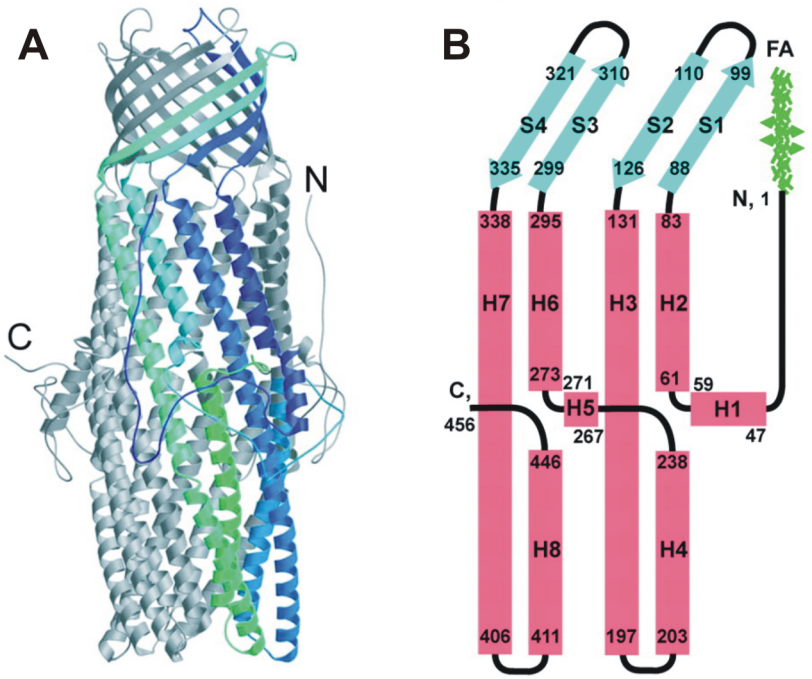

Fig. 1.

3D-Structure of OprM, the OMP of the MexAB system of *P. aeruginosa* (PDB ID code: 1WP1). A The biologically active, trimeric molecule is depicted in a ribbon diagram. One monomer is highlighted in blue and green. The N- and C- terminus are indicated (of two different monomers for simplicity). **B** Topology diagram for the OprM monomer. Adapted from [12]. FA = fatty acid acyl chain.

4.2 MexA

The structure of MexA was solved independently by two groups at 2.4 and 3.0 Å resolution, respectively [14, 15]. The structure presented by Akama et al. resolved residues 46 to 297 and the one by Higgins et al. residues 52 to 282 of the 383 residues protein. The N-terminal periplasmic signal sequence (residues 1-23) was either exchanged by another sequence or omitted and Cys24 was mutated to Ser to prevent the attachment of a fatty acid. The remaining residues were not ordered in the crystal. In both structures, the MexA monomer displays an elongated modular structure consisting of three main domains: a β-barrel, a lipoyl domain and a coiled-coil α-helical hairpin (Fig. 2A). The β-barrel domain contains six antiparallel β-strands and a single α-helix located at one entrance of the barrel. The lipoyl domain forms a β-sandwich consisting of two interlocking lipoyl motifs with four β-strands each. These two motifs are separated by the α-helical hairpin. Each helix has four heptad repeats.

Whereas MexA behaves as a monomer in solution, it formed a cylinder composed of two twisted arcs of six and seven monomers with a tight interaction of the α-helical hairpin domains in both crystals (Fig. 2B). All 13 copies displayed essentially the same conformation. This unusual oligomeric state, however, is not believed to be biologically relevant, as the tethering of MexA to the inner membrane via their lipid modified N-terminus would be impossible.

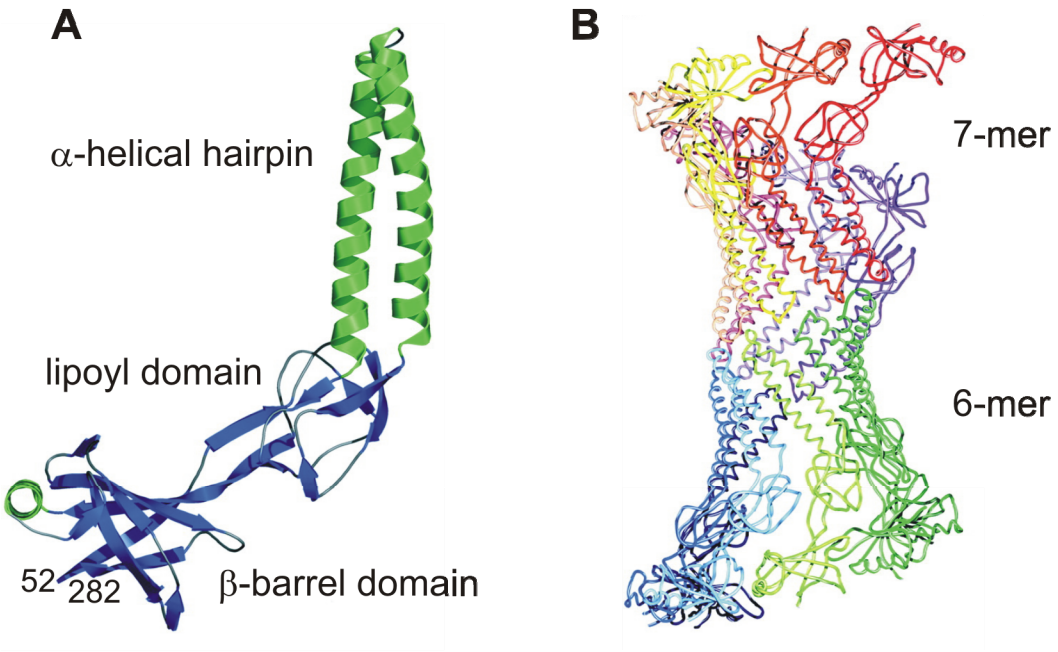

Fig. 2.

3D-Structure of MexA, the MFP of the MexAB system of *P. aeruginosa* (PDB ID code: 1T5E). A The MexA monomer is depicted in a ribbon diagram and colored by secondary structure. The last residues visible in the electron density and the three domains are indicated. **B** Cα traces of the 13 monomers in the asymmetric unit. Each monomer is colored differently. Adapted from [15].

4.3 MexB

Many studies leading to the understanding of the transport capability, energy needs and structural characterisation of the RND-transporter family and the whole tripartite systems, respectively, were actually performed rather with MexB than AcrB [16-18]. Surprisingly, despite the fact that a purification protocol of the protein was already described in 2005 [19], a crystal structure of this protein is not available yet. After the successful structure determination of AcrB we went one step further and solved the structure of the second member of the RND-transporter family, MexB. We further selected DARPin binders against MexB aiming for an alternative crystal form

which could support the observed conformational flexibility of one subunit in the structure of MexB alone (see chapter 4.5).

4.4 References

1. Li, X.Z., H. Nikaido, and K. Poole, *Role of mexA-mexB-oprM in antibiotic efflux in Pseudomonas aeruginosa.* Antimicrob Agents Chemother, 1995. 39(9): p. 1948-53.

2. Stover, C.K., et al., *Complete genome sequence of Pseudomonas aeruginosa PA01, an opportunistic pathogen.* Nature, 2000. 406(6799): p. 959-64.

3. Schweizer, H.P., *Efflux as a mechanism of resistance to antimicrobials in Pseudomonas aeruginosa and related bacteria: unanswered questions.* Genet Mol Res, 2003. 2(1): p. 48-62.

4. Kumar, A. and H.P. Schweizer, *Bacterial resistance to antibiotics: active efflux and reduced uptake.* Adv Drug Deliv Rev, 2005. 57(10): p. 1486-513.

5. Poole, K., et al., *Overexpression of the mexC-mexD-oprJ efflux operon in nfxB-type multidrug-resistant strains of Pseudomonas aeruginosa.* Mol Microbiol, 1996. 21(4): p. 713-24.

6. Kohler, T., et al., *Characterization of MexE-MexF-OprN, a positively regulated multidrug efflux system of Pseudomonas aeruginosa.* Mol Microbiol, 1997. 23(2): p. 345-54.

7. Mine, T., et al., *Expression in Escherichia coli of a new multidrug efflux pump, MexXY, from Pseudomonas aeruginosa.* Antimicrob Agents Chemother, 1999. 43(2): p. 415-7.

8. Aendekerk, S., et al., *Characterization of a new efflux pump, MexGHI-OpmD, from Pseudomonas aeruginosa that confers resistance to vanadium.* Microbiology, 2002. 148(Pt 8): p. 2371-81.

9. Chuanchuen, R., C.T. Narasaki, and H.P. Schweizer, *The MexJK efflux pump of Pseudomonas aeruginosa requires OprM for antibiotic efflux but not for efflux of triclosan.* J Bacteriol, 2002. 184(18): p. 5036-44.

10. Li, Y., et al., *A new member of the tripartite multidrug efflux pumps, MexVW-OprM, in Pseudomonas aeruginosa.* J Antimicrob Chemother, 2003. 52(4): p. 572-5.

11. Hassan, M.T., et al., *Identification of a gene cluster, czr, involved in cadmium and zinc resistance in Pseudomonas aeruginosa.* Gene, 1999. 238(2): p. 417-25.

12. Akama, H., et al., *Crystal structure of the drug discharge outer membrane protein, OprM, of Pseudomonas aeruginosa: dual modes of membrane anchoring and occluded cavity end.* J Biol Chem, 2004. 279(51): p. 52816-9.

13. Li, X.Z. and K. Poole, *Mutational analysis of the OprM outer membrane component of the MexA-MexB-OprM multidrug efflux system of Pseudomonas aeruginosa.* J Bacteriol, 2001. 183(1): p. 12-27.

14. Akama, H., et al., *Crystal structure of the membrane fusion protein, MexA, of the multidrug transporter in Pseudomonas aeruginosa.* J Biol Chem, 2004. 279(25): p. 25939-42.

15. Higgins, M.K., et al., *Structure of the periplasmic component of a bacterial drug efflux pump.* Proc Natl Acad Sci U S A, 2004. 101(27): p. 9994-9.

16. Guan, L., et al., *Membrane topology of the xenobiotic-exporting subunit, MexB, of the MexA,B-OprM extrusion pump in Pseudomonas aeruginosa.* J Biol Chem, 1999. 274(15): p. 10517-22.

17. Guan, L. and T. Nakae, *Identification of essential charged residues in transmembrane segments of the multidrug transporter MexB of Pseudomonas aeruginosa.* J Bacteriol, 2001. 183(5): p. 1734-9.

18. Nehme, D. and K. Poole, *Assembly of the MexAB-OprM multidrug pump of Pseudomonas aeruginosa: component interactions defined by the study of pump mutant suppressors.* J Bacteriol, 2007. 189(17): p. 6118-27.

19. Mokhonov, V., et al., *Multidrug transporter MexB of Pseudomonas aeruginosa: overexpression, purification, and initial structural characterization.* Protein Expr Purif, 2005. 40(1): p. 91-100.

4.5

THE MISSING PART OF THE BACTERIAL MEXAB-OPRM SYSTEM: STRUCTURE OF THE MULTIDRUG EXPORTER MEXB

GABY SENNHAUSER, MAGDALENA A. BUKOWSKA & MARKUS G. GRÜTTER

TO BE SUBMITTED.

Biological Sciences

Biochemistry

The Missing Part of the Bacterial MexAB-OprM System: Structure of the Multidrug Exporter MexB

Gaby Sennhauser, Magdalena A. Bukowska and Markus G. Grütter*

Department of Biochemistry, University of Zurich, Winterthurerstrasse 190, 8057 Zurich, Switzerland

*To whom correspondence should be addressed

Markus G. Grütter
Department of Biochemistry
University of Zurich
Winterthurerstr. 190
CH-8057 Zurich
Switzerland
Phone +41 44 635 55 80
Fax +41 44 635 6834
E-mail: gruetter@bioc.uzh.ch

Manuscript information: 17 text pages, 4 figures, 1 table.

Data deposition: The atomic coordinates and structure factors have been deposited in the Protein Data Bank, *www.pdb.org* (PDB ID code 2v50).

Author contributions: G.S. and M.G.G. designed research, analyzed data, and wrote the paper. G.S. and M.A.B. performed research.

Abstract

Three-component efflux systems play a major role in the intrinsic and acquired capability of Gram-negative bacteria to extrude a plethora of compounds including clinically relevant antibiotics. We here report the crystal structure of the *Pseudomonas aeruginosa* multidrug exporter MexB at 3.0 Å, an intensively studied member of the resistance-nodulation-cell division (RND) family of secondary transporters. MexB forms an asymmetric homotrimer where each subunit adopts a different conformation representing three snapshots of the transport cycle similar to the recently determined structures of its close homologue AcrB from *Escherichia coli*, the sole structurally characterized member of the superfamily so far. The conformation of one subunit is remarkably altered compared to AcrB, indicating conformational flexibility of the whole system. Furthermore, a molecule identified as dodecyl maltoside (DDM) bound in the internal multidrug binding cavity is consistent with the binding principles seen in other multidrug-binding proteins. As the only missing piece of the puzzle in the MexAB-OprM system, the X-ray structure of MexB completes the molecular picture of the major responsible pump mediating drug-resistance in *P. aeruginosa*.

Introduction

Pseudomonas aeruginosa is an opportunistic human pathogen causing severe infections. Its intrinsic resistance to multiple clinically relevant antibiotics and its ability to acquire high-level resistance makes this bacterium difficult to combat (1). The resistance mainly results from a synergy of a low-permeability outer membrane and the expression of drug efflux systems (2). Typically, such efflux systems consist of an energy-providing inner membrane protein, a channel-forming outer membrane protein (OMP) and a periplasmic membrane fusion protein (MFP) necessary for stabilization or maybe with a more active role in the transport event itself. Thereby these complexes achieve the direct extrusion of substrates across the two membranes of the Gram-negative bacteria. To date, several tripartite systems have been identified in *P. aeruginosa* participating in drug efflux. Among them, the MexAB-OprM tripartite system was the first identified (3) and as major system contributing to intrinsic multidrug resistance in this organism is by far the best-characterized.

The inner membrane component MexB belongs to the resistance-nodulation-cell division (RND) family of transporters, responsible for the specificity (4, 5) and for the energy of the transport process (6). Characteristic for the RND-transporter family, MexB transports its substrates using the proton electrochemical gradient and it can accommodate a very broad range of substrates, such as many antibiotics, biocides, dyes, organic solvents, and detergents. Furthermore, the transporter may also have some other export functions as in the export of virulence factors that are important for the colonization and infection of host cells (7).

The first crystal structure of an RND-transporter, namely AcrB, was determined by X-ray crystallography in 2002 and revealed the general architecture of this family of proteins (8). Recently, three independent structures of AcrB provided novel insights into the mechanism by which RND-transporters work (9-11). Compared to the first structure which exhibited three-fold symmetry, all recently determined structures displayed an overall asymmetric shape of the trimeric protein where each subunit adopted a different conformation, interpreted as consecutive snapshots of the transport process. This finally led to the proposal of a novel mechanism of drug transport in which each subunit cycles through the three conformations such that at any given time, each conformation is adopted only by one subunit. A channel leading through the periplasmic domain of the protein most likely forms the pathway for substrates, with alternate openings, in two subunits to the periplasm/outer leaflet of the inner membrane and in the third subunit towards the OMP. Protonation of charged residues within

the transmembrane region, most probably induce the opening and closing of the channel entrance and exit via conformational changes in a polypeptide stretch connecting the transmembrane and periplasmic domain. Importantly, further studies showed that the asymmetry does exist not only in the crystal structure, but also in vivo and in solution (11, 12).

MexB is highly homologous to its *E. coli* counterpart AcrB (69.8% identity and 83.2% similarity in a sequence of 1046 amino acid residues). Intriguingly, despite their high degree of homology it is not possible to interchange the two components with regard to their interaction partners without loosing activity (4, 13) even though their cognate OMPs OprM and TolC both are multispecific per se, working with multiple RND transporters (14) or in the case of TolC even with members of the ATP-binding cassette (ABC)- or of the major facilitator (MF)-superfamily. In addition, AcrA was reported to function with several RNDs (5).

Crystal structures have now been reported for the tripartite efflux pump components MexA (15, 16) and OprM (17) and for all three proteins of the homologous *E. coli* AcrAB-TolC system (8, 18, 19). In this study, we have determined the X-ray structure of the missing part MexB at 3.0 Å resolution. The structure confirms the asymmetric fold observed for AcrB recently but also shows altered relative orientations of the subunits, particularly in the subunit whose role in the transport process remained somewhat unclear. Furthermore, a bound detergent molecule in the periplasmic domain of one subunit supports the idea of a large multisite binding cavity with different residues involved in binding different substrates. The completion of the atomic resolution model of the MexAB-OprM drug export system, allows detailed comparison with the already fully resolved *E. coli* AcrAB-TolC system concerning the specificity of the respective MFPs and OMPs in the future.

Results

Overall structure of MexB. *P. aeruginosa* MexB was overexpressed in *E. coli*, purified from the membrane fraction and crystals belonging to space group P1 were grown. The structure was solved at 3.0 Å resolution by molecular replacement using the homologous asymmetric AcrB structure as search model (**Table 1**). The asymmetric unit contained two almost identical trimers (chains ABC and chains DEF) with a root-mean-square deviation (rmsd) of the superposition of mainchain traces of the two molecules of 0.1 Å. The final model was refined to R factors of R = 24.3 % and Rfree = 28.7 % applying two-fold non-crystallographic symmetry restraints for each chain. Small breaks in the electron density were observed and not included in the final structure: residues 1-3, 500-511 (loop between TM6 and the cytoplasmic horizontal helix), and 673-677 (loop connecting PC1 and PC2) in chain A; 253-261 (loop in the DN domain at the periplasmic end of the protein), 500-511, and 670-675 in chain D; 669-680, and 990-995 (loop connecting TM11 and TM12) in chain E.

The global structure of MexB is similar to that of AcrB (8), which is not surprising given their high homology (**Fig. S1**). Like AcrB, MexB forms a trimer consisting of three subunits (**Fig. 1**). Each monomer exhibits a complex topology, consisting of 12 transmembrane α-helices (TM) (TM 1-12) and an extensive periplasmic domain, formed by two long loops between TM1 and TM2, and TM7 and TM8, respectively. This periplasmic domain folds into six subdomains: PN1, PN2, PC1 and PC2 building the pore domain, and DN and DC building the docking domain to the OMP. The DN subdomain exhibits an elongated β-sheet which protrudes into the next subunit thereby interlocking the subunits and stabilizing the trimer. In the transmembrane region, a pseudo-twofold symmetry is observed, with TM1-7 related to TM8-12. TM4 and TM10 are surrounded by the other transmembrane helices and harbor well-conserved charged residues, among them Asp-407, Asp-408 (TM4) and Lys-939 (940 in AcrB) (TM10) which probably mediate proton translocation and have been shown to be indispensable for the proper function of the protein, since the mutation of these residues leads to a complete loss of drug resistance (20). MexB contains 1046 amino acids compared to 1049 amino acids of AcrB and has two internal amino-acid residue deletions at positions 711 (located in a loop in PC2) and at positions 955 (located in the cytoplasmic loop connecting TM10 and 11) of the AcrB sequence, respectively.

Comparison with the asymmetric AcrB structure. Close structural relationship is observed between *P. aeruginosa* MexB and *E. coli* AcrB. The overall superposition of MexB and a recently determined asymmetric AcrB structure (11) results in an rmsd for 2990 Cα positions of 1.4 Å. Figure 2 shows a comparison of MexB superimposed with the homologous structure of AcrB. As the transmembrane part is responsible for the proton translocation and is likely to be similar in all RND-family transporters we analyzed the differences between MexB and AcrB based on superpositions of the transmembrane domains. Indeed, this region is very well conserved in sequence (**Fig. S1**). Strikingly, almost all residues in the two central TMs - TM4 and TM10 - are conserved between MexB and AcrB, including the two aspartates and the lysin in the putative proton-translocation site (**Fig. S2**). In both MexB and AcrB, Lys-939 (940 in AcrB) of TM10 is engaged in a salt-bridge interaction with aspartate residues of TM4 (Asp-407 or Asp-408) in subunits A and B (**Fig. 2**). In subunit C however, the lysin is tilted towards Thr-976 (978 in AcrB) of TM11. This movement implicates a rigid body shift of TM5 towards TM4 and TM10 and conformational changes in TM8. The N-terminal end of this helix which connects the transmembrane with the PC2 domain adopts different conformations in the subunits and is believed to be the trigger for the large conformational changes observed in the pore domains that finally lead to the export of substrates (**Fig. 2**). This stretch varies in AcrB from a random coil conformation with only partially defined electron density in subunit A to a fully α-helical conformation in subunit C. Surprisingly, in MexB, the conformation of TM8 in subunit B resembles more the conformation in subunit C, in which it is fully helical.

Inspection of the MexB and AcrB structures reveals non-continuous channels located in the periplasmic domain reaching halfway from the periplasm to a large cavity formed by the four pore domain subdomains or from this cavity to the OMP docking domain at the periplasmic tip of the protein (**Fig. 3**). The channels are large enough to accommodate the common substrates proposed to be transported by these transporters. As observed in the asymmetric AcrB structures, conformation B exhibits a channel open to the periplasm and could probably capture the substrates from the periplasm whereas the channel in conformation C opens towards the TolC protein allowing substrates to be released. These two subunits are oriented very similar compared to the AcrB structure (rmsd of 1.0 Å each) (**Fig. 2**). The portal from the membrane bilayer leading to the channel of subunit B found in AcrB is not observed in MexB, most likely due to a more helical conformation of the N-terminal part of TM 8 as mentioned before which leads to a closure of this entrance. The most striking difference

between MexB and AcrB however, is the conformation of subunit A (rmsd of 1.6 Å). Subunit A shows motions particularly in TM 6-12 and remarkable shifts occur in the pore domain, most notably of the PC2 subdomain. Subdomain PC2 is significantly shifted towards the transmembrane domain and towards PC1. These conformational shift result in a closure of the entrance formed by the PC domains (**Fig. 2**). Therefore, there is neither a channel entrance nor a channel exit observed in subunit A of the MexB structure (**Fig. 3A**). In AcrB, an opening is present between PC2 and PC1 which extends to the proposed binding cavity similar to the conformation seen in subunit B (**Fig. 3B**).

The structures of the docking domains of MexB and AcrB, to which the corresponding OMPs have been shown to associate, are very similar, each consisting of two subdomains. One of the two subdomains forms a long protruding loop that inserts into the docking domain of the neighbouring subunit. Since OprM and TolC are not interchangeable between the MexAB and AcrAB system (4), this finding is somewhat surprising. The high specificity seems therefore more likely to rely on the MFP.

Substrate binding by multidrug transporters. The structure presented here was solved using crystals grown in the presence of the nonionic detergent DDM to keep the membrane protein in solution. Detergents are known to be transported by multidrug transporters (21). Unexpectedly, positive electron density is visible within one of the binding cavities in the MexB trimer (**Fig. 2 and Fig. 4A**). Consistent with the previous determined AcrB/substrate complex structures (9), the density is visible only in one of the three subunits of the trimer, namely the binding subunit B. We interpreted the density as two maltoside rings belonging to a DDM molecule cocrystallizing with the transporter and placed the maltoside part in an orientation that fits the density. The electron density could be observed in both trimers in the asymmetric unit albeit with slightly different occupancy.

The maltoside binds in a voluminous binding cavity created by the β-sheets of the pore domain to a region rich in polar amino-acid residues (**Fig. 4A**). Residues in close proximity (<4 Å) are Val-47, Ser-48, and Gln-125 of PN1; Val-177, Gly-179, and Ser-180 of PN2; and Gln-273, and Arg-620 of PC1. These residues interact with the substrate presumably via hydrogen-bonding and van der Waals interactions. Not surprisingly, the C12-carbohydrate tail was not resolved, presumably because of high mobility. This behaviour can be observed for

most of the three ordered detergents bound to the transmembrane helices of the protein as well.

The usage of different sets of residues for binding of structurally diverse substrates was demonstrated earlier in structures of the transcription repressor QacR harboring various cationic lipophilic drugs which explained the difference to substrate specific binding (22). The observed multisite binding seems equally valid for multidrug transporters. The binding site of the DDM bound to MexB corresponds to the minocycline and doxorubicin binding sites of AcrB (**Fig. 4A**). There, the minocycline is bound to residues of the PC1 and PC2 subdomains. The D-ring is wedged between Ile-277, Phe-615 and Phe-178. Asn-274 is tilted against the drug to form a hydrogen bond with the 12a-hydroxy group (unpublished results). Together, despite the chemical differences of the three substrates, they all bind in the binding cavity of the pore domain using a different but overlapping set of residues. The nature of this binding cavity seems to be conserved among the two homologs, exhibiting many polar residues at the distal end and more aromatic residues at the proximal end.

The substrate specificities of the two efflux pumps is very similar when expressed in the same organism, e.g. *E. coli* (4). Nevertheless, we were not able to obtain good quality MexB crystals in presence of minocycline to date and likewise AcrB crystals harboring DDM. This fact raises the question about the structural features that underlie this difference. The answer to this question is not yet clear, but one of the most obvious possibilities would be differences within the substrate-binding sites. But the size of the binding cavity (**Fig. 2B**) as well as the amino acids lining it is not dramatically different in the two transporters. In MexB, the electrostatic surface potential of the binding cavity seems to be slightly more positive due to two exposed arginine residues (**Fig. 4B**). However, it is hard to rationalize for these subtle differences, if they are important for determining the substrate specificity of the two transporters and future mutagenesis experiments will be required to uncover the structural features governing the substrate specificity of RND-family members.

Crystal packing. The reason for the large conformational differences in subunit A is unclear. The most obvious reason, however, could be the arrangement of the MexB molecules in the crystal (**Fig. S3**). The two trimers of MexB in the asymmetric unit of the crystal pack together in a head-to-head manner involving the periplasmic part heavily. Notably, the two trimers associate through extensive contacts involving mainly the PC2 subdomain of subunit A.

Approximately 700 $Å^2$ of surface area per molecule is buried at this interface. Thus, the observed altered conformation of subunit A could simply be a result of the crystal contact. However, there is evidence that the differences are functionally significant. First, similar crystal contacts occur between subunit B of a symmetry-related molecule and subunits B (E) and C (F) of the second molecule in the asymmetric unit which have no effect on the conformation (buried surface area around 450 $Å^2$). Second, there was also a triclinic P1 crystal form reported for AcrB where the molecules also pack head-to-head with their periplasmic part but with a different pore-pore domain interaction (10). Finally, the smallest sequence conservation between the transporters is seen in the PC1 and PC2 domains (**Fig. S2**), suggesting that the difference of these domains could be an intrinsic property of MexB and thus functionally important. Therefore, it is likely that the observed conformation of subunit A of MexB represents another naturally occurring alternative state of subunit A and crystal-packing effects are not likely to be responsible for the structural differences.

Discussion. In this study, we have solved the 3.0 Å crystal structure of MexB from *P. aeruginosa*. This trimeric protein is part of the multicomponent pump MexAB-OprM that confers *P. aeruginosa* resistance to several dyes, detergents, and clinical relevant antibiotics. As expected, MexB shares the same overall fold as its close homologue AcrB. Interestingly, MexB adopts an asymmetric conformation where each subunit adopts a slightly different conformation therefore confirming the asymmetric conformation of the RND-transport proteins and it supports the transport model derived from the AcrB structures.

Although the overall arrangement of MexB and AcrB is very similar, a prominent difference is seen in the pore domain of subunit A. The non-continuous channels identified clearly assign the binding and extrusion conformation to the conformation seen in subunit B and C, respectively. It is therefore suggested that subunit A presents an intermediate conformational state between the extrusion and binding of the substrates. Compared to AcrB, the positions of the pore domain subdomains of this subunit are clearly altered, with shifts particularly of the PC2 subdomain. This shift results in a closure of the periplasmic portal in this subunit and therefore no channel was found in this subunit. One might speculate that this conformation might represent a state in between, in which a substrate is fully captured, since two detected channels in a trimer per se do not unambiguously determine the direction of the rotation. But as we do not see a substrate bound in this subunit and we do so in subunit B we exclude this

possibility. The progression of a subunit through the three individual conformations is therefore rather ABC than ACB.

The flexible nature of subunit A in these structures could probably also be due to the absence of the interacting partners (MFPs and OMPs). It is known that RND-transporters interact with their cognate MFP components most probably via the pore domain. A chimeric analysis of MexB and AcrB indicated that residues 589-612 are involved in MFP specificity (4). Consistently, a study identified the nearby mutation T578I in MexB which compromised the transporters contribution to antibiotic resistance most likely by impairing its interaction with MexA (23). These residues are all located in the PC1 subdomain. Therefore, the structural flexibility seen in the pore domain may be functional important and could have impact on the tripartite complex association. The reason for the high specificity of the individual pump components remains uncertain, but the specificity seems to reflect rather only subtle changes of the assembly interaction surfaces than large structural variations.

The DDM molecule bound in subunit B together with the recently solved AcrB/substrate structures and the structural studies on multidrug-binding regulatory proteins expanded the knowledge of the capability to accommodate numerous structurally diverse compounds. The general properties of a multisite binding cavity seem to reiterate. All these protein/substrate complexes possess a large drug-binding cavity rich in polar and aromatic residues which provide several partially overlapping binding sites. The binding mode of the maltoside group of the DDM is reminiscent of the situation in the binding of maltose in the *E. coli* maltose transporter $MalFGK_2$, where the binding involves mainly aspargines and serines which form hydrogen bonds to some hydroxy groups of the maltose (24). But no aromatic residue stacking was observed in MexB maybe indicating a weaker binding and less specificity and therefore reflecting the fundamental differences of specific versus multidrug transporter.

Taken together, the observation that both AcrB and MexB adopt an asymmetric conformation suggests that bacterial RND-transporters share a common mechanism of coupling proton transport to substrate translocation. Furthermore, the mechanistic mobility of the system is reflected in the conformational flexibility of the individual subunits.

Materials and Methods

Protein preparation. MexB, amplified from *P. aeruginosa* strain PAO1 genomic DNA (ATCC 47085) using PCR, was cloned into a pET28 vector using NdeI and XhoI restriction sites and the protein was expressed with a C-terminal hexahistidine-tag in *E. coli* strain C43 (DE3; Novagen, EMD Biosciences). Bacteria were grown to an absorbance at 600 nm of 0.8 in the presence of 50 mg l^{-1} kanamycin at 37 °C, and induced with 1 mM isopropyl-β-d-thiogalactopyranoside for 4 hours at 30 °C. Cells were centrifuged and lysed by French press in 20 mM Tris-HCl pH 7.5, 150 mM NaCl, DNase I, 1 mM phenylmethyl sulphonyl fluoride (PMSF) and complete protease inhibitor cocktail. The membranes were collected for 1 hours at 100,000*g* and solubilized in buffer A 20 mM Tris-HCl pH 7.5, 150 mM NaCl, 10 mM imidazole, 1 mM PMSF, 10 % glycerol containing 1 % (w/v) *n*-dodecyl-β-D-maltoside (DDM) (Anatrace, D310LA Anagrade) for 2 h at 4 °C. The solubilized protein was centrifuged for 1 hour at 100,000*g* and the supernatant loaded onto a Ni-NTA affinity column (Qiagen) equilibrated with buffer A containing 0.03% DDM. The column was washed using this buffer and 30 mM imidazole, respectively, and the desired protein was eluted with 200 mM imidazole.

Crystal preparation. To obtain crystals of MexB, the protein was concentrated and further purified on a Tricorn Superdex 200 size exclusion column (Amersham Biosciences) equilibrated in 20 mM Tris-HCl pH 7.5, 150 mM NaCl, 10 % glycerol containing 0.03 % (w/v) DDM. The peak corresponding to the MexB trimer was concentrated, exchanged into 10 mM HEPES pH 7.5, 50 mM NaCl buffer containing 0.03 % (w/v) DDM, and finally concentrated to 20-25 mg ml^{-1}.

Initial crystallization screening was done in 96-well, sitting drop crystallization plates (Greiner Bio-One). The crystal used for data collection appeared within 20 d in 33% PEG400, 50 mM Na-Acetate pH 4.5, 230 mM NaCl in a sitting drop vapor diffusion experiment at 20°C. For cryo protection, the crystals were soaked in two steps in the mother liquor containing 35% PEG400 and flash frozen in liquid nitrogen.

Structure determination. Data were collected at the Swiss Light Source beamline PX on a PILATUS detector (Dectris). The data were indexed, integrated and scaled with XDS. The crystal belonged to space group P1, with a Matthews coefficient of 3.65 $Å^3$/Da, corresponding to an estimated solvent content of 66.0%.

The crystal structure was solved by molecular replacement with PHASER(25), using the asymmetric crystal structure of AcrB (Protein Data Bank code 2J8S) as a search model. Refinement of the structure was carried out through multiple cycles of manual adjustments and rebuilding using COOT (26) and refinement using PHENIX (27), resulting in a final model with an R factor of 24.3 and an R free factor of 28.7%.

ACKNOWLEDGEMENTS. We thank the beamline staff at the Swiss Light Source beamline X06SA for excellent support, C. Briand for help during data collection, and O. Eidam for crystallographic advice. This work was supported by the Swiss National Science Foundation in the framework of the National Center of Competence in Research (NCCR) Structural Biology.

References

1. Poole K, Srikumar R (2001) Multidrug efflux in Pseudomonas aeruginosa: components, mechanisms and clinical significance. *Curr Top Med Chem* 1:59-71.
2. Nikaido H (2001) Preventing drug access to targets: cell surface permeability barriers and active efflux in bacteria. *Semin Cell Dev Biol* 12:215-223.
3. Poole K, Krebes K, McNally C, Neshat S (1993) Multiple antibiotic resistance in Pseudomonas aeruginosa: evidence for involvement of an efflux operon. *J Bacteriol* 175:7363-7372.
4. Tikhonova EB, Wang Q, Zgurskaya HI (2002) Chimeric analysis of the multicomponent multidrug efflux transporters from gram-negative bacteria. *J Bacteriol* 184:6499-6507.
5. Elkins CA, Nikaido H (2002) Substrate specificity of the RND-type multidrug efflux pumps AcrB and AcrD of Escherichia coli is determined predominantly by two large periplasmic loops. *J Bacteriol* 184:6490-6498.
6. Zgurskaya HI, Nikaido H (1999) Bypassing the periplasm: reconstitution of the AcrAB multidrug efflux pump of Escherichia coli. *Proc Natl Acad Sci U S A* 96:7190-7195.
7. Piddock LJ (2006) Multidrug-resistance efflux pumps - not just for resistance. *Nat Rev Microbiol* 4:629-636.
8. Murakami S, Nakashima R, Yamashita E, Yamaguchi A (2002) Crystal structure of bacterial multidrug efflux transporter AcrB. *Nature* 419:587-593.
9. Murakami S, Nakashima R, Yamashita E, Matsumoto T, Yamaguchi A (2006) Crystal structures of a multidrug transporter reveal a functionally rotating mechanism. *Nature* 443:173-179.
10. Seeger MA, Schiefner A, Eicher T, Verrey F, Diederichs K, Pos KM (2006) Structural asymmetry of AcrB trimer suggests a peristaltic pump mechanism. *Science* 313:1295-1298.
11. Sennhauser G, Amstutz P, Briand C, Storchenegger O, Grutter MG (2007) Drug export pathway of multidrug exporter AcrB revealed by DARPin inhibitors. *PLoS Biol* 5:e7.
12. Seeger MA, von Ballmoos C, Eicher T, Brandstatter L, Verrey F, Diederichs K, Pos KM (2008) Engineered disulfide bonds support the functional rotation mechanism of multidrug efflux pump AcrB. *Nat Struct Mol Biol* 15:199-205.
13. Krishnamoorthy G, Tikhonova EB, Zgurskaya HI (2008) Fitting periplasmic membrane fusion proteins to inner membrane transporters: mutations that enable Escherichia coli AcrA to function with Pseudomonas aeruginosa MexB. *J Bacteriol* 190:691-698.
14. Aires JR, Kohler T, Nikaido H, Plesiat P (1999) Involvement of an active efflux system in the natural resistance of Pseudomonas aeruginosa to aminoglycosides. *Antimicrob Agents Chemother* 43:2624-2628.
15. Higgins MK, Bokma E, Koronakis E, Hughes C, Koronakis V (2004) Structure of the periplasmic component of a bacterial drug efflux pump. *Proc Natl Acad Sci U S A* 101:9994-9999.
16. Akama H, Matsuura T, Kashiwagi S, Yoneyama H, Narita S, Tsukihara T, Nakagawa A, Nakae T (2004) Crystal structure of the membrane fusion protein, MexA, of the multidrug transporter in Pseudomonas aeruginosa. *J Biol Chem* 279:25939-25942.
17. Akama H, Kanemaki M, Yoshimura M, Tsukihara T, Kashiwagi T, Yoneyama H, Narita S, Nakagawa A, Nakae T (2004) Crystal structure of the drug discharge outer membrane protein, OprM, of Pseudomonas aeruginosa: dual modes of membrane anchoring and occluded cavity end. *J Biol Chem* 279:52816-52819.

18. Mikolosko J, Bobyk K, Zgurskaya HI, Ghosh P (2006) Conformational flexibility in the multidrug efflux system protein AcrA. *Structure* 14:577-587.
19. Koronakis V, Sharff A, Koronakis E, Luisi B, Hughes C (2000) Crystal structure of the bacterial membrane protein TolC central to multidrug efflux and protein export. *Nature* 405:914-919.
20. Guan L, Nakae T (2001) Identification of essential charged residues in transmembrane segments of the multidrug transporter MexB of Pseudomonas aeruginosa. *J Bacteriol* 183:1734-1739.
21. Srikumar R, Kon T, Gotoh N, Poole K (1998) Expression of Pseudomonas aeruginosa multidrug efflux pumps MexA-MexB-OprM and MexC-MexD-OprJ in a multidrug-sensitive Escherichia coli strain. *Antimicrob Agents Chemother* 42:65-71.
22. Schumacher MA, Miller MC, Grkovic S, Brown MH, Skurray RA, Brennan RG (2001) Structural mechanisms of QacR induction and multidrug recognition. *Science* 294:2158-2163.
23. Middlemiss JK, Poole K (2004) Differential impact of MexB mutations on substrate selectivity of the MexAB-OprM multidrug efflux pump of Pseudomonas aeruginosa. *J Bacteriol* 186:1258-1269.
24. Oldham ML, Khare D, Quiocho FA, Davidson AL, Chen J (2007) Crystal structure of a catalytic intermediate of the maltose transporter. *Nature* 450:515-521.
25. McCoy AJ, Grosse-Kunstleve RW, Adams PD, Winn MD, Storoni LC, Read RJ (2007) in *Journal of Applied Crystallography*, pp. 658-674.
26. Emsley P, Cowtan K (2004) Coot: model-building tools for molecular graphics. *Acta Crystallogr D Biol Crystallogr* 60:2126-2132.
27. Adams PD, Grosse-Kunstleve RW, Hung LW, Ioerger TR, McCoy AJ, Moriarty NW, Read RJ, Sacchettini JC, Sauter NK, Terwilliger TC (2002) PHENIX: building new software for automated crystallographic structure determination. *Acta Crystallogr D Biol Crystallogr* 58:1948-1954.

Table 1. Data collection and refinement statistics.

Data collection and processing	
Wavelength, Å	1.0000
Space group	P1
Unit cell parameters, Å	a = 125.05, b = 134.58, c = 151.02
	α = 86.99, β = 69.70, γ = 88.16
Resolution, Å	50.00-3.0 (3.1-3.0)[a]
Total reflections	419193
Unique reflections	176904 (15057)
Completeness, %	95.7 (87.0)
R_{sym}	0.041 (0.70)
I/σ(I)	15.26 (1.73)
Refinement	
Resolution, Å	50-3.0
R/R_{free}, %[b]	24.3/28.7
No. atoms	46578
No. of detergent molecules	8
B-factors	88.33
rms deviations	
Bond lengths (Å)	0.004
Bond angles (º)	0.802
Ramachandran plot (%)	
Most favored	83.3
Allowed	16.1

[a]Values in parentheses are for the highest resolution shell.
[b]$R = \Sigma \mid F_{obs} - F_{cal} \mid / \Sigma F_{obs}$. The formula for R_{free} is the same as that for R, except it is calculated with a portion of the structure factors that had not been used for refinement.

Figure 1

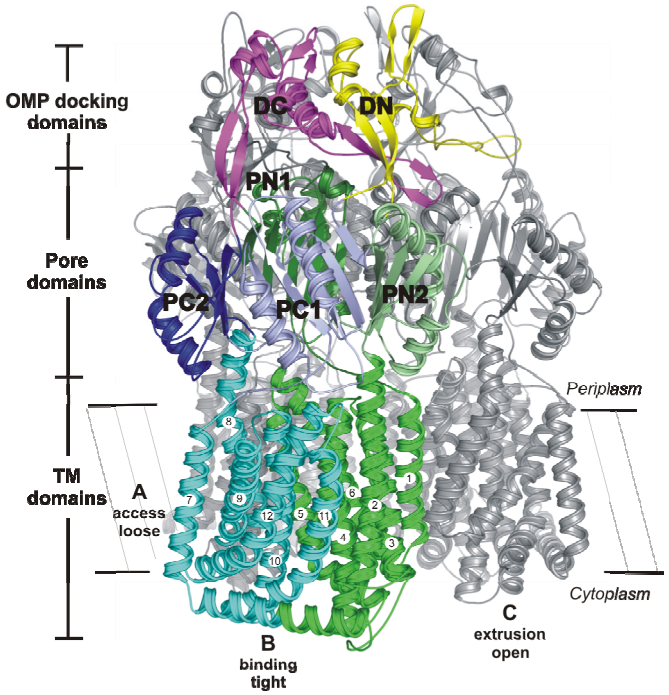

Fig. 1. Structure and architecture of MexB.
Ribbon diagram of the overall MexB trimer viewed in the membrane plane. The locations of the three prominent domains and the approximate position of the inner membrane are indicated. One monomer is colored according to its subdomains, with subdomains labeled and α-helices numbered. The common terms for the naming of the three subunits are listed (9-11). All figures of the molecular models were generated with PyMol (www.pymol.org).

Figure 2

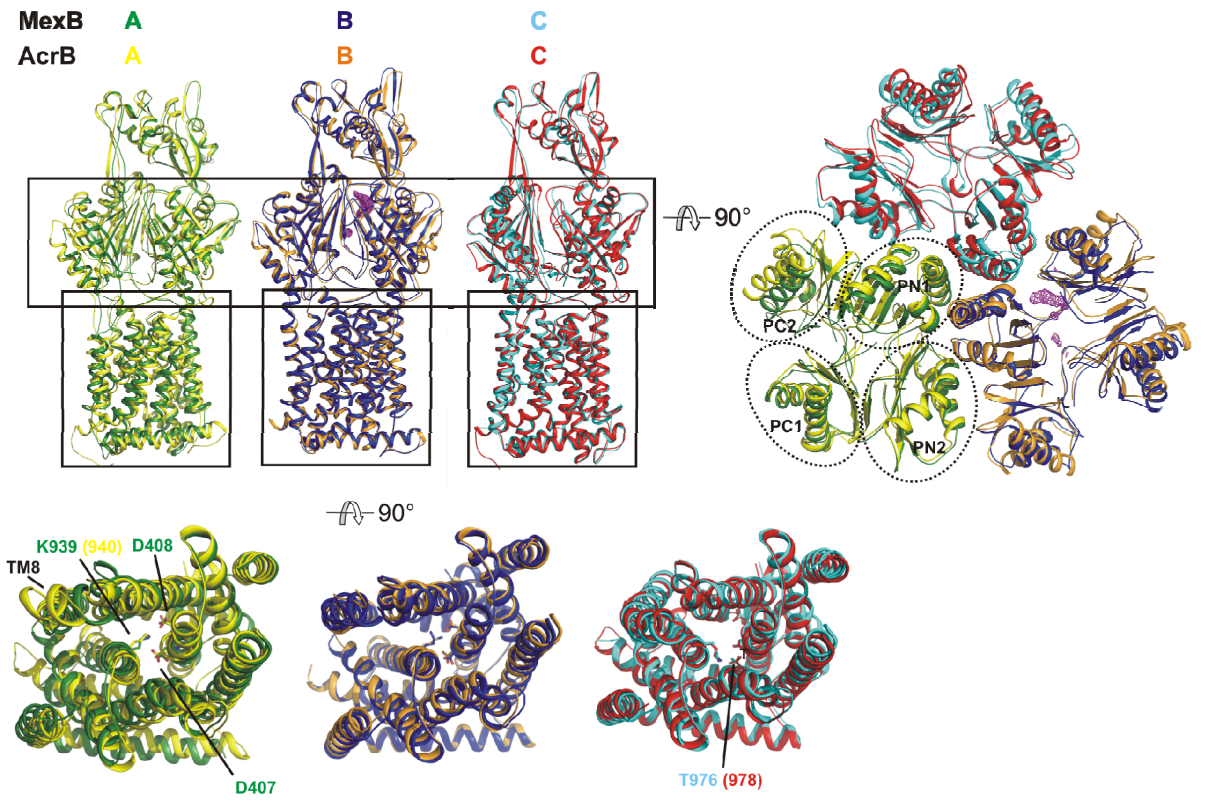

Fig. 2. Comparison of MexB and AcrB structures.
The MexB trimer is superimposed with the AcrB trimer (PDB ID code 2J8S) based on their transmembrane helices. For clarity, the subunits are individually represented in the same orientation. Also shown is the Fo-Fc electron density (contoured at 2.5σ) observed in one of the binding cavities of the trimer, as purple mesh. The right panel shows a close-up view of the structural differences occurring in the pore domain. The lower panel shows a close-up view of the TM domains illustrating the side chain conformations in the putative proton translocation site.

Figure 3

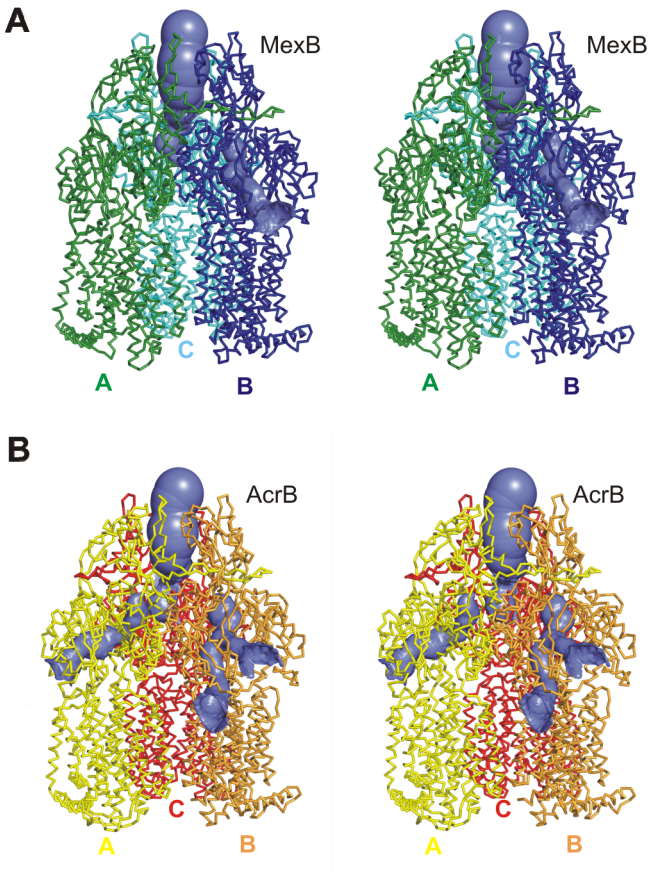

Fig. 3. Stereo view of the channels leading to the drug binding cavity.
(*A*) The channels detected in MexB are shown as blue surfaces. The subunits are individually colored: green (A), blue (B), and cyan (C). No channel can be observed in subunit A due to the conformational changes observed for the PC2 domain. The channels were calculated using the program CAVER (http://loschmidt.chemi.muni.cz/caver).
(*B*) Channels detected in AcrB (PDB ID code: 2J8S). The subunits are individually colored: yellow (A), orange (B), and red (C).

Figure 4

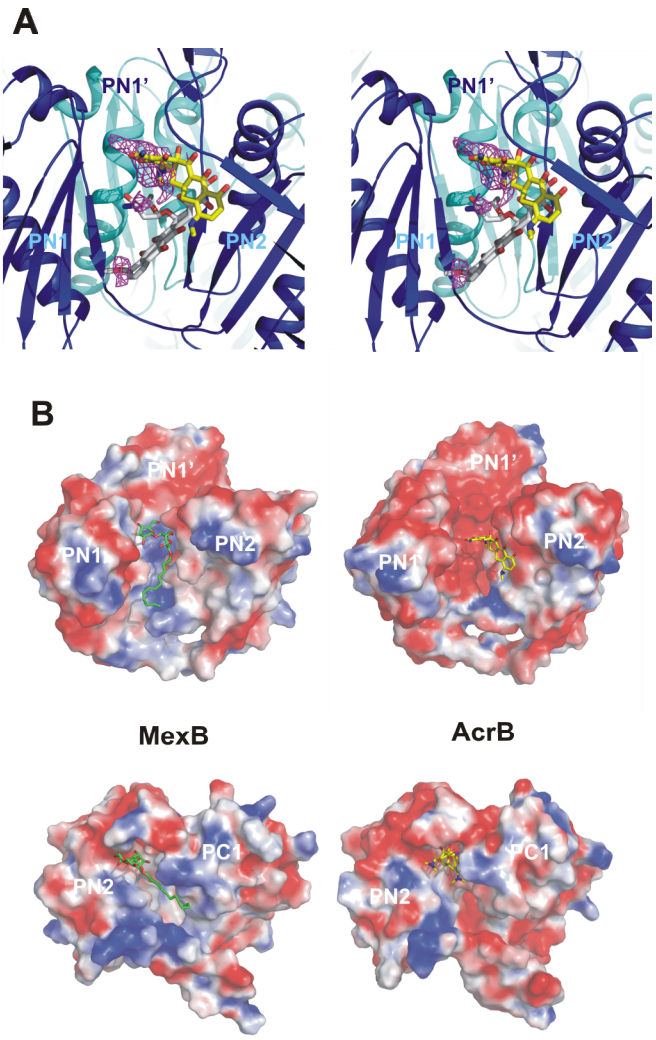

Fig. 4. Multisite binding pocket of RND-transporters.
(*A*) Stereo view of the binding cavity with the Fo-Fc map contoured at 2.5σ. Minocycline and doxorubicine binding sites in AcrB are shown as yellow and grey sticks, respectively. The view is as for the individual subunits in Fig. 2 with PC subdomains omitted for clarity.
(*B*) Comparison of the electrostatic surface potential of the binding pockets of MexB and AcrB (calculated with APBS). The upper panel has the same orientation as Fig. 4A. The view in the lower panel is from the PN1 and PC2 domains. The surface is colored blue for potentials > 10 kT/e and red for potentials < -10 kT/e. DDM and minocycline are shown as green and yellow sticks, respectively.

Fig. S1. Sequence alignment.

Alignment of the *P. aeruginosa* MexB sequence with its close homologue *E. coli* AcrB. The secondary structure elements are indicated above the sequence (based on subunit C of the MexB crystal structure). The subdomains are individually colored and labeled according to Fig. 1.

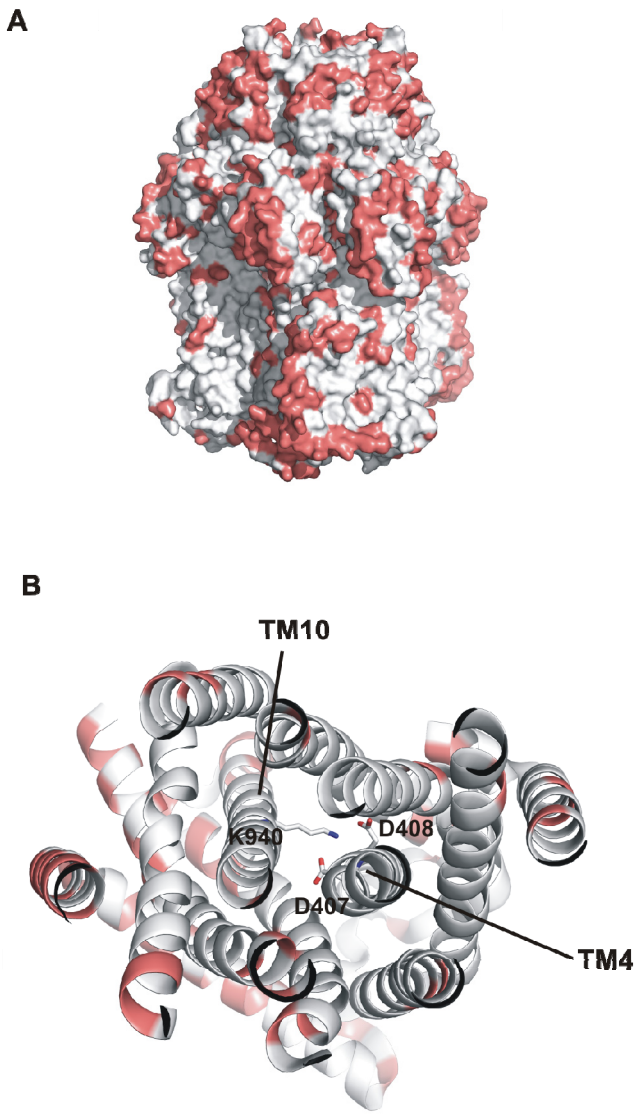

Fig. S2. Structural alignment of MexB and AcrB.
(A) Structural alignment of MexB and AcrB. The protein surface of AcrB is colored according to sequence conservation with the homologous MexB. Conserved residues are colored in grey. The sequence differences are mainly in the periplasmic domain. This image was prepared with ProtSkin (http://www.mcgnmr.ca/ProtSkin/intro/index.html).
(B) Conservation in the transmembrane domain of AcrB. The TMs of subunit B are shown in ribbon representation and the charged residues in the putative proton translocation site are shown as sticks.

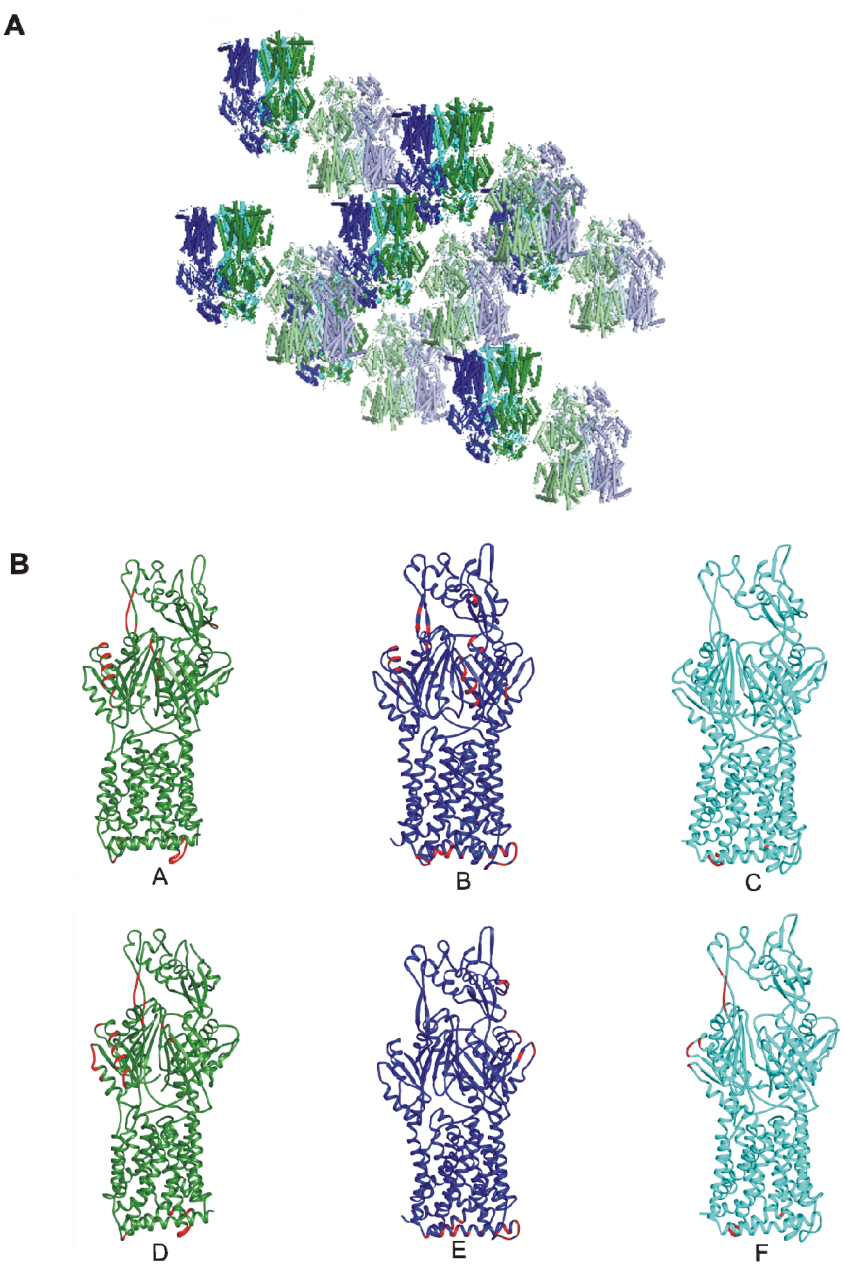

Fig. S3. Packing of MexB in the crystal.
(A) Crystal packing of MexB. The individual subunits are colored: Green, blue and cyan for A, B, and C, respectively and lighter colors for D, E, and F.
(B) Individual subunits of MexB are shown in ribbon representation. Interfaces of crystal contacts are colored in red. Calculated with the Protein interfaces, surfaces and assemblies service (PISA) (www.ebi.ac.uk/msd-srv/prot_int/pistart.html).

4.6 Selecting DARPins for the structural analysis of RND-transporters

Gaby Sennhauser, Markus G. Grütter

Among the five known superfamilies of multidrug transporters, the resistance-nodulation-division (RND) family is especially effective in generating antibiotic resistance in Gram-negative bacteria [1]. Within a species there are normally multiple genes encoding RND transporters and these proteins typically share a high degree of sequence homology. *Escherichia coli* AcrB and *Pseudomonas aeruginosa* MexB are constitutively expressed and mainly responsible for the intrinsic resistance to a wide variety of substances in these bacteria. The function of other close homologues such as AcrD and AcrF from *E. coli* (66% and 77% identity to AcrB, respectively) is less characterized since the investigation is more complicated. The substrates transported by these homologous are often overlapping and the range is not as broad. AcrD is believed to transport aminoglycosides since its deletion decreased the MIC of such compounds and lead to the accumulation of radioactive aminoglycosides [2]. The function of AcrF is more obscure since its deletion did not alter the drug-susceptibility of wild-type *E. coli* [3]. A great deal of research is being undertaken to understand the precise mechanisms of these RND transporters and how specificity for different drugs is achieved. The key to understand how these pumps work involves the determination of the structures of several representative proteins to atomic resolution.

After the successful structure determination of AcrB in complex with a DARPin, the aim of this work was to select specific DARPin binders to close homologs of it. These binders could then facilitate the crystallization of these proteins in a similar way as with AcrB.

The RND transporters AcrD and AcrF were cloned, expressed and purified in a similar way as MexB (see chapter 4.5). All proteins carried a Hexahistidine-Tag at their C-terminus and could be efficiently purified in presence of DDM via Immobilized Metal Affinity Chromatography (IMAC). Size exclusion chromatography was used as polishing step in purification and to roughly assess the oligomeric behaviour of the proteins (Fig. 1). Whereas MexB and AcrF showed only a small tendency to

aggregate and eluted predominantly as a symmetric peak in SEC with a molecular weight corresponding to a trimer, we observed a significant percentage of other oligomeric states for AcrD (monomer or dimer). For immobilization on streptavidin coated plates, the proteins were chemically biotinylated following the procedure for AcrB [4].

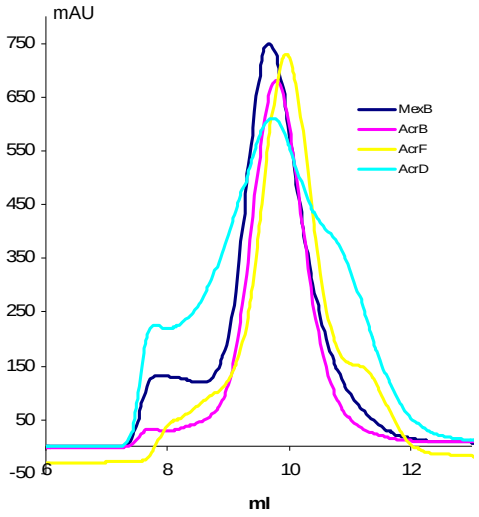

Fig. 1.

SEC profiles of all investigated RND transporters. Recombinant proteins from 0.5l *E. coli* culture were purified and applied to a Tricorn Superdex 200 column.

Four rounds of ribosome display were carried out against biotinylated MexB, AcrD and AcrF in the presence of 0.03% DDM using an N2C DARPin library (Fig. 2) [4]. Two prepanning steps against maltose binding protein were included in all rounds and in the last round the washing step was extended to two hours.

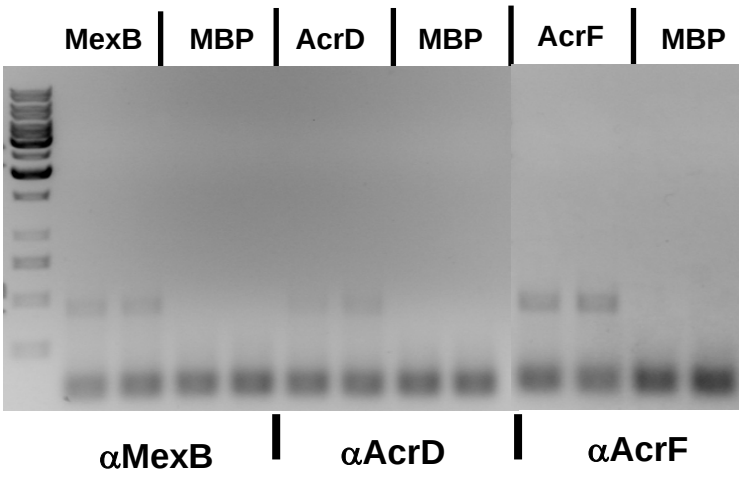

Fig. 2.

Fourth round of ribosome display against three AcrB homologs. The round was done in duplicates and the DNA was analyzed after reverse-transcription PCR. The binding was tested against the target protein (first two lines) and background binding against maltose binding protein (second two lines).

The pools obtained were then cloned into the pQE30 vector (Qiagen). To test if the crude extract ELISA protocol still works in the presence of detergent, a test assay was performed using the AcrB binder which lead to the crystal structure and an old DARPin pool generated against AcrB [4] as controls. Then the newly generetated pools against the homologs were analyzed (data not shown). The binders giving the highest signal to background ratio were sequenced, purified and further analyzed by competition ELISA (data not shown). 96 clones per target were analyzed in a crude extract ELISA. 6 binders for AcrB, 5 for MexB, 5 for AcrF and none for AcrD showed a specific recognition in a competition ELISA (Fig. 3). These DARPin binders were able to form a stable complex also during size exclusion chromatography. The kinetic constants of the MexB binders were further determined by Biacore experiments and showed that all binders possess dissociation constants in the low nanomolar range (Fig. 4). For the AcrF binders Biacore measurements were not possible due to a severe decay of baseline signal over time. This behaviour was also observed for MexB albeit to a much lesser extend. This problems could have been due to an improper immobilization technique or instability of the proteins.

AcrB binders

```
N3C     MRGSHHHHHHGSDLGKKLLEAARAGQDDEVRILMANGADVNAXDXXGXTPLHLAAXXGHLEIVEVLLKXGADVNAX
110819  ........................R.................A.VV.W.......YW...........N......Y
3A      ..........................................R.FT.W.......HF...........N......K
3C      ..........................................S.HV.W.......YF...........N......D
9E      ..........................................R.II.W.......YF...........H......E
12E     ..........................................R.II.W.......YF...........H......E
5B      ..........................................F.FT.W.......YF......V....Y......T
7C      ..........................................N.YS.K.......RR...........H......I

        DXXGXTPLHLAAXXGHLEIVEVLLKXGADVNAXDXXGXTPLHLAAXXGHLEIVEVLLKXGADVNAQ
        .TL.S.......HF...........N......K.DN.I.......NR...........Y.......
        .SL.V.......RR...........N......S.SH.F.......KR...........N.......
        .SL.T.......DR...........N......N.HN.F.......NI...........H.......
        .TL.S.L.....HT...........H......M.SN.H.......RL...........Y.......
        .TL.S.L.....HT...........H......M.SN.H.......RL...........Y.....T.
        .TI.Y.......QK...........N......N.HN.F.......NI...........Y.V.....
        .NW.Y.......YW...........H......L.KI.N.......DC...........H.......

        DKFGKTAFDISIDNGNEDLAEILQKLN**
        ............N..............**
        ..........................**
        ................S.........**
        ..........................**
        ..........................**
        ..........................**
        ..........................**
```

MexB binders

```
N2C     MRGSHHHHHHGSDLGKKLLEAARAGQDDEVRILMANGADVNAXDXXGXTPLHLAAXXGHLEIVEVLLKXGADVNAX
12E     ..........................................I.HN.M.......YR...........Y......W
8F      ................................V.......I.HN.M.......YR...........Y...I..W
2C      ..................KT.....................T.FS.I.R.....SK...........Y......Q
7B      ............N.............................I.FK.N.......VK...........N.....VQ
6E      ..........................................I.WN.S.......LR...........N......A

        DXXGXTPLHLAAXXGHLEIVEVLLKXGADVNAQDKFGKTAFDISIDNGNEDLAEILQKLN**
        .IW.A.......HS.....F.....H.................................**
        .IW.A.......YT...........H.................................**
        .FF.L.......SN...........N.................................**
        .FY.W.......TW...........Y.................................**
        .FY.W.......TF...........N.................................**
```

AcrF binders

```
N2C     MRGSHHHHHHGSDLGKKLLEAARAGQDDEVRILMANGADVNAXDXXGXTPLHLAAXXGHLEIVEVLLKXGADVNAX
5E      ..........................................K.SW.Q.......TY...........H......D
6C      ..........................................N.DY.Q......TTY...K.......Y......S
12B     ....................T.....................N.DY.Q......TTY...........YS.....S
9D      ..........................................N.DY.Q......TTY...........Y......S
9A      ..........................................D.NH.F.......HY...........Y.....DH

        DXXGXTPLHLAAXXGHLEIVEVLLKXGADVNAQDKFGKTAFDISIDNGNEDLAEILQKLN**
        .ME.F.......IT...........Y.................................**
        .QM.F.......IL...........Y.................................**
        .QM.F.......IL...........Y.................................**
        .QM.F.......HT.R.........Y.........I.......................**
        .LI.W.......YL.R.........Y..............L...............RN*
```

Fig. 3.

Sequences of DARPins binding to RND transporters.

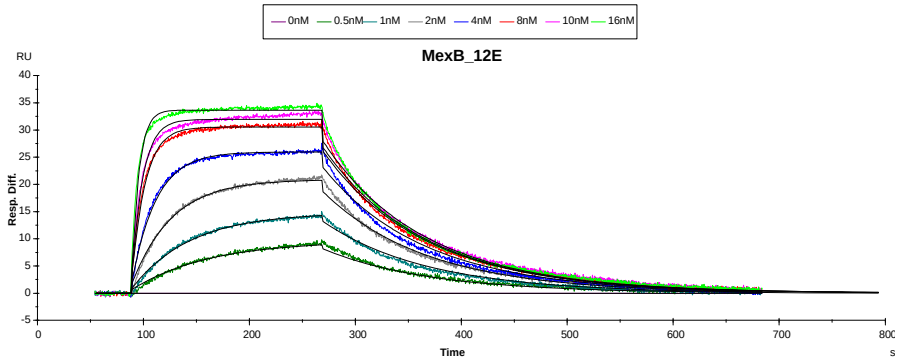

Fig. 4.

The association and dissociation rate constants were determined using SPR. For the MexB binding DARPin 12E, a dissociation constant of 1.2 nM was calculated.

Finally, we found that the selected DARPin molecules were extremely specific. Despite the close homology all DARPins specifically recognized only the target protein against which they were selected (Fig. 5).

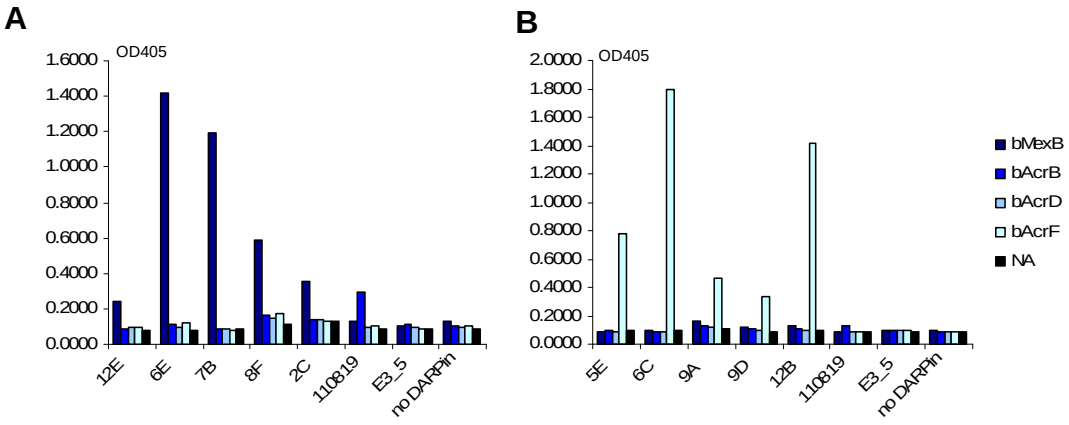

Fig. 5.

Specificity of the DARPins (each 50 nM; control with no DARPin) with immobilized MexB, AcrB, AcrD, AcrF and neutravidin is shown. **A** MexB binders and the AcrB binder 110819. **B** AcrF binders and the AcrB binder 110819.

All RND-transporter-specific DARPins in complex with their corresponding target were subjected to crystallization. No crystals were obtained for AcrF/DARPin complexes. Among the five MexB binders, one binder, termed 12E yielded crystals. Indeed the conditions leading finally to the MexB structure were originally obtained in presence of 12E in the protein solution. However, it turned out that the complex must

have dissociated under the specific crystallization condition since no density could be seen for a bound DARPin.

1. Nikaido, H., *Multidrug efflux pumps of gram-negative bacteria.* J Bacteriol, 1996. 178(20): p. 5853-9.

2. Rosenberg, E.Y., D. Ma, and H. Nikaido, *AcrD of Escherichia coli is an aminoglycoside efflux pump.* J Bacteriol, 2000. 182(6): p. 1754-6.

3. Nishino, K. and A. Yamaguchi, *Analysis of a complete library of putative drug transporter genes in Escherichia coli.* J Bacteriol, 2001. 183(20): p. 5803-12.

4. Sennhauser, G., et al., *Drug export pathway of multidrug exporter AcrB revealed by DARPin inhibitors.* PLoS Biol, 2007. 5(1): p. e7.

ACKNOWLEDGEMENTS

My gratitude goes to Prof. Markus Grütter for giving me the possibility to work in his group on such an interesting project. I appreciated his confidence, his interest and the freedom he left me in my project.

I would also like to thank the members of my PhD examination committee Raimund Dutzler and Andreas Plückthun for reviewing this thesis as well as their effort.

Very special thanks to Patrick Amstutz for teaching me almost everything from project planning, techniques, writing, to work as fast as possible. I learned really a lot from him and I am deeply grateful for how much time he dedicated to me and for his immense support. Thanks of course also to the rest of the Molecular Partners crew, I am still proud to have been their first collaborator and I am really looking forward to my future employment in their team.

I would like to thank future MD Otso Storchenegger for his effort in this project and Martin Pos at the Institute of Physiology for continuous discussion about RND-transporters. Thanks as well to former and present members of our research group. Annette Haisch for the initial support, Christophe Briand for introducing me into crystallographic programs and for enormous support at the SLS, Heinz Gut and Oliv Eidam for the many crystallographic advices in difficult times, Daniel Frey for the good time in the lab, Beat Blattmann for the excellent management of the crystallization facility, Eva Jenny for the never running out of materials, and Andi Schweizer for moral support and the athletic challenge of course.

Finally, my love and gratitude to my friends in and around Zurich who have been great support along the way, being there for motivating words with a glass of wine, a beer or good music. Immense thanks also to my brother Sven for his never-ending very professional IT-support. Last but not least I would like to thank my parents, to whom I owe everything. They supported me throughout my education, and they funded my beloved horse that I unfortunately lost during the period of this PhD thesis. I am deeply grateful to you, there aren’t words...

Curriculum vitae

Name	Sennhauser
First Name	Gaby
Date of birth	May 23, 1980
Citizenship	Kirchberg SG, Switzerland

Education

2004 – now	PhD studies in the research group of Prof. Dr. Markus G. Grütter Institute of Biochemistry, University of Zürich
2003 – 2004	Diploma thesis at the Department of Biochemistry, University of Zürich Supervisor: Prof. Dr. Markus G. Grütter Subject: *Cloning, overexpression, purification and crystallization of two Escherichia coli ATP-binding cassette (ABC) transporters*
2000 – 2004	Studies of Biochemistry at the University of Zürich Side subject: Immunology
1995 – 2000	Swiss Federal Matura “Typus B” Kantonsschule Zürcher Oberland, Wetzikon ZH

Publications

Sennhauser G., Amstutz P., Briand C., Storchenegger O., Grütter M.G. Drug Export Pathway of Multidrug Exporter AcrB Revealed by DARPin Inhibitors. *PLoS Biology* (2007) **5**(1), e7.

Sennhauser G., Grütter M.G. Chaperone-assisted Crystallography with DARPins. Review
Submitted

Sennhauser G., Bukowska M.A., Grütter M.G. The Missing Piece of the Bacterial MexAB-OprM system: Structure of the Multidrug Exporter MexB.
To be submitted

Oral and Poster Presentations

2008	Keystone Symposia Frontiers in Structural Biology, Steamboat Springs (CO), USA: Poster presentation (Supported with a travel grant from the Swiss Biochemical society)
2007	BioMedical Transporters 2007 5th International Research Conference, Bern, Switzerland: *Poster presentation*; *prize for best poster*
2007	University of Konstanz, Germany: *Invited lecture* ”Selection and crystallization of a DARPin against the multidrug transporter AcrB, revealing the drug export pathway”
2006	20th REGIO Meeting, Konstanz, Germany: *Oral presentation*
2006	5th International NCCR Symposium on New Trends in Structural Biology, Zürich, Switzerland: *Poster presentation*
2006	3rd International Conference on Structure, Dynamics and Function of Proteins in Biological Membranes, Ascona, Switzerland: *Poster presentation*